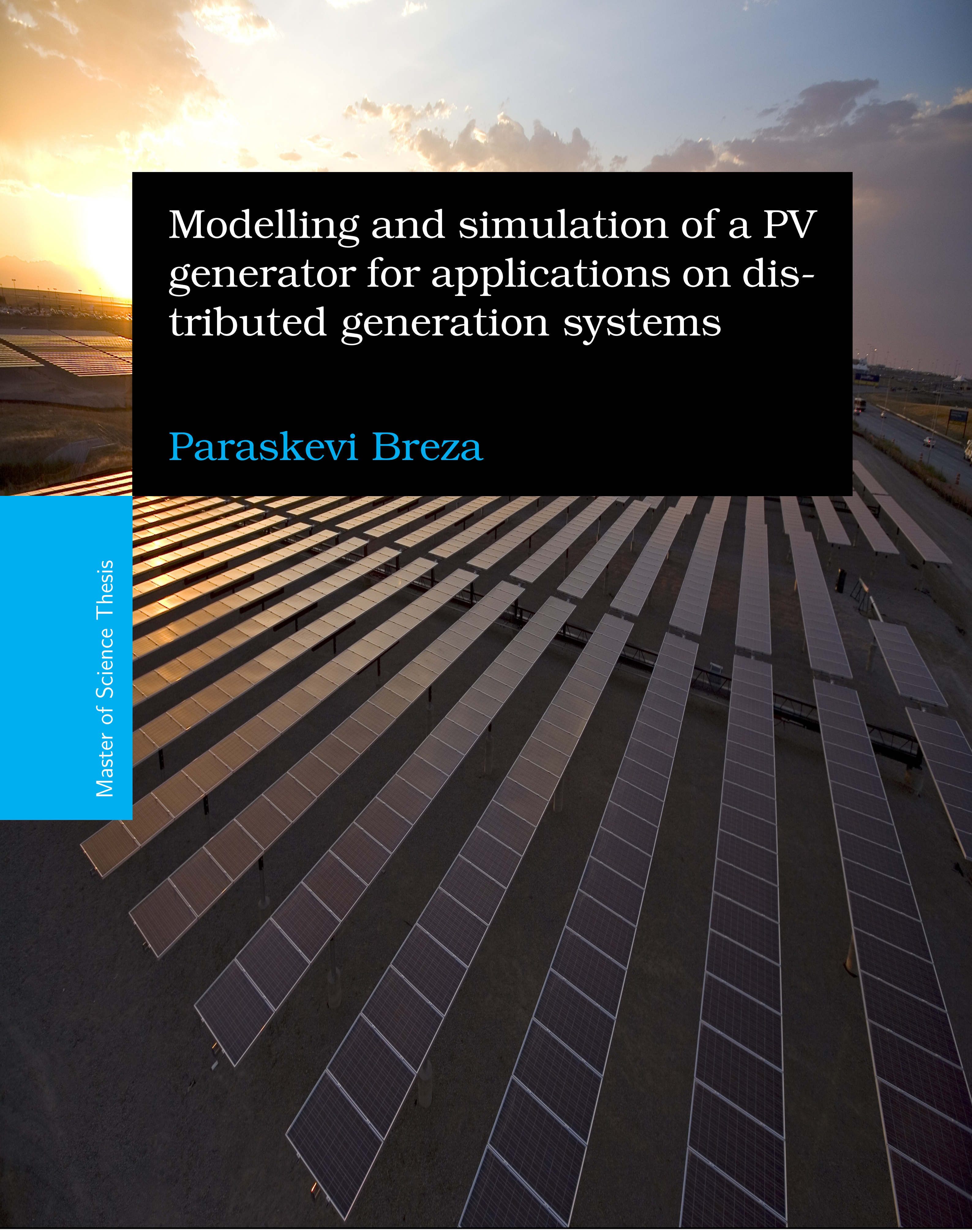

Modelling and simulation of a PV generator for applications on distributed generation systems

Paraskevi Breza

Master of Science Thesis

Delft University of Technology

Intelligent Electrical Power Grids

Modelling and simulation of a PV generator for applications on distributed generation systems

Master of Science Thesis

For the degree of Master of Science in Sustainable Energy Technology
at Delft University of Technology

Paraskevi Breza
4184122

November 15, 2013

Faculty of Applied Sciences (TNW) · Delft University of Technology

Delft University of Technology

Cover photo by: Denver International Airport (2008). 2 MW PV system at the Denver International Airport. [photograph]. Retrieved November 14, 2013, from:
http://images.nrel.gov/viewphoto.php?imageId=6311939

Delft University of Technology
Faculty of
Electrical Engineering Mathematics and Computer Science (eemcs)

The undersigned hereby certify that they have read and recommend to the Faculty of Applied Sciences (TNW) for acceptance a thesis entitled

Modelling and simulation of a PV generator for applications on distributed generation systems

by

Paraskevi Breza

in partial fulfillment of the requirements for the degree of

Master of Science Sustainable Energy Technology

Dated: November 15, 2013

Supervisor(s): ______________________

Dr.Ir. Marjan Popov

Reader(s): ______________________

Prof.Dr.Ir. Miro Zeman

____

Dr.Ir. Armando Rodrigo Mor

Abstract

Solar energy is expected to play a great role in the grid's future infrastructure as a distributed source, due to the fact that it is an easily available renewable source of energy. The expected high penetration of Photovoltaic (PV) power into the existing electricity grid demands a more detailed study and analysis of the interaction between PV systems and the grid, to enable safe and reliable operation. Until recently, in the case that an electromagnetic transient software package was used for a PV system study, a PV generator model had to be developed by simulating a complex block-circuit. Therefore, the simulation of a less complex PV generator model implemented in an electromagnetic transient program would be of great significance.

In this project, a simplified electrical model of PV generator, simulated in Electromagnetic Transients Program (EMTP), is proposed. The equivalent circuit of the generator is based on a linearisation process using the Newton-Raphson algorithm, in order to uncouple its current and voltage quantities. This scheme has been developed explicitly for association with electromagnetic transient packages for power system studies. The simplified model is represented by a dependent current source in parallel with a variable conductance.

The association of the proposed model with RLC circuits is simulated and the results are compared with measurement results. The systems show good transient response and settle to the steady state quite fast, so the model can successfully predict the nonlinear performance of a PV generator. An optimisation scheme is also proposed, in order for the PV generator to follow the changes of atmospheric conditions. When solar irradiance and temperature change the generator shows good response and reproduces already validated values.

The model is also combined with a single-phase grid-connected system, of which all the components are developed in EMTP. The evaluation and modelling of the PV system is performed with data from real PV modules. Results of the modelling and PV characteristics are described, showing good agreement with initial nonlinear models. An important remark is that the harmonic content of injected current into the grid is found significantly high, due to the assumptions made in this project and the limitations of the system. For the system's improvement a Maximum Power Point Tracking (MPPT) algorithm is developed and integrated, based on the concept of appropriately firing the inverter's switches. The algorithm corresponds successfully to variable initial conditions and the system response is validated by numerical calculations.

For the three-phase grid-connected case, an already established hybrid PV/battery model, simulated in MATLAB/Simulink, is used. The circuit parameters of the PV generator model are estimated from data of the output characteristic of the EMTP-based model, extracted in Excel and inserted in the Simulink model in terms of a system function. Case studies simulated prove the expandability of the proposed PV generator model in three-phase systems and the adaptation potential in large-scale systems.

Keywords
electromagnetic transients, photovoltaic generators, photovoltaic generation systems, transients, nonlinear circuits, hybrid systems, distributed generation

Table of Contents

List of Figures

List of Tables

Acknowledgements

First of all, I would like to express my profound gratitude and deep regards to my supervisor Dr.Ir. M. Popov for his guidance, monitoring and constant encouragement throughout the making of this thesis. Furthermore, I would like to thank Dr. A. Theocharis for his supervision and constant counsel during the first period of this project. I also take this opportunity to express a deep sense of gratitude to Prof.Dr.Ir M. Zeman and Dr.Ir. A. Rodrigo Mor, who graciously agreed to serve on my committee.

Special thanks also go to all my friends I met during these two years. I thank you for your friendship and patience. Although, I cannot mention you all, do know that everyone had an impact on my life for which I am thankful.

Last but not least, I would like to thank my parents for their endless support and for allowing me to realize my own potential. You were always there for me, ready to sacrifice a lot, especially during these hard times, so I could gain this amazing experience.

As closing remark, I would like to thank Nick for the endless courage and support he gave me when I needed it. Thank you for the smile on my face every time I see you.

Delft, University of Technology — Paraskevi Breza
November 15, 2013

“What you get by achieving your goals is not as important as what you become by achieving your goals.”

— *Henry David Thoreau*

Chapter 1

Introduction

Since global warming and environmental pollution are nowadays two of the main worldwide concerns, renewable energy can play a significant role on the reduction of environmental problems and delay of fossil fuel depletion [1]. The world is running out of non-renewable energy resources, consequently the need of using green energy sources gains more importance. Wind energy, solar energy and biomass are considered to be the most popular renewable energy sources. Research and development, focused on each of these areas, is being carried out globally, with solar energy playing a leading role given the fact that is one of the cleanest and least expensive sources of energy [1].

Even though a few years ago the penetration of solar energy into the electricity market was negligible, recent statistics show a significant change in this tendency. According to the European Photovoltaic Industry Association (EPIA), the Photovoltaic (PV) market in 66 sunbelt countries potentially could have 250GW installed PV capacity by 2020 and 1.1TW capacity by 2030 [1]. The PV industry is experiencing rapid growth and solar energy is highly promoted. Conforming with the technical report [1], there was an increase of 74% in PV plants installation in 2011, while in 2012 more than 100GW of PV systems were installed internationally. Europe is the leader in terms of cumulative capacity, with more than 70GW as of 2012, with China also being a strong player in the solar energy sector, followed by the USA and Japan. Europe's market has developed rapidly over the past decade, driven mostly by the "evolution" of PV installations in Italy and Germany [2]. Worldwide PV system installations between 2000 and 2012 are shown in Figure 1-1.

PV market reports published by various organizations, show that the installation of large scale grid-connected PV plants is currently the major trend. While more people are getting acquainted with solar energy, an increase of small scale installations is expected as well. Such a raise can result in high penetration of large amount of PV energy into the electricity grid. Europe accounts for the predominant share of the global PV market in this case as well, even though 17.2GW of PV capacity was connected to the grid in Europe in 2012, compared to 22.4GW in 2011. Germany was the top market in 2012, with 7.6GW of newly connected systems, followed by China with an estimated 5GW and Italy with 3.4GW. According to the technical report [2], PV was the main new source of electricity generation installed in

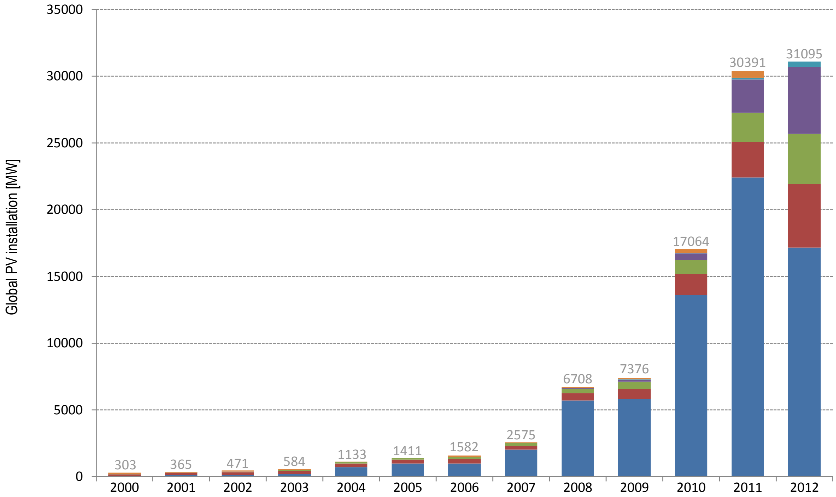

	2000	2001	2002	2003	2004	2005	2006	2007	2008	2009	2010	2011	2012
ROW	88	56	80	77	29	10	105	42	76	80	284	508	*
MEA	n/a	n/a	n/a	n/a	1	n/a	n/a	1	1	22	46	121	410
China	19	5	19	10	10	8	10	20	40	160	500	2500	5000
Americas	24	32	47	66	104	106	150	213	346	543	1029	2179	3758
APAC	117	140	191	230	282	303	324	271	535	742	1583	2672	4769
Europe	56	133	135	202	707	984	992	2028	5710	5830	13622	22411	17159
Total	303	365	471	584	1133	1411	1582	2527	6708	7376	17064	30391	31095

Figure 1-1: Evolution of global PV annual installation 2000-2012 (MW) (ROW: Rest of the World, MEA: Middle East and Africa, APAC: Asia Pacific) [2]

Europe. Figure 1-2 shows the increase of grid-connected PV systems in Europe until 2011, while a small reduction in 2012 is obvious, mainly as a consequence of the financial crisis. On the other hand, in Europe the grid-connected capacity is extremely high compared to the off-grid PV capacity, which accounts for less than 1% of the installed capacity. Nevertheless, in other countries, such as the USA, Australia and Korea the off-grid capacities installed every year account for many megawatts and thus are considered to play a significant role in the penetration of solar energy into the total energy market [2].

In conclusion, PV systems can currently provide approximately 2.6% of the electricity demand in Europe, up from 2% at the end of 2011. A clear overview can be drawn from Figure 1-3. PV systems can actually produce 5.2% of the peak electricity demand in the European Union (EU) 27, a result achieved in just a few years, proving how the development of PV energy in Europe is occurring at a rate faster than expected [2]. On the other hand, even though by the end of 2011 the contribution of PV towards the global electricity demand was 0.5% and only 1% towards the peak power demand, the future looks quite promising [3]. With the PV cell manufacturing costs decreasing every year, the use of solar energy is becoming more appealing. With organised support schemes by governing bodies along with better R&D, this renewable energy source can become a fair player in the world energy market [2].

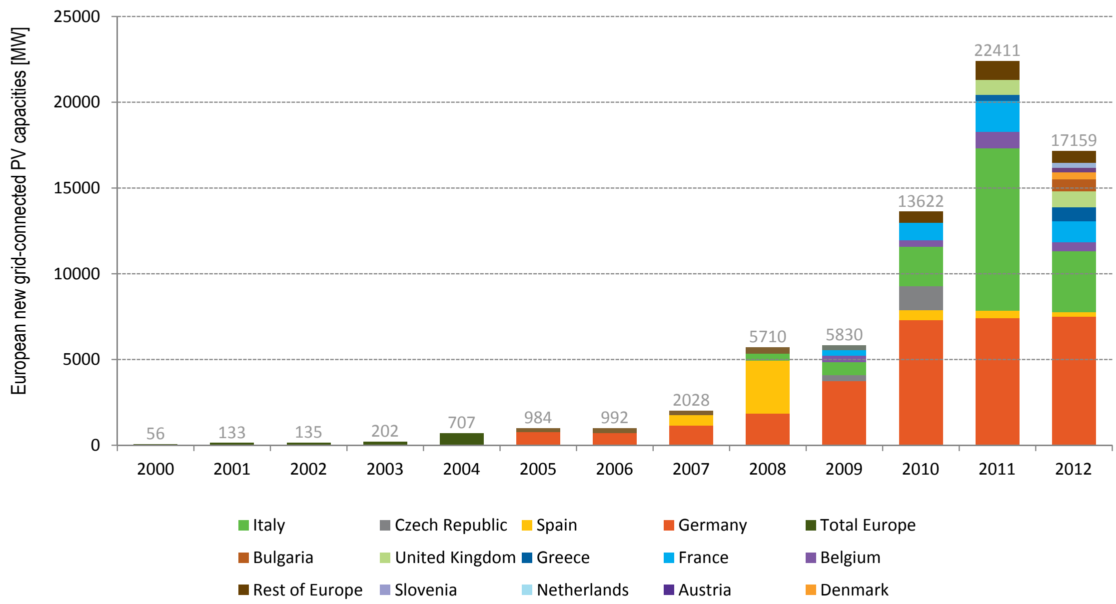

Figure 1-2: Evolution of new grid-connected PV systems in Europe (MW) [2]

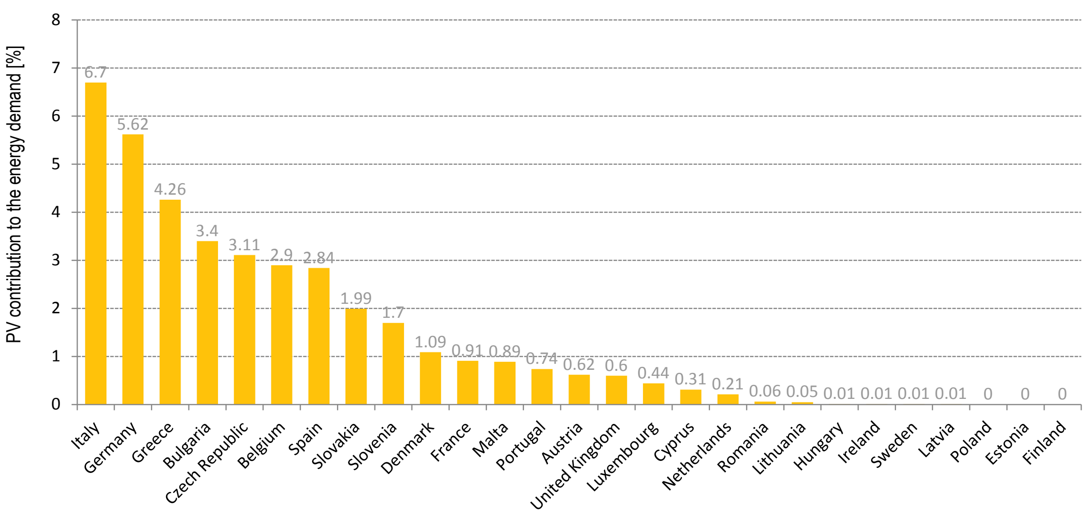

Figure 1-3: PV contribution to the energy demand in the EU 27 in 2012 based on cumulative installed capacity [2]

1-1 Project objective

The expected high penetration of PV power into the existing electricity grid demands a more detailed study and analysis of the interaction between PV systems and the grid, to enable safe and reliable operation. Concerning performance studies on PV systems, two ways are mainly used; measurements on operating installations and digital simulations. Generally digital simulations, while compared to measurements, are considered faster, low cost and appropriate for sensitivity analysis on different design parameters [4]. For the digital simulation studies, the interest is focused not only on the improvement of the models of the individual components of the PV systems, but also on the control side of the PV systems, in order to enable its operation in high efficiency and under maximum power conditions [4]. Digital simulations are executed either by using differential equations or electromagnetic transient software programs, based on nodal analysis on equivalent resistive circuits, such as EMTP, ATP, SPICE etc.

Although many nonlinear equations have been successfully used to describe PV generators, representing in that way their behaviour, they cannot directly be used with models based on differential equations or with electromagnetic transient software packages. When the PV system modelling is based on differential equations the most common problems that occur are [4]:

- an iterative procedure for the solution of the non-linear equation of the PV generator should be used, so that the operational point on the plane is designated;
- the PV system limitations, regarding its description by using differential equations, lead to restrictions to employ methods of circuit analysis;
- advanced algorithms should be used in order to avoid numerical instability problems.

It is clear that the aforementioned limitations have an impact on the derivations of the system equations, increasing the computational load at the same time. In order to overcome these problems, a linearised equivalent circuit for the representation of the PV generator, based on differential equations in standard form, has been developed and shown in Theocharis et al.[4].

In the case that an electromagnetic transient program is used for a PV system study, a PV generator model has to be developed by simulating a block-circuit using various elements and control demands. This task is quite complex, since there is no incorporated element suitable for the representation of a PV generator and all components included in the study have to be described with regard to linear and algebraic node equations [4]. Therefore, the simulation of a simple PV generator model implemented in an electromagnetic transient program would be of great significance.

Aiming to discuss and analyse some of the above discussed issues, such as the analytical implementation of the linearised equivalent electrical circuit of a PV generator proposed in Theocharis et al.[4], simulations in the electromagnetic transient software EMTP/ATPDraw are performed. The developed model is then used for utility grid-connection studies. Consequently, a PV system analysis is implemented. In case of a single-phase system, the analysis covers the modelling of the PV generator, the inverter controller design, that can also be termed as the AC side of the PV system, and the execution of the Maximum Power Point

Tracking (MPPT) algorithm which ensures maximum system's output power. In the three-phase case, a hybrid PV/battery system, presented in a previous graduation project and built in MATLAB/Simulink, is used combined with the EMTP-based model of the PV generator. The analysis then covers issues such as the DC side design of a PV system and the inverter controller design, which includes many other control mechanisms such as DC voltage regulation, active power control, etc.

1-2 Project contribution

The technical and scientific contribution of this thesis project has been formulated as follows:

- ✓ Modelling of a PV generator using EMTP/ATPDraw as the simulation tool, also suitable for implementation in other electromagnetic transient programs.
- ✓ Analysis of detailed PV system's elements design in EMTP, simplified with the proposed schemes.
- ✓ Development of comprehensive EMTP-based PV system models suitable for utility grid-connection studies.
- ✓ Combination of the EMTP-based PV generator model, with established Simulink grid-connected model.

1-3 Project outline

The thesis consists of seven chapters. Chapters 1 to 3 review the literature, to obtain the knowledge of solar energy and the state of art of individual components required for the proposed PV generator and PV system interfaces. Chapters 4 to 6 present the design, implementation and results of the proposed systems. Finally, the conclusions are presented in the last chapter.

Chapter 2 presents the theory behind the photovoltaic solar energy and provides information, such as the basics of a PV cell, to facilitate the understanding of the project. Widely used electrical models of PV cells are also presented.

Chapter 3 includes a review of PV systems. The definition and configuration of typical PV systems are presented. The principles of operation of PV converter topologies and a review of maximum power point tracking methods are discussed briefly at the end of the chapter.

The development of the proposed simulation model of a PV generator is presented in **Chapter 4**. Specifically, a well-behaved simulation model of a PV generator with known limitations is developed using EMTP/ATPDraw software package. Different applications and their results are discussed for validation of the proposed PV model, along with a proposed optimisation scheme.

A single-phase grid-connected PV system is also designed, simulated and analysed. **Chapter 5** presents the design and implementation of all the system's elements. Furthermore, the maximum power point algorithm and the behaviour of the converter used are discussed in particularly. Simulation results are analysed for different case studies and a comparative analysis with experimental results is presented.

A validation analysis of the proposed PV generator model is performed by testing it as a part of an established three-phase grid-connected model and presented in **Chapter 6**. Moreover, the proposed PV system's behaviour and outputs under load power and solar irradiance variations are discussed.

Chapter 7 provides an overview of the work performed in this project. It narrows down the discussion to the main findings and finally potential future work and recommendations for researchers are presented.

Chapter 2

Theory behind photovoltaic solar energy

The Sun is one of the most significant sources of renewable energy. In one hour the Earth receives enough energy from the Sun to meet its needs for nearly a year. A Photovoltaic (PV) cell is a semiconductor device that directly converts the energy of solar radiation into electric energy. In general, an element that converts sunlight into electricity is called a PV device. The fundamental PV device is the PV cell, while a set of connected cells form a panel or module. As an array either a module or a set of modules can be considered [5].

The purpose of this chapter is to provide an introduction into the photovoltaic solar energy and to present a brief introduction to the behaviour and functioning of the PV devices, without the intention of providing in-depth analysis of the PV phenomenon and the semiconductor physics.

2-1 Solar energy conversion

Photovoltaic (PV) energy conversion is often described as the direct conversion of solar radiation into electricity, by means of the photovoltaic effect. Generally, the term photovoltaic effect refers to the generation of a potential difference at the junction of two different materials in response to visible or other radiation. Thus, the broad study area of solar energy conversion into electric energy is denoted as photovoltaics [5].

2-1-1 Solar radiation

As explained above, the basic process of solar cell operation is the generation of the electron-hole pairs as a result of the absorption of visible or other electromagnetic radiation by a semiconductor material [5]. The Sun is a light source with a radiation spectrum that can be compared to the spectrum of a black body at a temperature of nearly 6000K. A black body

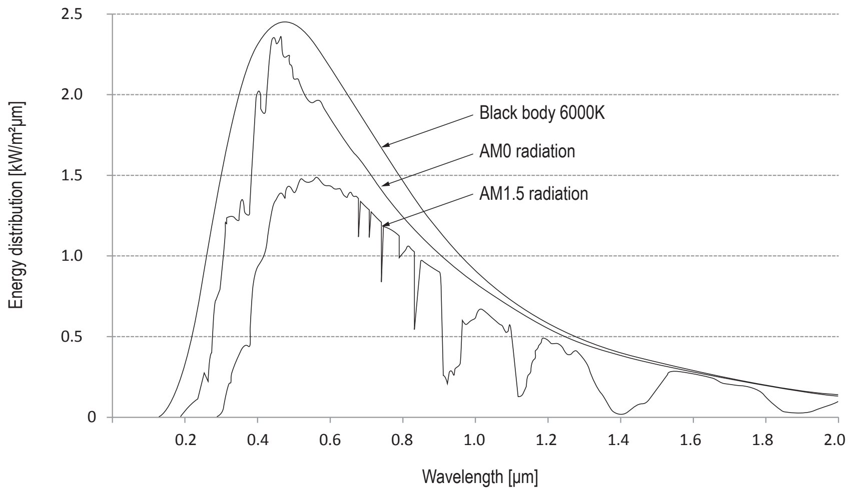

Figure 2-1: Spectral distribution of the black body radiation and the Sun radiation in the extraterrestrial space (AM0) and on Earth's surface (AM1.5) [6]

absorbs and emits electromagnetic radiation in all wavelengths and its theoretical distribution of wavelengths can be described by Planck's law. In Figure 2-1 the spectral distribution of the black body radiation compared to the extraterrestrial and terrestrial solar radiations is shown.

The spectrum of the sunlight on the surface of the Earth is influenced by different factors, like the variation of temperature on the solar disc and the influence of the atmosphere, making the study of the effect of the solar radiation on PV devices quite complicated. At an average distance between the Earth and the Sun, the irradiance, the flux of solar radiation incident on the surface outside of the atmosphere is about 1.373kW/m^2, while on the Earth's surface is in the order of 1kW/m^2 [7]. According to the American Society for Testing and Materials (ASTM) there are two standard terrestrial spectral distributions; the direct normal and the global AM1.5. The perpendicular radiation that reaches the sun-facing surface directly from the Sun corresponds to the direct-normal standard condition, where the global standard coincides with the spectrum of the direct and diffuse radiations. The atmospheric haze and the reflection on the Earth's surface are the factors forcing radiation to diffuse. The AM1.5 standards are defined for a PV device with a surface 37^o tilted, while facing the Sun [8].

The AM represents the air mass, more specifically the mass of air between a surface and the Sun, that influences the spectral distribution and intensity of the sunlight. The AM_x number represents the length of the path of the solar radiation through the atmosphere. Longer paths lead to more light deviation and absorption. The above phenomena have an impact on the spectral distribution of the light received by the PV device. The x coefficient of AM_x indicates the length of the path of the sunlight and is defined as:

$$x = \frac{1}{cos\theta_z} \tag{2-1}$$

where θ_z is the angle of the Sun with reference to the zenith [8], as can be seen in Figure 2-2.

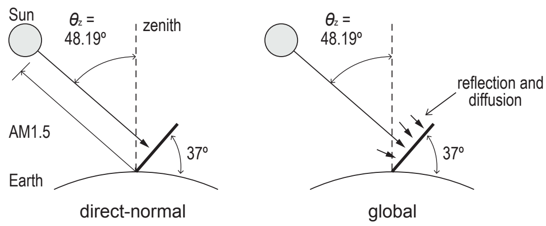

Figure 2-2: Illustration if the AM1.5 path and the direct-normal and global incident radiations on a sun-facing surface tilted 37^o [8]

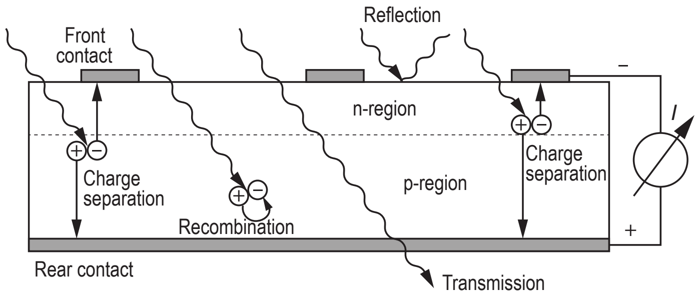

Figure 2-3: Processes in an irradiated solar cell [3]

The bigger the x the longer the path and the greater the air mass between the Sun and the surface of the PV device. The standard AM1.5 distributions correlates with the solar radiation with a solar angle θ_z= 48.190^o. In Figure 2-2 the definitions of the AM1.5 path and the direct-normal and global radiations can be seen.

Depending on the geographic position, time, day of the year, climate conditions, composition of the atmosphere, altitude, etc. the intensity and the spectral distribution of the solar radiation can change. As a result of all the aspects that can affect the solar radiation, the AM1.5 spectral distributions can only be considered as average estimations that can support the evaluation and comparison of different PV devices. In the PV industry the AM1.5 distribution serve as standard and PV modules' datasheets bring information about the characteristics and performance of PV devices with respect to the Standard Test Conditions (STC), which indicate an irradiance of 1000W/m^2 with an AM1.5 spectrum at 25^{o}C [8].

2-1-2 PV cell operation

A PV cell is a semiconductor p-n junction photodiode, that can generate electrical power when exposed to light [9]. There are several types of semiconductor materials used for PV cells production. The most common types known commercially are mono-crystalline, polycrystalline and amorphous silicon (Si) [9]. The principal operation of a PV cell is based on the phenomenon termed as the photovoltaic effect, depicted in Figure 2-3. This effect can be defined as a phenomenon in which an electron gets ejected from the conduction band, as a consequence of the absorption of sunlight of a certain wavelength by a material either metallic,

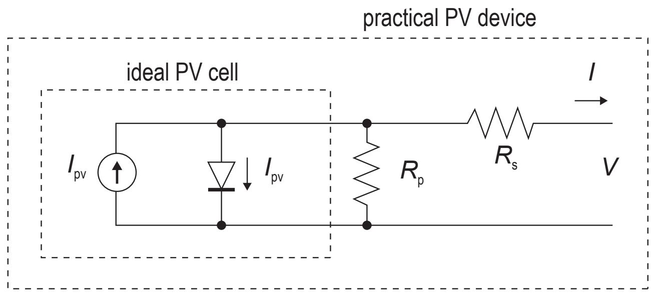

Figure 2-4: Single-diode model of ideal PV cell and equivalent circuit of practical PV device

non-metallic, solid, liquid or gas. Thus, when light strikes the surface of a PV cell a proportion of the solar energy is absorbed in the semiconductor material. In case the absorbed energy is greater that the bandgap energy of the semiconductor, the electron from the valence band jumps to the conduction band. Therefore, pairs of hole-electron are created in the illuminated region of the semiconductor. That way the electrons created in the conduction band are able to move freely. The free electrons have to move in a particular direction by the action of the electric field present in the PV cells. These flowing electrons compose a current, which can be drawn from external use by connecting a metal plate on top and bottom of the cells. Finally, current and voltage, created because of its built-in electric field, generate electric power [9]. The flux of incident light along with the capacity of absorption of the semiconductor affects mainly the rate of generation of electric carriers. The performance of the cell relies on various factors, such as the semiconductor bandgap, the reflectance of the cell surface , the intrinsic concentration of carriers of the semiconductor, the electronic mobility, the recombination rate and the temperature [8].

The study of the physics behind the PV cells is noticeably complicated and is out of the scope of this project. In order to study electronic converters for PV systems, it is sufficient to know the electric characteristics of the PV device. Manufacturers of PV devices provide either a set of empirical data that can be used to obtain the mathematical equation of the current-voltage (I-V) curve of the device or provide I-V curves retrieved experimentally for various operating conditions [8].

2-2 Modelling of PV devices

2-2-1 Ideal PV cell

To simplify the analysis of PV cells in electrical circuits, an electrical model of a PV cell is introduced. Figure 2-4 shows the equivalent circuit of an ideal PV cell [8]. It consists of a current source driven by sunlight and an ideal diode. The equation based on the theory of semiconductors that mathematically describes the I-V characteristics of an ideal PV cell is the following equation:

$$I = I_{pv,cell} - I_{0,cell}\left[exp\left(\frac{qV}{\alpha kT}\right) - 1\right] \tag{2-2}$$

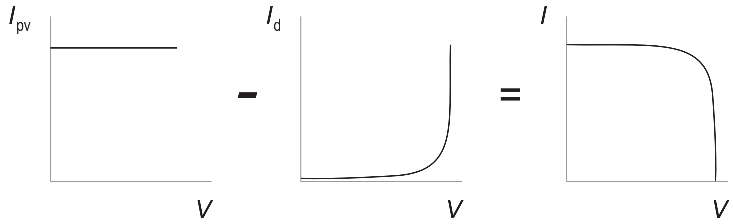

Figure 2-5: Characteristic I-V curve of a PV cell [8]

Where [8]:

- $I_{pv,cell}$ is the current generated by the incident light and is directly proportional to the solar irradiance $[A]$
- $I_{0,cell}$ is the leakage current of the diode $[A]$
- q is the electron charge (1.602x10^{-19} C)
- k is the Boltzmann constant (1.3806x10^{-23} J/K)
- T is the temperature of the p-n junction $[K]$
- α is the diode ideality constant.

The second part of the equation (2-2) is equal to the Shockley diode current I_d. In Figure 2-5 the I-V curve of a PV cell can be seen, where the net cell current is calculated as the sum of the light generated current I_{pv} and the diode current I_d, as the equation (2-2) shows.

2-2-2 Modelling of modules and arrays

Since a single PV cell is generating relatively small output voltage and a relatively high current, multiple cells are connected in series and enclosed in a common frame to form a photovoltaic panel or module. By connecting many cells in series, the voltage of the PV module is increased and the conduction losses in the cables are minimised. A PV module represents the basic building block for large scale PV power production. Multiple PV modules can be stacked in series forming strings of modules. As a result, the voltage increases. By connecting multiple strings in parallel, PV arrays are formed. For an array to perform well all the modules must not be shaded. Otherwise it will act as a load resulting in heat, which may damage the solar cell. Bypass diodes are used to avoid damage, however resulting in a cost increase. Integration of bypass diodes in some large modules during manufacturing is not uncommon and reduces the extra wiring required [8]. The typical power level of a PV string can range from a few hundred watts up to 5 kW. For PV arrays, power ratings can range from a few hundred watts up to hundreds megawatts in case of very large scale PV plants [4]. In Figure 2-6 the procedure of how PV cells are connected in modules and how modules can be connected in PV arrays is presented.

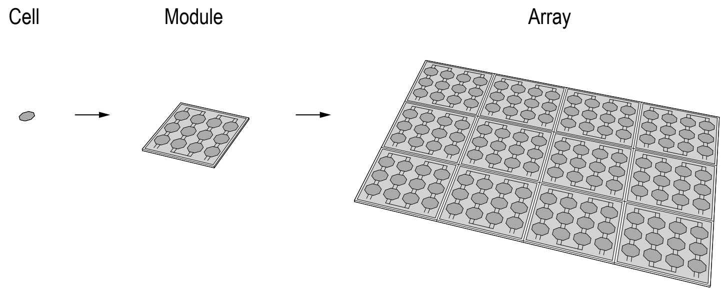

Figure 2-6: Construction of PV array

However, the basic equation of the ideal PV cell does not correspond to the I-V characteristic of a practical PV array. The observation of the characteristics at the terminal of the PV array requires also additional parameters shown in the equation (2-3) below:

$$I = I_{pv} - I_0 \left[exp\left(\frac{V + R_s I}{V_t \alpha}\right) - 1 \right] - \frac{V + R_s I}{R_p} \tag{2-3}$$

Where [8]:

- I_{pv} is the PV current $[A]$
- I_0 is the saturation current $[A]$
- V_t is the thermal voltage of the array $[V]$
- R_s is the equivalent series resistance of the array $[\Omega]$
- R_p is the equivalent parallel resistance of the array $[\Omega]$
- α is the diode ideality constant.

Equation (2-3) describes the single-diode model of a PV cell. However more accurate models have been proposed, such as the double exponential model with an extra diode, to represent the effect of the recombination carriers, or with three-diodes, to include the influence of effects that are not considered in the previous models [8]. However, the single-diode model is widely used in literature, since it offers a good compromise between simplicity and accuracy [9].

In the case that Np parallel connection of cells compose an array the saturation current is equal to $I_{pv} = I_{pv,cell} \cdot Np$ while respectively the saturation current is $I_0 = I_{0,cell} \cdot Np$.

From equation (2-3) the I-V and P-V curves of a practical PV device can be produced, as show in Figure 2-7. Some remarkable points of the curves should be highlighted; the short circuit point (0, I_{sc}) where the power is zero, the open circuit point (V_{oc},0) where the power is also zero, and the Maximum Power Point (MPP) (V_{mp}, I_{mp}), where the power is maximum [7]. Similarly to a single PV cell, the maximum power point exists also in case of an array of modules. The maximum power point is the operating point at which a PV panel or array of panels delivers maximum output power (P_{mp}) at a specific level of solar irradiance. In

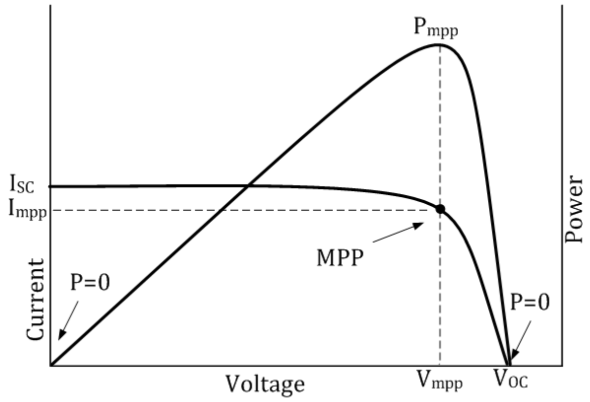

Figure 2-7: Characteristic I-V and P-V curves of practical PV device [5]

addition, the fill factor of a PV module or array describes how square the I-V curve is, and is defined as the ratio of two areas by the I-V curve, as illustrated in Figure 2-7 [7]. The fill factor accounts for the ideality of the PV module; any impairment that reduces the fill factor will reduce the output power. The fill factor is represented by the following equation [7]:

$$FF = \frac{P_{mp}}{V_{oc} \cdot I_{sc}} = \frac{V_{mp} \cdot I_{mp}}{V_{oc} \cdot I_{sc}} \tag{2-4}$$

It is quite common that PV modules' manufacturers provide only some data about thermal and electrical characteristics, instead of the I-V equation. So, the basic information found in datasheets are: the nominal open circuit voltage ($V_{oc,n}$), the nominal short circuit current ($I_{sc,n}$), the voltage at the MPP (V_{mp}), the current at the MPP (I_{mp}), the open circuit voltage/temperature coefficient (Kv), the short circuit current/temperature coefficient (KI) and the maximum experimental peak output power ($P_{max,e}$). This information is always provided with reference to STC of temperature and solar irradiance. Most of the time, manufacturers provide I-V curves for several irradiance and temperature conditions, which makes the adjustment of the mathematical I-V equation easier [8].

2-2-3 Factors affecting PV characteristic curves

The electrical characteristics of the PV cell represented by the current-voltage and the power-voltage curves, as presented in Figure 2-7, are totally dependent on the particular climatic conditions. Specifically, the I-V and P-V characteristics depend on the irradiance incident on the PV device and the environmental temperature. Figure 2-8 highlights the effect of different levels of irradiance on the characteristic curves of a PV panel. It is clear that the short circuit current I_{sc} is semi-linearly dependent on irradiance, while the change in the open circuit voltage V_{oc} is minor. Thus, the output power at the maximum power point P_{mpp} increases as the irradiance increases. More accurately, the power increases in a faster rate than the irradiance and can it be concluded that the efficiency is higher for high irradiance. Normally, the characteristics are given for STC, but in practice the irradiance on a PV device is lower, when light concentration is absent. So, the efficiency is usually lower than the rated value [7].

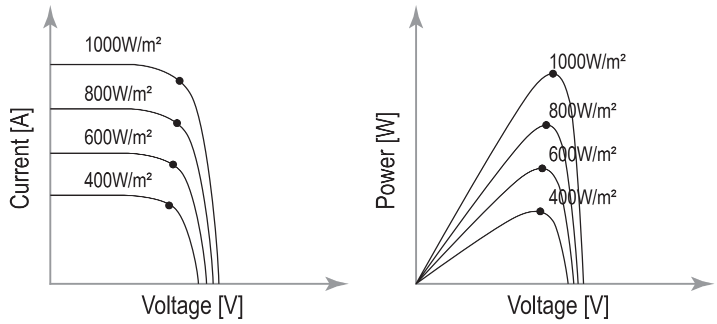

Figure 2-8: Irradiance effect on the PV characteristics [7]

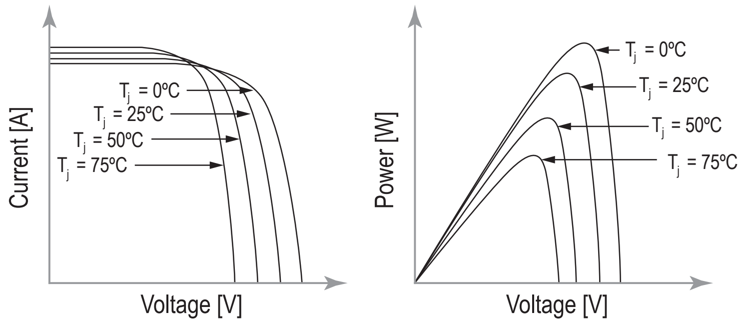

Figure 2-9: Temperature effect on the PV characteristics [7]

Temperature also has an effect on the PV characteristics. With an increase in the internal temperature Tj, the short circuit current I_{sc} marginally increases, as a result of exceptional light absorption. On the other hand, the open circuit voltage V_{oc} is affected strongly by the temperature and decreases significantly. In real life situations, under sunshine conditions, the internal temperatures are often higher than the one under STC, and consequently the efficiency of the PV device is lower [7]. The characteristics for different levels of temperature can be seen in Figure 2-9.

Chapter 3

PV Systems

Photovoltaic (PV) systems are composed of interconnected components designed to accomplish specific goals, ranging from powering a small device to feeding electricity into the main distribution grid. More specifically, PV devices convert sunlight into DC electricity. Such energy is transferred to the load or to the utility grid by means of a subsystem, that is generally known as the balance of the system BOS [10]. It involves all the components of a PV system, other than the PV devices, and includes the following [11]:

- supporting structures for mounting PV modules
- power conditioning units, that adjust and convert the produced DC power to AC power of required frequency and magnitude
- cables and protection devices, that allow a safe passage for current
- storage devices that store PV generated electricity, to be used when generation is not sufficient.

The structures are usually weather proof and are placed so that the modules' orientation ensures the highest energy production. As for most of the PV systems the main goal is to harvest all the available energy from the sun constantly, therefore power conditioning units are needed. The power conditioning units not only maximise the energy harvested but perform many other functions, like the conversion of DC to AC power or the provision of galvanic isolation between the PV field and the AC grid. In off-grid applications the power conditioning equipment is also responsible for managing the energy storage equipment. Due to solar energy's intermittent nature, storage systems are usually included into the BOS. They are mostly adopted in off-grid systems, whenever the extra energy produced by the PV array must be used during times there is power deficiency (such as during cloudy days or during night). Batteries are the most common devices used to store energy, although their environmental impact is an issue, since they use heavy metals and their lifetime is considerably shorter than that of the PV array [5].

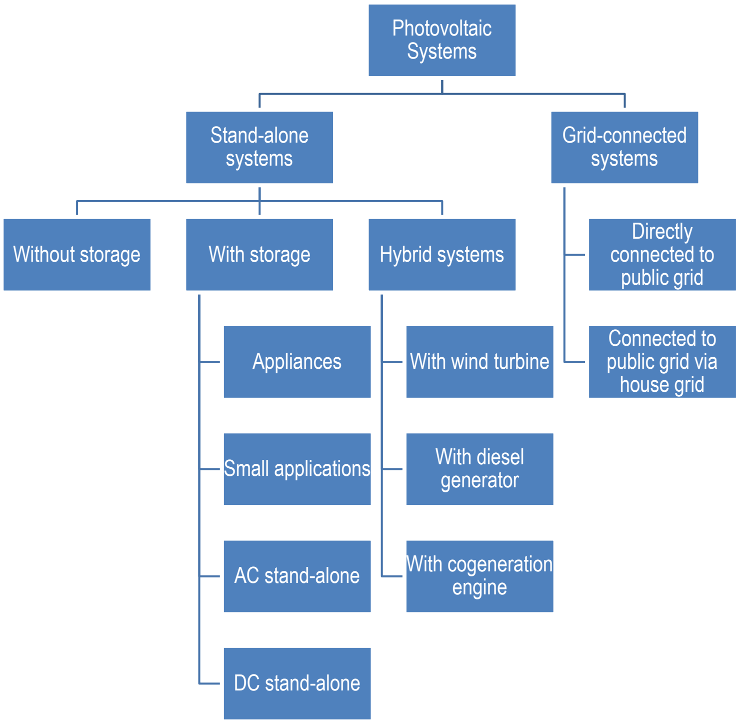

Figure 3-1: Classification of PV systems

3-1 Types of PV systems

Photovoltaic systems are classified according to the diagram in Figure 3-1. The two main classifications as depicted in the figure are the stand-alone and the grid-connected systems, however the hybrid systems are of significant value as well [12]. The main distinguishing factor between these two categories is that in stand-alone systems the solar energy output is matched with the load demand. When a PV system is interconnected with the utility grid, it might deliver excess PV energy to the grid or use the grid as a backup system, in case of insufficient PV generation. In these systems a suitable interfacing circuitry has to be incorporated, so that the PV system will be disconnected from the grid in case of a grid failure [13].

3-1-1 Stand-alone

Historically the first cost-effective applications of PVs were stand-alone systems in remote areas, where a connection with the utility grid was not feasible. An example of a stand-alone system can be seen in Figure 3-2. Even though stand-alone systems are mostly used in the cases of rural electrification, they can also be used in mobile equipment, communication and water pumping systems. Typically, a stand-alone system is comprised of the solar device, the power-conditioning and control units, the storage equipment and the load [12].

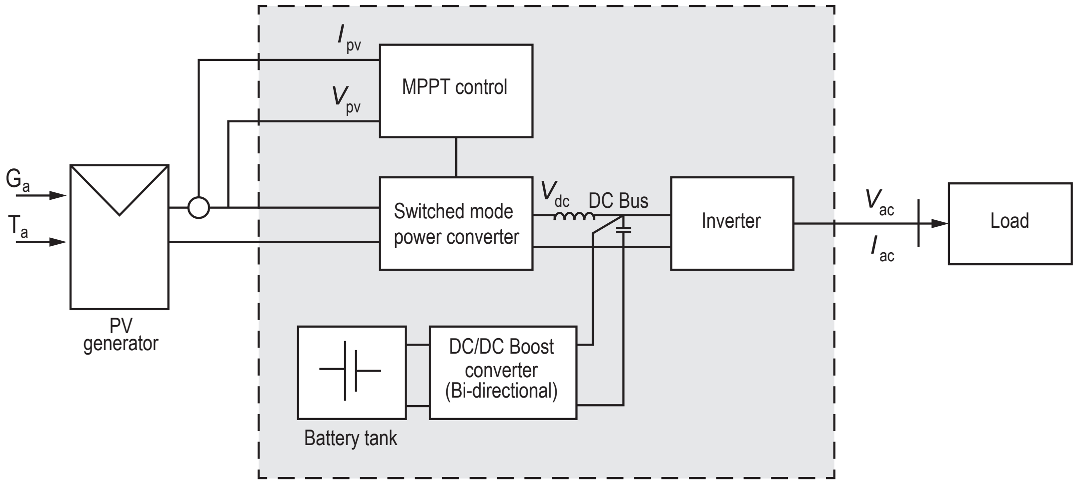

Figure 3-2: Stand-alone PV system

3-1-2 Hybrid systems

When the energy from PV devices can not be supplied in an economically and practically feasible way, other means are used. In many cases the PV system is used in combination with a diesel generator. In such a system the energy demands are ensured to be met, while fully utilising the PV supply [12]. A typical hybrid system can be seen in Figure 3-3.

3-1-3 Grid-connected systems

Grid-connected PV systems offer the opportunity to their users to be self-sufficient in terms of energy and sustainable in terms of protecting the environment. As mentioned in the introduction part of this report, the installation of grid-connected systems has increased considerably in the last years. A further increase is expected in the upcoming years, since more governments are introducing legislations to promote the use of renewable energy and PV systems' costs continue to go down. A great advantage of the grid-connected systems is that they offer the opportunity of generating significant amounts of energy near the consumption point, minimising that way the transmission and distribution losses. The operation of such systems is in parallel with existing electricity grids, so that the exchange of electricity from and to the grid is allowed [12]. As shown in Figure 3-1, grid-connected PV systems can be classified in decentralised and central grid-connected systems [7].

In decentralised PV systems, the energy storage can be committed, since the power provided by the solar radiation in the residencies can be injected into the utility grid in case of surplus. The central grid-connected PV systems, can be in a range up to MW and can be connected to a medium or a high voltage grid [7].

With the Institute of Electrical and Electronics Engineers (IEEE) adopting standard 929-2000 in 2000, most of the technical issues regarding the connection of a PV system to the utility

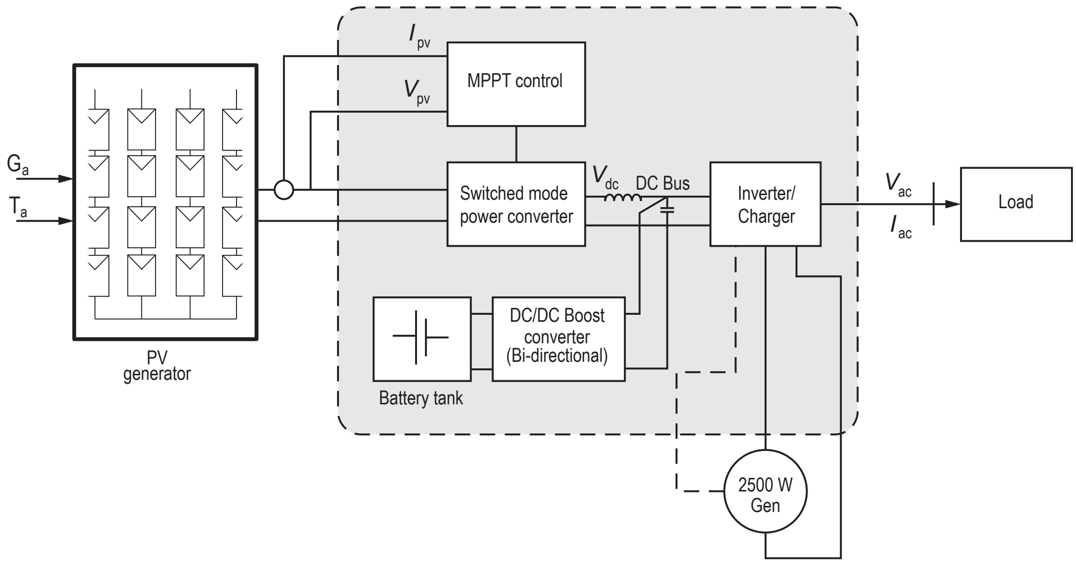

Figure 3-3: Hybrid PV system

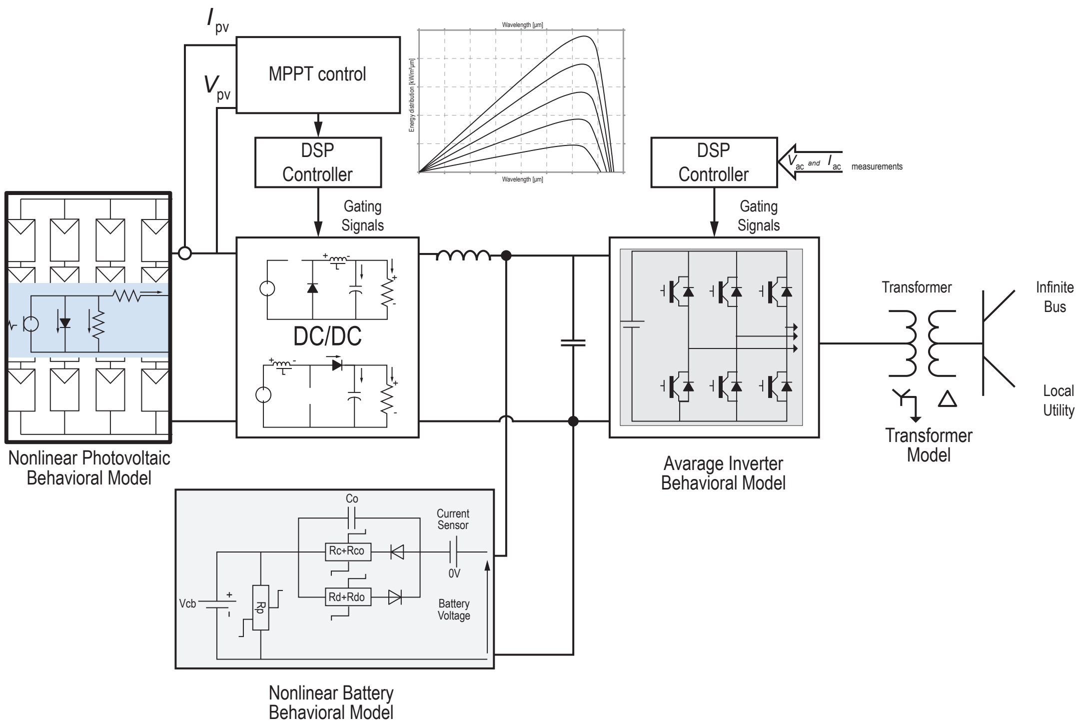

Figure 3-4: Grid-connected PV system

Table 3-1: Distortion limits as recommended in IEEE Std 519-1992 for six-pulse converters

Odd harmonics	Distortion limit
3^{rd}-9^{th}	<4%
11^{th}-15^{th}	<2%
17^{th}-21^{st}	<1.5%
23^{rd}-33^{rd}	<0.6%
above 33^{rd}	<0.3%

grid have been determined [12]. In this standard, the PV systems' integration is divided in two main categories; safety and power quality. In the IEEE Std 929 it is declared that the limits of the total harmonic distortion, caused by the PV system at the point of common coupling (PCC), must comply with Clause 10 of IEEE Std 519-1992 [14]. These limitations are shown in Table 3-1. Regarding safety, a main issue that has extensively been studied is the issue of islanding. Islanding refers to the condition in which a distributed generator continues to power a location, even though the power from the utility grid is no longer present [15]. In this case, the inverter is forced to automatically shut down, given that the source of power is disconnected from the network. Another issue that has to be taken into consideration is the Radio Frequency Suppression, that demands proper filtering and shielding [14].

3-2 Photovoltaic converters

A main technology linked to PV systems is the technology of power electronic converters. PV power has to be converted from DC to AC, in order to feed the power grid or AC loads in general [13]. An ideal PV converter should be able to supply the maximum power, drawn from the PV device, to the load side. For grid-connected systems, this has to be done with the minimum harmonic content in the current and at a power factor close to one. In case of stand-alone PV systems the output voltage must also be regulated to the desired value. In this section a short analysis of various topologies often associated with PV systems is presented. All the semiconductors switches used below are considered to be ideal [13].

3-2-1 DC/DC converters

In order for someone to be able to understand the switch-mode power conversion, the simple idea behind DC/DC power converters has to be explained first. There are three basic DC/DC topologies: buck, boost and buck/boost [13]. A simple PV system with a DC/DC converter is presented in Figure 3-5. DC/DC converters are supposed to control the voltage across the load, even in cases in which the input voltage varies [4].

Buck converter

The simplest version of a buck DC/DC converter is shown in Figure 3-6. During the on state of the switch, the input voltage is applied to the load. When the switch is off, the voltage

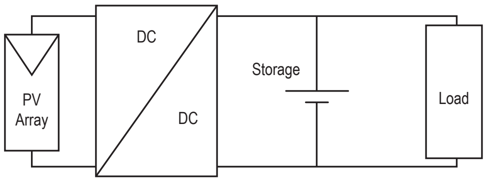

Figure 3-5: A basic PV system with DC/DC converter

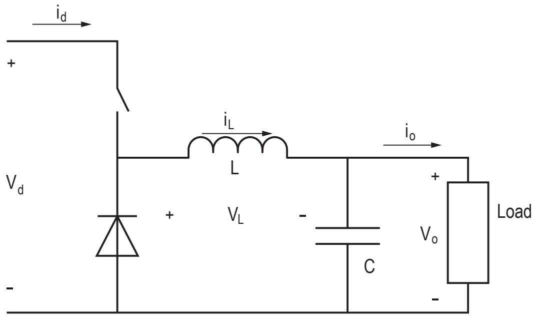

Figure 3-6: A buck converter

across the load is zero [16].

The average output voltage can be found from the unfiltered voltage as [16]:

$$V_0 = \frac{1}{T_s}\int_0^{T_s} v_o(t)dt = \frac{1}{T_s}(t_{on} \cdot V_d + t_{off} \cdot 0) = \frac{t_{on}}{T_s} \cdot V_d \tag{3-1}$$

In order to make the understanding more simple we will now define a new term, the duty cycle as:

$$\frac{t_{on}}{T_s} = D \tag{3-2}$$

and therefore

$$V_o = D \cdot V_d \tag{3-3}$$

In general this output voltage contains undesirable high harmonics, thus filtering is required [16].

Boost converter

This converter boosts the output DC voltage to a value higher than the input DC voltage. Applying the inductor volt-second balance we get [16]:

$$V_d \cdot t_{on} + (V_d - V_0) \cdot t_{off} = 0 \tag{3-4}$$

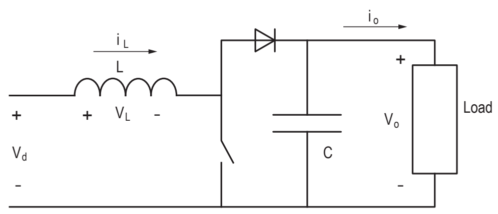

Figure 3-7: A boost converter

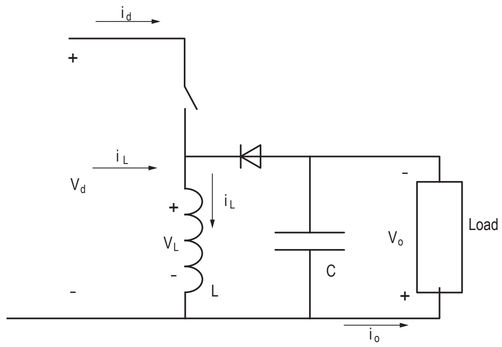

Figure 3-8: A buck-boost converter

Equation (3-4) can be solved in order to obtain the ratio for the input to output voltage [16]:

$$\frac{V_0}{V_d} = \frac{1}{1-D} \tag{3-5}$$

Equation (3-5) is valid in the continuous conduction mode, where the output current never goes to zero between switching cycles. The principle behind it is that energy stored in the inductor, during switch on operation, is later released against higher voltage V_0. That way the energy is transferred from lower to higher voltage [16].

Buck-boost converter

In a buck-boost converter the output voltage can be either higher or lower than the input voltage [16]. By using inductor volt second balance, we obtain:

$$V_d \cdot t_{on} + (-V_0) \cdot t_{off} = 0 \tag{3-6}$$

and

$$\frac{V_0}{V_d} = \frac{D}{1-D} \tag{3-7}$$

in the continuous conduction mode [16].

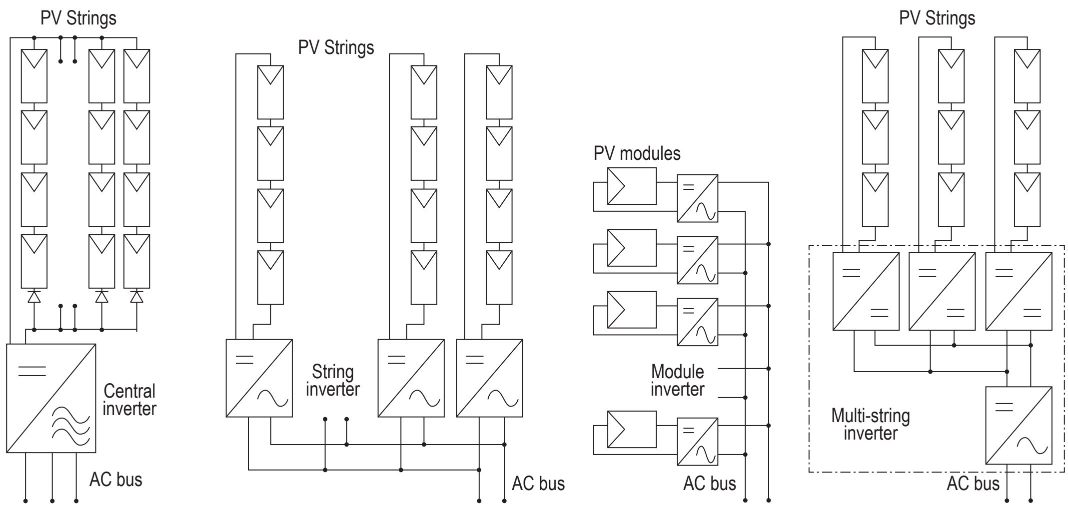

Figure 3-9: System architectures employed in PV systems [17]

3-2-2 DC/AC converters

System configurations

In this part a general overview of different system architectures, in block diagram form, will be presented. The system architecture regulates how PV modules are interconnected to the grid or AC loads via a power converter. Employment of these architectures in PV plants depends on different factors, such as the environment of the plant, scalability and costs [13]. In Figure 3-9 an overview of types of system architectures is given [13]. Each of these system configurations will be briefly explained in the following paragraphs, focusing on the main advantages and disadvantages.

Even though each of these systems has specific properties, there is a main line that all have to follow. Some of the general characteristics are [18]:

- designed for high efficiency
- capable of special safety features, such as islanding detection
- low harmonic limits of the line currents
- designed for high ambient power
- designed for over 20 years operation under extreme environmental conditions
- operate silently.

Central inverters

A system with central inverter is the most simple architecture employed in PV systems. The PV modules are connected in strings, hereby increasing the system's voltage, while strings are connected in parallel forming arrays of modules. The entire array is then connected to one central inverter which performs maximum power point tracking and power conversion, as can be seen in Figure 3-9. This configuration is mainly used in very large scale PV power production, with the central inverter often being DC to three phase [17]. Centralised configuration offers the lowest specific cost (cost per kWp of installed power). These configurations are employed in large scale PV power plants, as mentioned before, where high reliability is required. The easiest way to achieve that is by using a minimal number of components as in the central inverter [17].

Despite of their advantages, central inverters suffer from a significant number of drawbacks [17].

1. Due to the system's design, a large amount of power is transferred over noticeable distances using DC wiring. This can lead to safety issues, since faulty DC currents are difficult to interrupt.

2. The most significant disadvantage is the mismatch losses in the modules, due to the fact that all strings operate at single maximum power point. The overall system output can therefore be reduced in case mismatches exist between sections.

3. The configuration of this system is low in flexibility and expandability, since it is designed as a unit.

4. In order to prevent current circulation in the strings, diodes have to be put in series with each string causing extra power losses.

Module integrated or module oriented inverters

Unlike the central inverters, module integrated inverters, as shown in Figure 3-9, can operate directly on one or several PV modules. The power rating for these inverters is a couple hundred of watts and often require a two stage power conversion, due to the low voltage rating of the PV module. The first stage boosts the voltage to the required value, while the second stage inverts DC voltage to AC. In order to ensure full galvanic isolation, quite often a high frequency transformer is incorporated, enhancing system flexibility even further. These inverters are integrated with the PV panels, contributing to the great flexibility and expandability of the system. In this configuration the mismatch losses, due to mismatch in maximum power point between different PV modules, are minimised [13]. However all the aforementioned advantages come at certain costs. Inverters need to operate in harsh environmental conditions, which puts strains in the design and reliability of the system, increasing additionally the specific costs [4].

String inverters

String inverters combine the advantages of central and module integrated inverter concepts. PV modules connected in series forming a string, with power rating up to 5kWp can be connected to the utility grid by using a number of smaller inverters [13]. However in this topology the high DC voltage requires significant consideration. Due to the fact the string

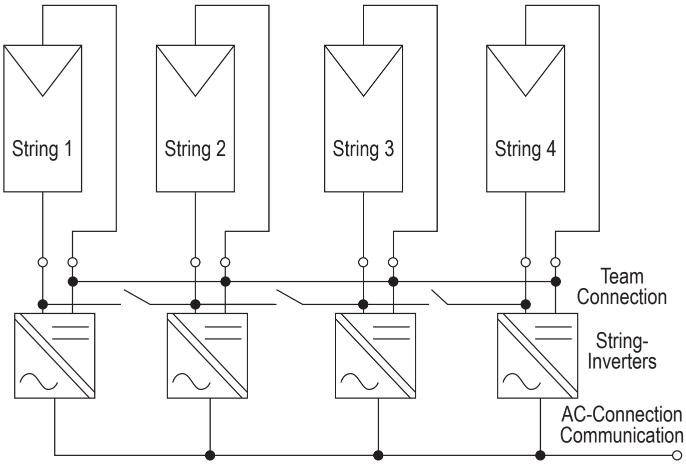

Figure 3-10: Team concept of inverters

inverters are commonly installed on dwellings or office buildings, the protection of the system requires special attention, especially the use of proper DC cabling [13]. Each string can operate at its MPP and there is no need of using series diodes, because strings are not connected in parallel. This fact reduces the losses, although there is always the risk of a hot-spot to occur, because of the unequal current and power sharing inside the string [13].

Multi string inverters

The multi string inverter concept, as shown in Figure 3-9, is combining the advantage of higher energy yield of a string inverter with the lower costs of a central inverter. Every individual string is connected to a lower power DC-DC converter, having independent MPP tracker optimising the energy output from each string. The system can easily be expanded, within a certain power range, by simply adding a new string with its DC/DC converter. Then all the DC/DC converters are connected via a DC bus through a central inverter to the utility grid. This central inverter is a Pulse Width Modulation (PWM) inverter, using the robust and relatively cheap IGBT technology [19].

Team concept

Of course many other concepts have been presented in the literature the past few years. However, the concepts explained above are the most common ones. One of the alternative configurations, is the team concept. In this concept the string technology is combined with the master-slave concept [20]. A combination of several string inverters working with the team concept is shown in Figure 3-10 [20]. At very low solar irradiance conditions, the whole PV array is connected to a single inverter. That way the overall losses are reduced. By increasing irradiance more inverters are connected, dividing the PV array into smaller units, until every string inverter operates close to its rated power. Every string operates separately with its

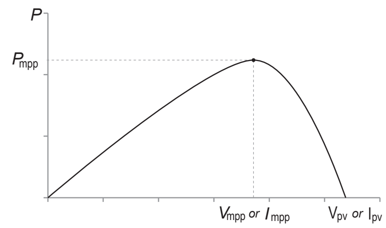

Figure 3-11: Power versus voltage (or current) at a PV module

own MPP controller. At low irradiance the inverters are being controlled, in the so-called master-slave way [20].

3-3 Maximum power point tracking (MPPT)

Another essential part of the PV system is tracking the maximum power point of a PV array. The maximum power point tracking (MPPT) control by definition allows the PV array, usually combined with a DC/DC converter, to produce the maximum continuous power, for specific meteorological conditions [7]. There are many methods used, that differ in complexity, the convergence speed, cost, popularity etc. The power output from a PV panel is related to the voltage (or current) at which power is drawn from. In Figure 3-11, the relationship between delivered power and current (or voltage), applicable for a single PV module with uniform irradiance throughout the module's surface, is shown.

The idea behind MPPT is to automatically find the maximum voltage V_{mp} or current I_{mp}, that the PV array has to operate in, in order to obtain the maximum power output P_{mpp}, under given temperature and irradiance conditions. The most difficult part in this operation happens under partial shading conditions, when is possible to have multiple maxima and it is more difficult to define the absolute maximum power point.

3-3-1 MPPT techniques

There are many different techniques proposed for maximum power point tracking. In the survey report as presented in Esram et al.[21], nineteen distinct methods are described. The most famous techniques are the perturb and observe method, the incremental conductance method, the fractional open-circuit voltage, the fractional short-circuit current, the ripple correlation control, the DC-link capacitor droop control, the load current or voltage maximisation and the dP/dV or dP/dI feedback control.

The MPPT technique used in this project, will be analytically explained in the following chapters.

Chapter 4

Modelling of a photovoltaic generator in EMTP

A photovoltaic (PV) generator is a nonlinear device having irradiance-dependent volt-ampere characteristics [22]. More specifically, a PV generator is a collection of interconnected solar cells and other components. The entire array is assumed to be treated as a system constituting N strings in parallel, having M cells connected in series per string, with all the cells being identical. Many electrical models of photovoltaic generators were developed to represent the nonlinear behaviour of the device, like the single-diode model presented in Chapter 2. In the following parts the electrical model of the PV generator, developed in this project, will be explained and will be followed by its digital simulation in Electromagnetic Transients Program (EMTP) and the results of different applications.

4-1 ENRC of a PV generator

In this part, the theory behind the method of modelling a PV generator as a linearised equivalent circuit model, appropriate for implementation in electromagnetic transient programs, is presented. The mathematical model is based on linearisation of the initial nonlinear $\mathrm{i}_{pv}(v_{pv})$ PV characteristic, using the fundamental Newton-Raphson algorithm (Appendix A). This uncoupling of the electrical quantities, in each timestep Δt of the digital simulation, can be represented by an equivalent linearised current source in parallel with a linearised ohmic conductance. This equivalent electrical circuit is called "Equivalent Newton-Raphson Circuit"(ENRC) [4]. The procedure obtaining the ENRC is based on an already published $i_{pv} - v_{pv}$ characteristic nonlinear equation shown in Lalouni et al.[23]. Therefore the development of a new characteristic is not necessary.

4-1-1 Existing PV generator model

A nonlinear model, called "Four-Parameter Model", has been extensively used in different software programs. This model uses four parameters under STC and can successfully predict the performance of mono and poly-crystalline PV arrays [23]. The equivalent circuit current of the generator i_{pv} based on that model, can be expressed as a function of the generator's voltage v_{pv}:

$$i_{pv} = I_{sc}\left\{1 - k_1[exp(k_2 v_{pv}^m) - 1]\right\} \tag{4-1}$$

where the coefficients k_1, k_2, k_3, k_4 and m are defined as:

$$k_1 = 0.01175 \tag{4-2}$$

$$k_2 = \frac{k_4}{V_{oc}^m} \tag{4-3}$$

$$k_3 = \ln\left[\frac{I_{sc}(1+k_1) - I_{mpp}}{k_1 I_{sc}}\right] \tag{4-4}$$

$$k_4 = \ln\left(\frac{1+k_1}{k_1}\right) \tag{4-5}$$

$$m = \frac{\ln(k_3/k_4)}{\ln(V_{mpp}/V_{oc})} \tag{4-6}$$

where V_{mpp} is the maximum power point voltage, V_{oc} is the open circuit voltage, I_{mpp} is the maximum power point current and I_{sc} is the short circuit current [23].

The i_{pv}-v_{pv} curve is affected by the variation of the solar irradiance and the temperature, as shown in the previous chapter. The adaptation for different levels of solar irradiance and temperature in this case, can be done by using the curve that corresponds to equation (4-1) as a reference curve. The new characteristic curve $i_{pv,new}$-$v_{pv,new}$ then is represented by the following equations:

$$\Delta T_\alpha = T_\alpha - T_r \tag{4-7}$$

$$\Delta i_{pv} = \alpha_r\left(\frac{G}{G_r}\right)\Delta T_\alpha + \left(\frac{G}{G_r} - 1\right) I_{scr} \tag{4-8}$$

$$\Delta v_{pv} = -\beta_{oc}\Delta T_\alpha - r_s \Delta i_{pv} \tag{4-9}$$

where G corresponds to the solar irradiance, T_α to the temperature, G_r is the solar irradiance under reference conditions, α_r is the current temperature coefficient, β_{oc} is the voltage temperature coefficient, r_s is the series resistance and T_r is the temperature and I_{sc} is the short circuit current under reference conditions [23].

So, the new values of the PV generator's voltage and current are given by:

$$v_{pv,new} = v_{pv} + \Delta v_{pv} \tag{4-10}$$

$$i_{pv,new} = i_{pv} + \Delta i_{pv} \tag{4-11}$$

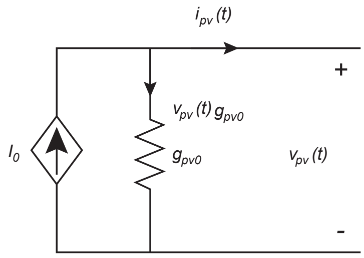

Figure 4-1: ENRC of a PV generator at the time instant t=$t_0+\Delta t$ [4]

4-1-2 Derivation of the ENRC of a PV generator

Using the model presented previously, we will see in this section in-depth the derivation of the ENRC of a PV generator as proposed in Theocharis et al.[4]. Assuming that at time t_0, the operation point of the PV generator is [$v_{pv}(t_0)$,$i_{pv}(t_0)$], in the next time instant t=$t_0+\Delta t$ the operation point becomes respectively [v_{pv}(t),i_{pv}(t)]. Δt is the timestep and depends on the time constant of the system, that the PV generator is a part of. The value of the timestep should be appropriate, so that the (4-1) can be linearised. By choosing an initial $i_{pv}(v_{pv})$ relation, expanding it in a Taylor series in the space [$v_{pv}(t_0)$,$i_{pv}(t_0)$], and by evaluating the expression at [t,v_{pv}(t),i_{pv}(t)], the following equation is derived, by keeping only the first two terms:

$$i_{pv}(t) = i_{pv}(t_0) + \left.\frac{di_{pv}}{dv_{pv}}\right|_{[i_{pv}(t_0),v_{pv}(t_0)]} [v_{pv}(t) - v_{pv}(t_0)] \tag{4-12}$$

From the $i_{pv}(v_{pv})$ characteristic curve it is clear that:

$$\left.\frac{di_{pv}}{dv_{pv}}\right|_{[i_{pv}(t_0),v_{pv}(t_0)]} < 0 \tag{4-13}$$

and the incremental conductance of the system at the point [t_0,$v_{pv}(t_0)$,$i_{pv}(t_0)$] can be defined as:

$$g_{pv0} = -\left.\frac{di_{pv}}{dv_{pv}}\right|_{[i_{pv}(t_0),v_{pv}(t_0)]} \tag{4-14}$$

By substituting equation (4-14) into (4-12) and by rearranging the terms we get the following equation:

$$i_{pv}(t) = I_0 - g_{pv0}v_{pv}(t_0) \tag{4-15}$$

where:

$$I_0 = i_{pv}(t_0) + g_{pv0}v_{pv}(t) \tag{4-16}$$

In conclusion, equation (4-15) gives the operation point of the PV generator at the time t=$t_0+\Delta t$, using values for the previous time instant, via I_0 and g_{pv0}. Finally, equation (4-15) can be represented by the equivalent circuit as can be seen in Figure 4-1. I_0, updated by using equation (4-16), is represented by a current source, since its value depends on the irradiance G, the absolute temperature T_α and the position of the operation point at the previous time instant t_0. That way the trajectory of the operation point of the PV generator, at any time instant, can be predicted using the tangent at the reference nonlinear curve at the time instant t_0, by suitably updating the parameters I_0 and g_{pv0} at each time interval Δt [4].

The parameter g_{pv0} is updated using a linear algebraic equation, which arises by the substitution of equation (4-14) in (4-1). So we can derive the derivative with respect to the voltage v_{pv} of the equation (4-1), evaluated at the point $[v_{pv}(t_0),i_{pv}(t_0)]$:

$$\left.\frac{di_{pv}}{dv_{pv}}\right|_{[i_{pv}(t_0),v_{pv}(t_0)]} = \left.\left[\frac{d}{dv_{pv}}(I_{sc}) - I_{sc}k_1\frac{d}{dv_{pv}}(e^{k_2 v_{pv}^m}) + \frac{d}{dv_{pv}}(I_{sc}k_1)\right]\right|_{[i_{pv}(t_0),v_{pv}(t_0)]} \tag{4-17}$$

Since in equation (4-17) the first and the last terms are zero, considering the equation (4-14), g_{pv0} is given by:

$$g_{pv0} = (I_{sc}k_1k_2m)\,[v_{pv}(t_0)]^{m-1}\,e^{k_2[v_{pv}(t_0)]^m} \tag{4-18}$$

In conclusion, the procedure for updating equation (4-18) is based on the calculated value of $v_{pv}(t_0)$, at the time instant t_0. The next step is to calculate $i_{pv}(t_0)$ from equation (4-1), so we can follow the tangent in the initial $i_{pv} - v_{pv}$ nonlinear curve. The explained method can be directly applied on various types of selected initial models, such as the double-diode model or other based on nonlinear exponential equations. This application will lead to the ENRC, presented in Figure 4-1, and then, based on the an initial $i_{pv} - v_{pv}$ nonlinear curve, the interrelated equation for the incremental conductance g_{pv0} will be obtained [4].

4-2 The EMTP-based PV generator model

4-2-1 EMPT/MODELS

The big increase of installed PV systems, either connected to the grid or as stand-alone systems, has also increased the power quality problems. For that reason detailed analysis of all the PV system's parameters is required. Tools have been developed to estimate the energy output characteristics of new systems and new models, based on parametric analysis, have been introduced for this purpose [24].

PV system analysis, including system and field condition analysis, can be performed with a transient phenomenon analysis software for electric power systems. As it has been mentioned in the introduction part of this report, in order for a PV system to be developed, either laboratory tests or digital simulation are required. Digital time domain simulation programs, such as Electromagnetic Transients Program (EMTP), have been a key part in the design and analysis of power apparatus and systems [24]. EMTP can be applied in practically every problem requiring time domain simulation and is mainly used through ATPDraw. The latter is a graphical preprocessor of the Alternative Transients Program (ATP) version of EMPT on the MS-Windows platform [25]. ATP has extensive modelling capabilities and additional important features besides the computation of transients. One of the integrated simulation modules, the recently introduced MODELS enables the control of the interaction between the power system and the protective system operations. MODELS is a simulation language, supported by a set of simulation tools for studying time-variant systems. The description of the model is self-documenting, so it can be used as the description document, used for representing the system and as the data used in the actual simulation. With MODELS, the monitoring and controllability parameters of the power system and algebraic operations for programming can be calculated. Using MODELS, the user can represent the power system by describing the physical constants and/or the physical subsystems of the systems to be examined [25].

In ATPDraw there is also a number of embedded models that can be directly used in a defined network. These models can be transformer models, machine models or various types of sources and switches etc. All these components can be sufficient for building a power system network and apply both steady-state and transient analysis. However, for some studies these embedded components are not enough, and user defined models should be applied. This can be done by using either Transient Analysis of Control Systems (TACS) or MODELS, interfaced to ATPDraw. TACS and MODELS can read a variable from a network in time domain and use it for the computation of another parameter, and can export parameters back to the network, such as controlled resistances, current, voltage, etc. [26].

In this section the technique of modelling the EMTP-based generator will be presented. All the procedures of the components of the PV system are in an EMTP formatted file.

4-2-2 Modelling of the photovoltaic generator

So far a DC source has been used instead of a PV generator in EMTP simulations since there is no such a component embedded in the program. Due to all the restrictions of using a PV model compatible with electromagnetic transient programs, explained in the introduction part, an introduction to a PV generator model, ideal for implementation in EMTP and based on the ENRC procedure, has been given in this project.

As we saw in Figure 4-1 the ENRC of the PV generator results in the representation of the generator by a dependent current source I_0 in parallel with a variable conductance g_{pv0}, where both are updated in each time interval Δt by using simple linear algebraic equations. For the computation of the different parameters and equations that lead to the ENRC some of the already embedded TACS will be used, while some new parameters imported in MODELS will be introduced.

The idea of setting up the ENRC concept in ATPDraw was based on Popov[26], where a nonlinear inductance has been modelled by means of a variable resistance type-91 in a parallel combination with a current controlled type-60 source, as presented in Figure 4-2. The concept behind this representation, is that in electromagnetic transients programs, the fundamental differential equations of inductors and capacitors are converted into algebraic form by using the trapezoidal rule. So by applying the trapezoidal rule in the equation that governs the behaviour of an inductor:

$$v(t) = L\frac{di(t)}{dt} \tag{4-19}$$

and by rearranging the terms, the current $i(t)$ becomes:

$$i(t) = G(t)\left(v(t) + v(t-\Delta t)\right) + i(t-\Delta t) \tag{4-20}$$

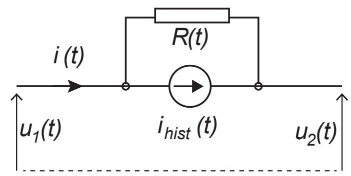

Figure 4-2: Equivalent scheme of a nonlinear inductance

or

$$i(t) = G(t)v(t) + i_{hist}(t) \tag{4-21}$$

where

$$i_{hist}(t) = G(t)v(t - \Delta t) + i(t - \Delta t) \tag{4-22}$$

$i_{hist}(t)$ is the history of the current and $G(t)$ is the variable conductance. The variable resistance type-91 is in this case:

$$R(t) = \frac{1}{G(t)} \tag{4-23}$$

So, in order to build the PV generator in this project, one of the default MODELS in ATPDraw will be used. In this new PV generator model the inputs should be the V_{oc}, I_{sc}, V_{mpp} and the I_{mpp}, in order to build the equations explained in the procedure of obtaining the ENRC. With the coefficient k_1 constant and the inputs known, the first step in the designing procedure is to calculate the coefficients k_2, k_3, k_4 and m. Our PV model will then start the iteration procedure of calculating all the parameters by a starting point t_0, in which we set an initial $v_{pv}(t_0)$ value. With all the above values calculated, the model developed will calculate g_{pv0} by using equation (4-18) and then from equation (4-15) the $i_{pv}(t_0)$ will also be calculated. In the following step the model will calculate I_0 by using equation (4-16). The new introduced MODEL will have as outputs the i_{hist} that will go to the current controlled type-60 source and the $G(t_0)$ conductance value. And then the generator is ready to proceed to time instant t.

4-3 Application and results

Since a PV generator constitutes a special power source, due to its transcendental current-voltage characteristic, the known performance of linear electrical circuits and systems energised by conventional sources has to be re-examined. So, in this section the PV generator is associated with equivalent RLC circuits.

4-3-1 Analysis of RLC circuits empowered by a PV generator

In general, the necessary background for studying the transient performance of complex electrical systems, is provided through studying circuits involving either one or two independent energy-storing elements. The same practice in the case of a photovoltaic system could be an

(a) Equivalent circuit of a PV//R//L circuit **(b)** Equivalent circuit of a PV//R//C circuit

Figure 4-3: Parallel R,L,C loads energised by the PV generator

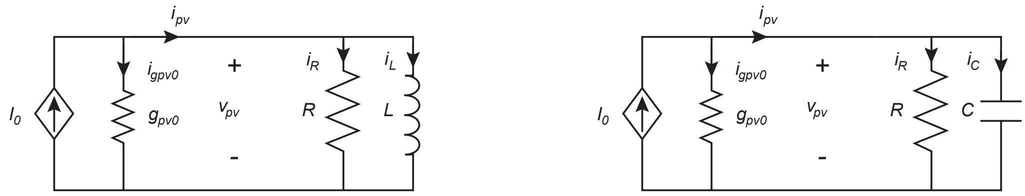

(a) PV//R//L circuit **(b)** PV//R//C circuit

Figure 4-4: Equivalent circuits where the PV generator is described by the ENRC

intriguing aspect for an engineer. So, the dynamic behaviour of first-order circuits (circuits that contain two types of passive elements, namely resistors and one capacitor C or just one inductor L, along with a network of DC sources and switches, characterised by first-order differential equations) powered by a PV generator can be the starting point towards that direction [27]. However, the transient behaviour of circuits involving R,L,C elements in different combinations, especially that of the linear second-order RLC circuits (where both a capacitor and a inductor are present simultaneously), can also be of particular interest for many reasons [27], and will be explained in the following sections.

The method to prove that the proposed PV generator model is functional in EMTP, is to combine it with equivalent electrical circuits involving R,L,C elements and provide a transient response analysis of these circuits. As it is known, in case a circuit contains one or more storage elements, the circuit response to a sudden change will go through a transition period prior to settling down to a steady state value [27]. Roughly speaking, the time varying current and voltage resulting from a sudden application of sources are called transients, while the steady state value is the magnitude of voltage or current, after the circuit has reached stability. It is this transition period that shows how fast the circuit responds to changes and is the significant part of a transient analysis. So, two first-order, parallel PV//R//L and PV//R//C, and a second-order, series-parallel PV-RLC, circuits will be examined. In addition, the predicted results from the simulations will be compared with results retrieved from measurements.

In Figure 4-3a and in Figure 4-3b the parallel PV//R//L and PV//R//C are shown respectively. These two circuits have the same resistive circuit. In Figure 4-4a and in Figure 4-4b the equivalent circuits can be seen, where the PV generator is represented by the ENRC.

Table 4-1 shows the PV panel's data under STC for a SIEMENS SM 110-24 module [28],

Table 4-1: Data for the PV//R//L and PV//R//C circuits simulation

	PV generator	PV//R//L	PV//R//C
STC	$P_{pv} = 110W$		
	$I_{mpp} = 3.15A$		
	$V = 35V$		
	$P_{mpp} = 110W$		
	$I_{sc} = 3.45A$		
	$V_{oc} = 43.5V$	$R = 22.59\Omega$	$R = 60.45\Omega$
	$\alpha_r = 1.4mA/^oC$	$L = 0.3H$	$C = 10^{-3}$F
	$b_{oc} = -152mV/^oC$	$\Delta t = 10^{-5}s$	$\Delta t = 10^{-5}s$
Measurement conditions	$G = 900W/m^2$		
	$T_\alpha = 35^oC$		

which is used for the simulations. The experimental characteristics were obtained by Lalouni et al.[23] and have been also used in the measurements' explanation part of Theocharis et al.[4]. For the experimental characteristics a prototype of the PV system, as described in Lalouni et al.[23], was designed and implemented at the university of Bejaia (Algeria).

In order to start the implementation in EMTP all the components of the aforementioned circuits have to be simulated in the ATPDraw interface. As explained before the new MODEL, representing the PV generator, will have as inputs the V_{oc}, I_{sc}, V_{mpp} and the I_{mpp}. In the component dialog box of the new model object, where the DATA and NODES attributes are shown, the values from Table 4-1 are inserted, as can be seen in Figure 4-5. On the *Library* page the link to the original file on disk is given and the *Reload* option becomes available. The input and outputs of the MODEL and its interface with the rest of the circuit are automatically managed by ATPDraw. The model descriptions are written directly in the ATP file [25].

Figure 4-6 shows a diagram of the PV//R//C circuit, which is similar to the diagram of the PV//R//L circuit. The PV generator is modelled using ATP/MODELS and TACS components, as explained previously. Each of the presented systems has to be energised by setting an initial voltage value $v_{pv}(t_0)$ for the time instant t_0, depending on the structure and on the values of the system's components. The transient response of the PV//R//C and PV//R//L circuits can be shown in Figure 4-8a and Figure 4-9a respectively. In Figure 4-8b and Figure 4-9b one can see the trajectories of the operation points from the time instant $t_A = 0s$ until the steady state on the $i_{pv} - v_{pv}$ plane. In both graphs the point A corresponds to the time instant $t_A = 0s$, while the point B corresponds to the steady state of the PV generator.

From the graphs it is obvious that an initially uncharged capacitor, for $t_A = 0s$ behaves as a short circuit and the system starts to operate at the point A, while for the steady state the capacitor behaves as an open circuit, so the operating point is B, as it is shown in Figure 4-8b. Additionally, Figure 4-8a points out several important things. The initial current through the PV//R//C circuit, in which the capacitor is originally uncharged, is at a maximum. It is not until charge begins to accumulate that the charge flow begins to diminish. The graphs also identify a particular point in time, which is of great importance, the time constant $\tau = RC$. This constant gives an indication of how rapidly the system responds to sudden changes and

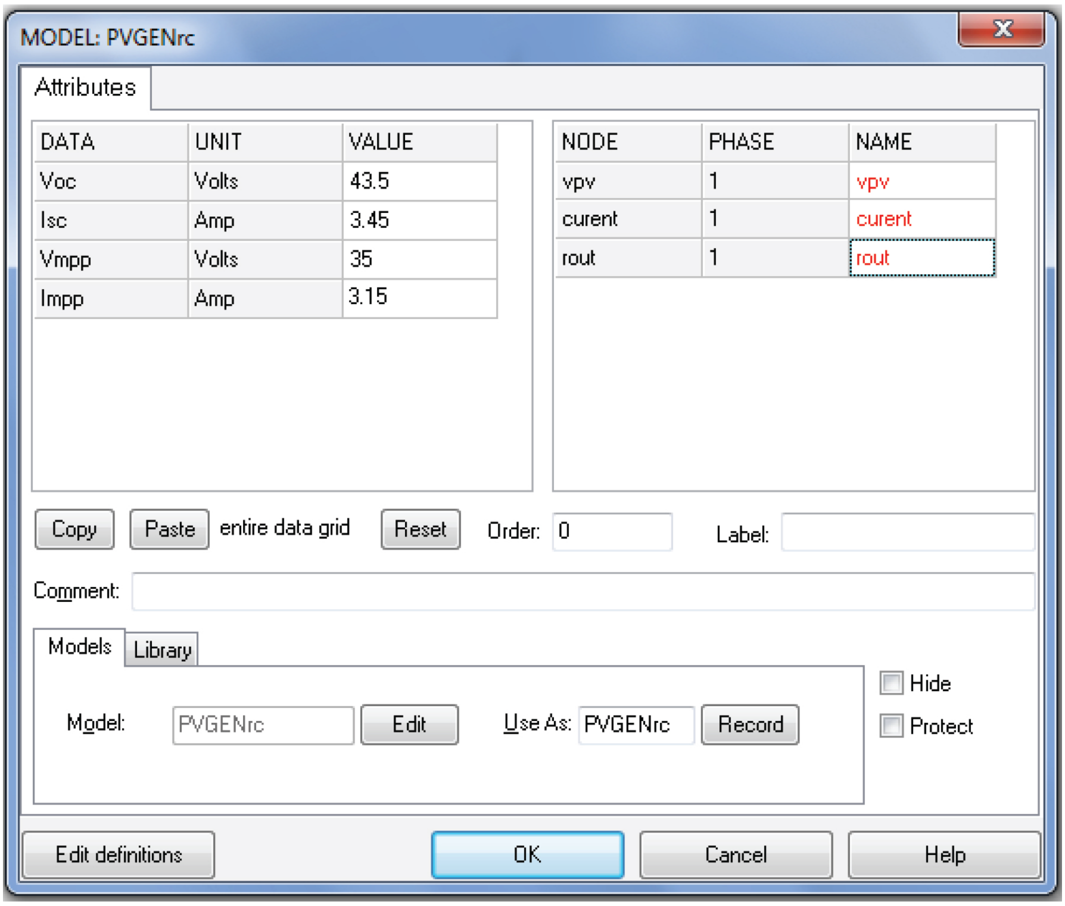

Figure 4-5: The component dialog box of MODEL object

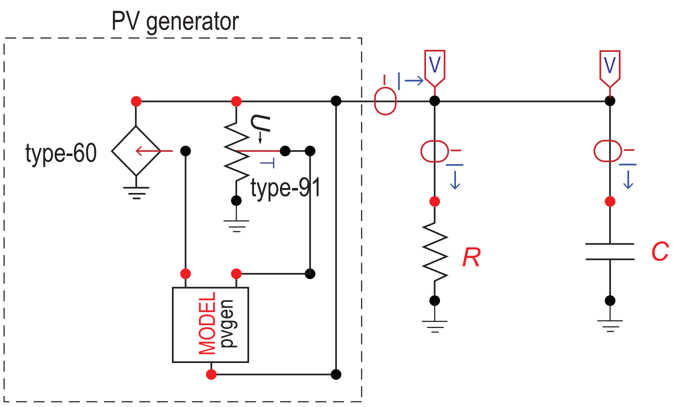

Figure 4-6: PV//R//C EMTP-based circuit

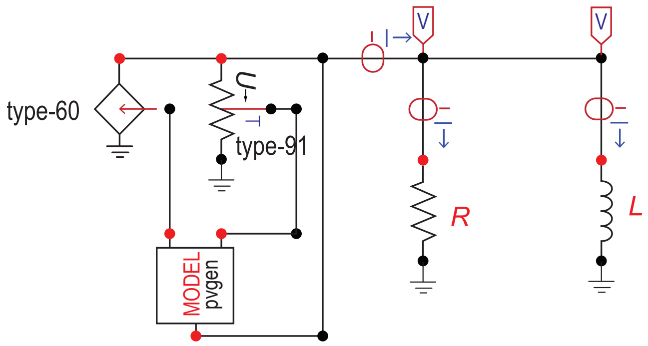

Figure 4-7: PV//R//L EMTP-based circuit

determines when it settles to its final values. In conclusion, it is clear that the response of the circuit has a transient which dies out eventually and after the response time, a period of time almost of $t = 0.025s$, the circuit reaches and remains on its the final steady state value.

Similarly, an initially uncharged inductor for $t_A = 0s$ behaves as an open circuit, while in steady state behaves as a short circuit. So, the dynamic route starts from the point A and terminates on the point B, as shown in Figure 4-9b. As for the transient response, it is clear that the i_{pv} current initially starts from a point that is defined by the values of V_{oc} and R, while the current at the inductor i_L, as the transient effect dies, it approaches the I_{sc} current. The time constant in this case is defined as $\tau = L/R$ and the response time is again about $t = 0.025s$, until the system settles at its steady state.

To conclude, the response of the system for first-order circuits is fixed by the time constant, which provides information about the speed of response of the system. The smaller the τ the more rapid the change, while on the other hand a system with a larger time constant provides a slow response, since it takes longer to reach the steady state. The most important point however is that in both cases the predicted values show perfect matching with the measurements, as presented in Lalouni et al.[23]. Apart from that, the simulated curves are also in perfect match with the predicted curves obtained by using the ENRC of the PV generator and the same R,L,C elements as presented in Theocharis et al.[4].

As a second step, in order to verify the EMTP-based model in a second-order case, a series-parallel PV-RLC circuit is used. The second-order circuits also exhibit a transient response, which is of great interest, since these types of circuits frequently take place in PV engineering. However, as these circuits are more complex, their response varies depending on the respective values of R,L,C. Furthermore, the study of such a circuit is really valuable, because the behaviour of many higher-order PV systems are often described in terms of an equivalent second-order circuit. The equivalent PV-RLC circuit shown in Figure 4-10a, can be transformed in the one shown in Figure 4-10b using the equivalent circuit of the ENRC of the PV generator as presented previously. Figure 4-11 shows the diagram of the test system in EMTP used in this project.

The PV module's data are the same as the ones presented in Table 4-1, since once more the SIEMENS SM 110-24 module was used for both the simulations and for retrieving the experimental data. The new data of the R,L,C elements of the series-parallel PV-RLC circuit

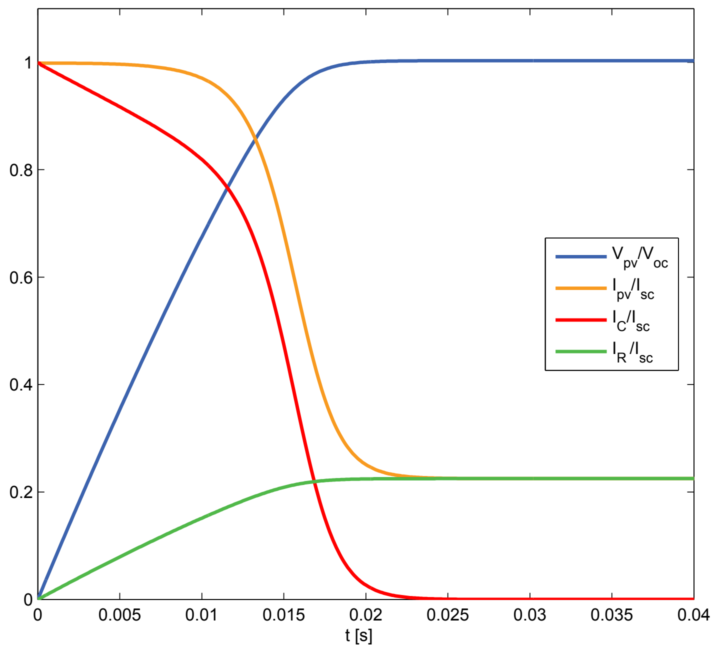

(a) Transient behaviour

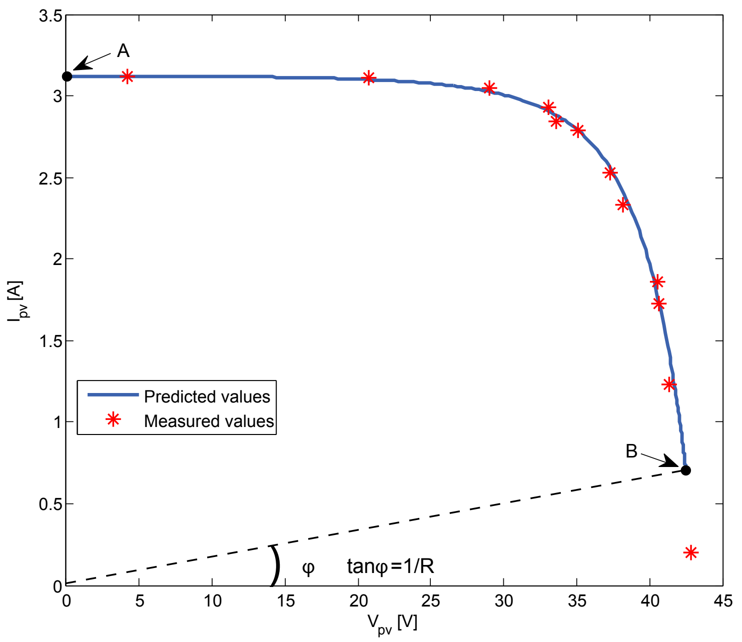

(b) $i_{pv} - v_{pv}$ trajectories

Figure 4-8: Transient response of the PV//R///C circuit

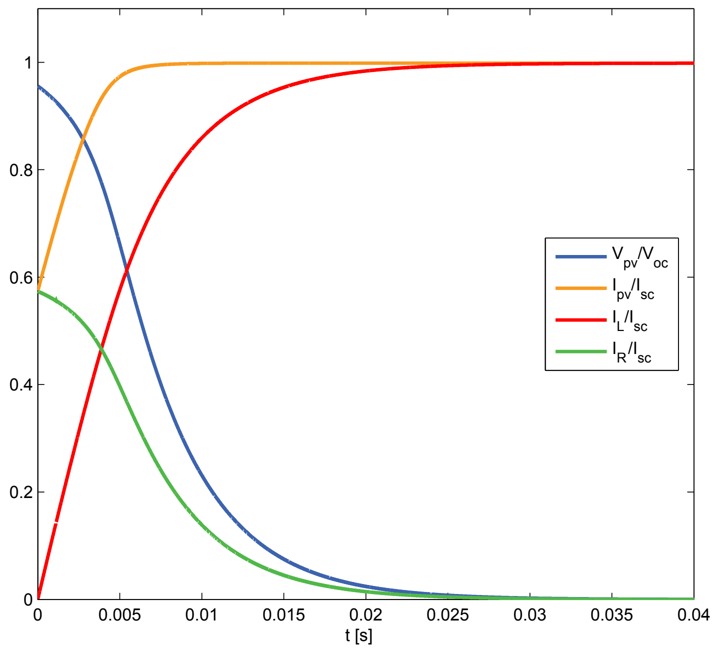

(a) Transient behaviour

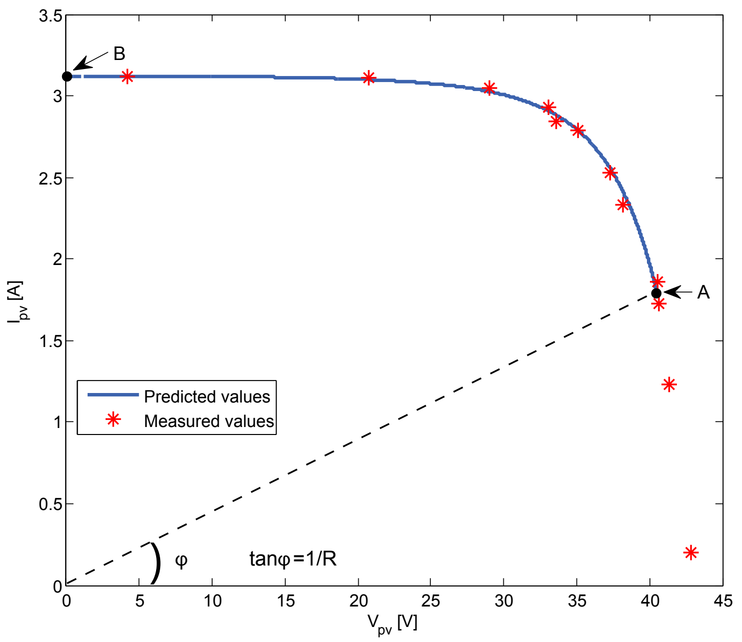

(b) $i_{pv} - v_{pv}$ trajectories

Figure 4-9: Transient response of the PV//R///L circuit

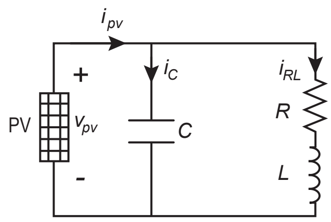

(a) RLC equivalent circuit using lumped L and C elements

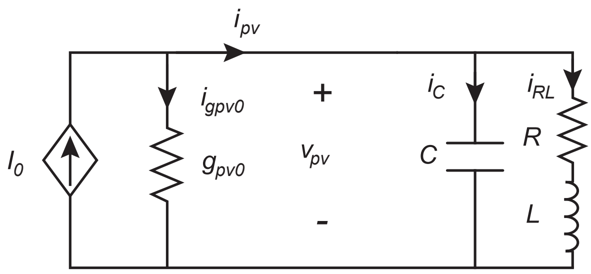

(b) Equivalent circuit where the PV generator is described by the ENRC

Figure 4-10: RLC circuit energised by the PV generator

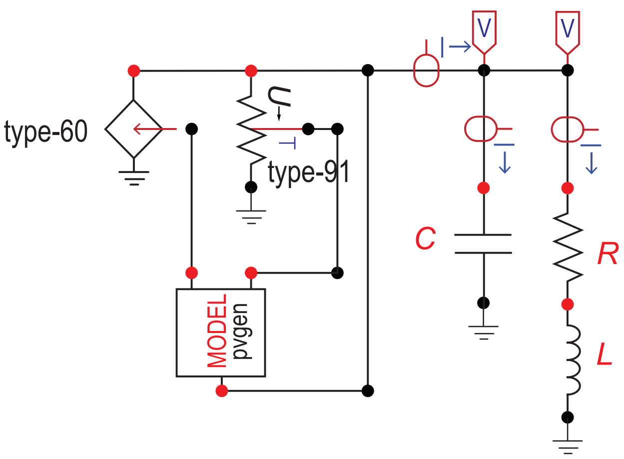

Figure 4-11: PV-RLC EMTP-based circuit

Table 4-2: Data for the simulation of the PV-RLC circuit

RLC
$R = 122.592\Omega$
$L = 10mH$
$C = 0.1mF$
$\Delta t = 10^{-5}s$

can be seen in Table 4-2, as shown also in Theocharis et al.[29].

Figure 4-12a shows the characteristic transient responses of the circuit to the PV generator applied at $t = 0s$, while the trajectories for the time interval from $t_A = 0s$ to the steady state on $i_{pv} - v_{pv}$ and $p_{pv} - v_{pv}$ planes can be seen in Figure 4-12b and Figure 4-13, respectively. The values chosen for R,L,C determine the magnitude of the damping factor of the circuit's response.

The curves in Figure 4-12b and Figure 4-13 are carried out for three levels of irradiance and temperature. In either case, the circuit response starts from the short circuit point and terminates on the point determined by R. The experimental characteristics obtained are compared to the simulation characteristics for the same operation conditions ($G = 450W/m^2, T_c = 25^oC$; $G = 650W/m^2, T_c = 33^oC$; $G = 900W/m^2, T_c = 35^oC$). As one can see, the predicted $i_{pv} - v_{pv}$ and $p_{pv} - v_{pv}$ curves, using the ENRC of the PV generator implemented in EMTP, are in excellent agreement both with the measured values, shown in Lalouni et al.[23] and in Theocharis et al.[29], and the predicted values obtained by following the node equations in the equivalent resistive circuit of the PV-RLC circuit, as shown in Theocharis et al.[29]. As also expected, I_{sc} increases, while V_{oc} slightly changes with increasing irradiance. Additionally, the maximum power P_{mpp} increases highly with irradiance, while slightly decreases with temperature. All the curves presented are notable. Indeed, the circuit examined in this subsection is frequently encountered in PV applications. The solution of a PV system with an embedded power converter connected to a RL load with a capacitor filter can be obtained via analogous circuits and its response may be comprised out of a succession of segments of similar curves to those shown in this section [27].

Since all the above simulations have been conducted with a timestep equal to $\Delta t = 10^{-5}s$, the considerable relation of the linearised circuit with the timestep should also be mentioned. After conducting many simulation trials in EMTP, based also on the results of Theocharis et al.[29], the conclusion reached is that the timestep strongly affects the predicted curves. In the case when the chosen timestep is used, a very good agreement with the measured values is observed. Additionally, in this case the digital simulation results in EMTP of the PV generator model present great numerical stability. So, at different studies excellent agreement can be achieved by choosing the appropriate timestep.

For comparison purposes, the response of the same circuit, driven by a constant voltage source, is also presented. This constant voltage has been taken equal to the open circuit voltage (V_{oc}) of the PV generator. As an example, the circuit current and capacitor voltage versus time are plotted for an initially de-energised series-parallel RLC circuit. In Figure 4-14 the transient response of the current of the PV-RLC circuit in time can be seen, along with the current

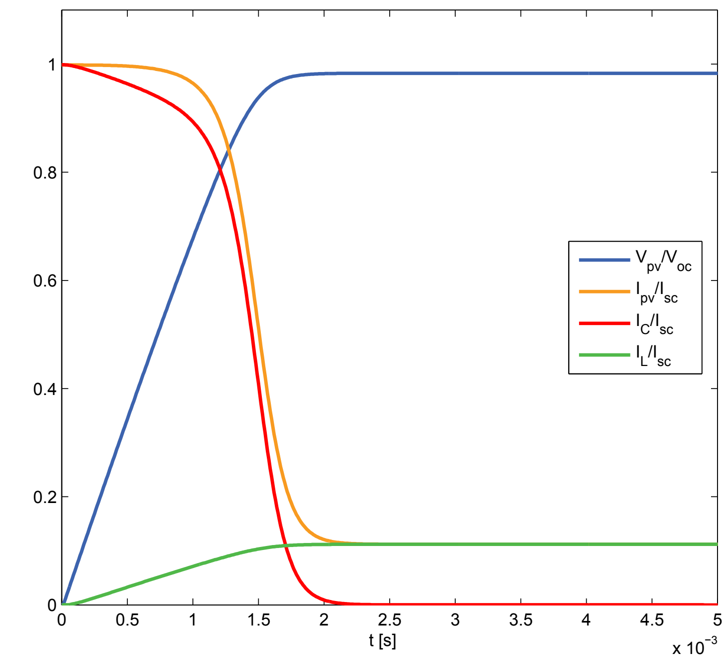

(a) Transient behaviour from $t = 0$ to steady state

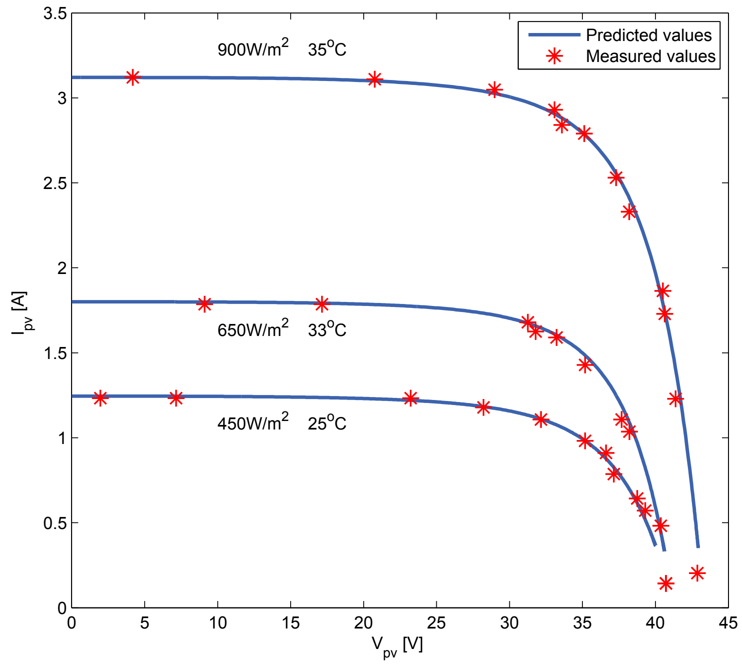

(b) $i_{pv} - v_{pv}$ trajectories from $t = 0$ to steady state for different levels of irradiance and temperature

Figure 4-12: Transient response of the PV-RLC circuit

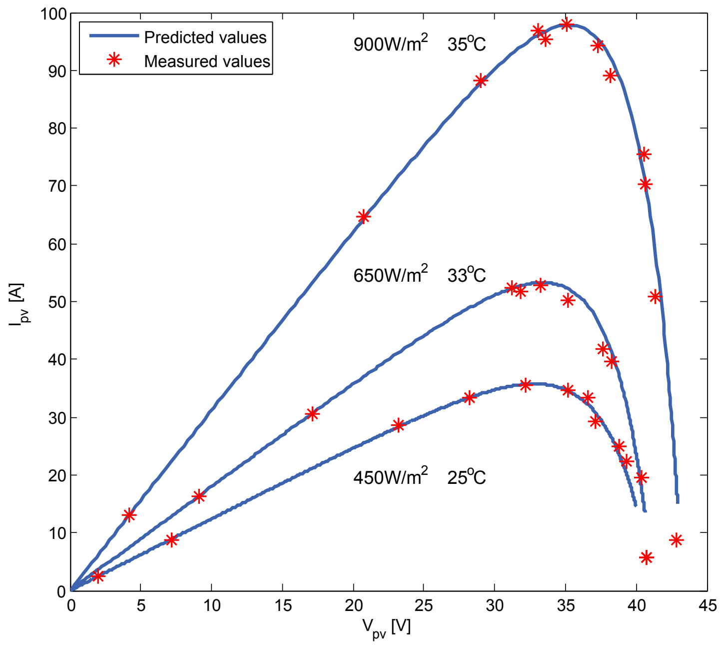

Figure 4-13: $p_{pv} - v_{pv}$ curves for different levels of irradiance and temperature of the PV-RLC circuit

response of the RLC circuit, while a DC voltage source is used as an input. Comparing, the two circuits we can easily see quite some differences in their transient behaviour. It is obvious that the PV-RLC circuit reaches the steady state faster. More specifically, in Figure 4-15 the capacitor voltage response of the two RLC circuits is presented. Analogous to the above mentioned cases, it is clear that for the situation where the PV drives the system the circuit reaches the steady state faster. The difference in the voltage limits for the two cases is due to the voltage drop along a series source resistance used while connecting the DC voltage source when designing the circuit, this is due to EMTP limitations. In Figure 4-14 the curves indicate that the PV system shows a more abrupt current decay, compared to the DC circuit, and settles down quickly to the steady state.

In conclusion, although the transient performance of second-order circuits powered by a PV generator exhibits the general characteristics of their input response, it presents a variety of unique features which are not met in conventionally powered circuits. Furthermore, the performance characteristics presented provide a rough approximation of the general behaviour expected for higher-order circuits. The most important conclusion of our comparison is that the same approach seems to apply for any circuit involving all three basic circuit elements in all possible combinations, a fact that makes it extremely important for the study of more realistic solar electrical systems.

After verifying the PV generator model by studying two parallel PV//R//C and PV//R//L circuits and a series-parallel PV-RLC circuit, we can conclude that the ENRC implemented in EMTP, can successfully predict the nonlinear performance of the PV generator and thus the proposed EMTP-based model is a strong tool. Also, as it has been proved, the PV

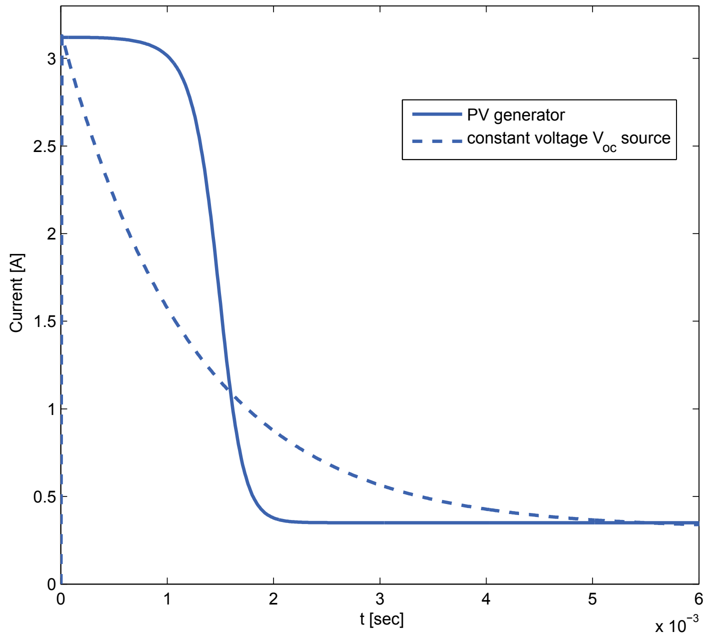

Figure 4-14: Current response of a series-parallel RLC circuit supplied by a PV generator or a constant voltage V_{oc} source

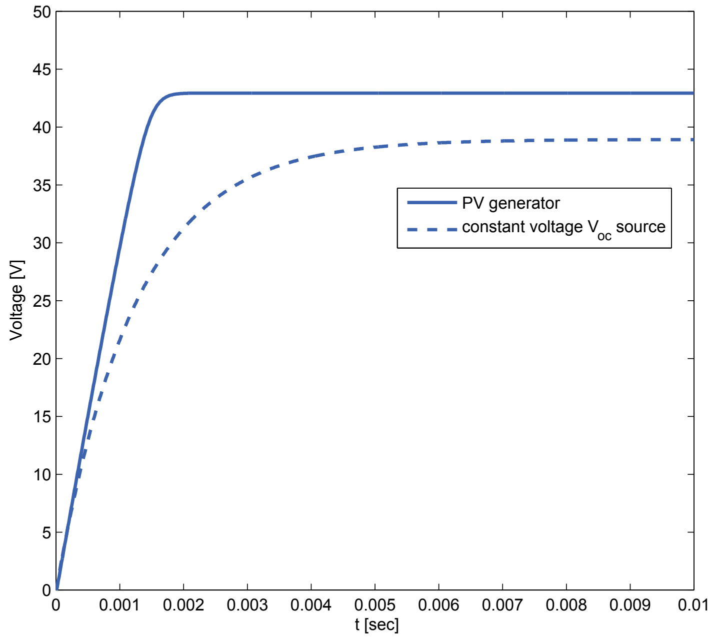

Figure 4-15: Capacitor voltage response of a series-parallel RLC circuit supplied by a PV generator or a constant voltage V_{oc} source

generator may introduce responses unattainable in circuits driven by conventional sources due to principal reasons.

4-4 Model optimisation

4-4-1 Temperature and irradiance dependence

As presented in a previous section, the equations used to describe how the parameters of the PV model change with respect to the irradiance and temperature changes, are (4-8), (4-9), (4-10) and (4-11). However, one can see that these equations depend on the series resistance r_s of the single-diode model, that has been described in Chapter 2. A point to note is that the PV generator model, presented in this project, has been built in EMTP in a different way than the single-diode model. It is only applicable at one particular irradiance level G and cell temperature T_c per simulation and the absence of r_s inhibit the use of the afore-stated equations. Thus, in order to expand and optimise the model suitable equations had to be found, therefore a reference I-V curve was translated regarding the irradiance and PV module temperature changing conditions.

In Marion et al.[30], the Module Energy Ratings (MER) methodology is presented, which uses indoor tests to characterise the electrical performance of the PV module and to determine factors to correct the nonlinear performance, when the irradiance and the temperature vary. Based on this study, the PV generator's temperature and irradiance correction factors and functions are determined from a matrix of short circuit current (I_{sc}) and open circuit voltage (V_{oc}), as resulting from the I-V curve measurements over a range of six irradiances and six operating temperatures. From this procedure three correction factors and functions are determined. The (I_{sc}) correction factor for temperature, α; the (V_{oc}) correction for temperature as a function of irradiance G, $\beta(G)$; and the (V_{oc}) correction for irradiance as a function of the PV module temperature T, $\delta(T)$.

As found in Marion et al.[30], using the incident irradiance and the PV module's temperature, I_{sc} and V_{oc} are calculated and a reference I-V curve is translated to determine the current at a steady voltage and thus at the maximum power. These procedures were based on modifications to ASTM E1036-96 (Standard Test Methods for Electrical Performance of Non-concentrator Terrestrial Photovoltaic Modules and Arrays Using Reference Cells) and use the following equations to calculate I_{sc} and V_{oc}:

$$I_{sc} = \frac{G}{G_r} I_{sc_r} \left[1 + \alpha(T - T_r)\right] \tag{4-24}$$

$$V_{oc} = V_{oc_r} \left[1 + \beta(G_r)(T - T_r)\right] \left[1 + \delta(T) \ln(G/G_r)\right] \tag{4-25}$$

where the subscript r refers to the reference curve.

In order to determine the I-V curve for the desired conditions, a reference I-V curve is selected to be translated. The reference curve can be the one measured under the irradiance and temperature conditions closest to those desired. That way the errors caused by the I-V translation, without taking into account the changes in fill factor due to the changes in temperature and irradiance, can be minimised.

Table 4-3: Irradiance and temperature correction factors and functions

PV Module	α (°C^{-1})	β (E) = mE + b (°C^{-1})			δ(T) = mT + b (dimensionless)	
		β(E_0)	m	b	m	b
a-Si/a-Si/a-Si:Ge, S/N 1736	8.50e-4	-3.97e-3	1.17e-6	-5.14e-3	5.20e-4	4.72e-2
CdS/CulnGaSSe, S/N 5165	-1.32e-4	-3.75e-3	1.34e-6	-5.09e-3	6.07e-4	4.97e-2
CIS, S/N 114	1.94e-4	-4.94e-3	2.22e-6	-7.16e-3	8.39e-4	7.39e-2
Mono-Crystal Si, S/N 0442	3.60e-4	-3.63e-3	0.98e-6	-4.61e-3	3.21e-4	4.15e-2
Multi-Crystal Si, S/N581836	2.58e-4	-3.57e-3	1.02e-6	-4.59e-3	4.80e-4	3.55e-2
a-Si/a-Si:Ge, S/N SYS49	8.36e-4	-3.52e-3	1.56e-6	-5.08e-3	5.36e-4	5.53e-2
CdS/CdTe, S/N 14407	0.60e-4	-2.38e-3	1.21e-6	-3.59e-3	6.00e-4	1.61e-2

The I-V data pairs of the reference curve can be then translated into the desired conditions by using equations (4-26) and (4-27):

$$I = I_r \frac{I_{sc}}{I_{sc_r}} \tag{4-26}$$

$$V = V_r \frac{V_{oc}}{V_{oc_r}} \tag{4-27}$$

By using this methodology the fill factor does not change, thus the reference I-V curve data pair for maximum power becomes the translated I-V curve data pair for maximum power. In order to determine the current at a specific voltage, the current has to be interpolated by using the two adjacent I-V curve data pairs from the translated I-V curve, with voltages above and below the desired voltage.

4-4-2 Simulation and results

For the simulation in ATPDraw the same series-parallel PV-RLC circuits shown in the previous section are used. As reference values are taken the data from Table 4-1 under STC, since the SIEMENS SM 110-24 module is used again for the simulations. As for the irradiance and temperature correction factors and functions needed for the equations shown above, Table 4-3, as given in Marion et al.[30], is used. According to this table, a group of 7 PV modules representing different technologies were used in order to determine the irradiance and temperature correction factors and functions, as explained in the previous section. To use equation (4-25), the table gives values of β evaluated for G_r.

The SIEMENS SM 110-24 PV module is made out of mono-crystalline Si cells, thus the highlighted row of correction factors, as shown in Table 4-3, is being used as data in the ATP/MODELS of the generator, along with the STC data of the module and the desired temperature and irradiance. The timestep in these simulations is again $\Delta t = 10^{-5}s$. The results of the simulation can be seen in Figure 4-16. At this point, it has to be mentioned that the simulations use as a reference curve the one corresponding to the PV data under STC, shown in Table 4-1. This curve has also been successfully reproduced using the aforementioned procedure. Based on the reference curve two more new curves have been successfully

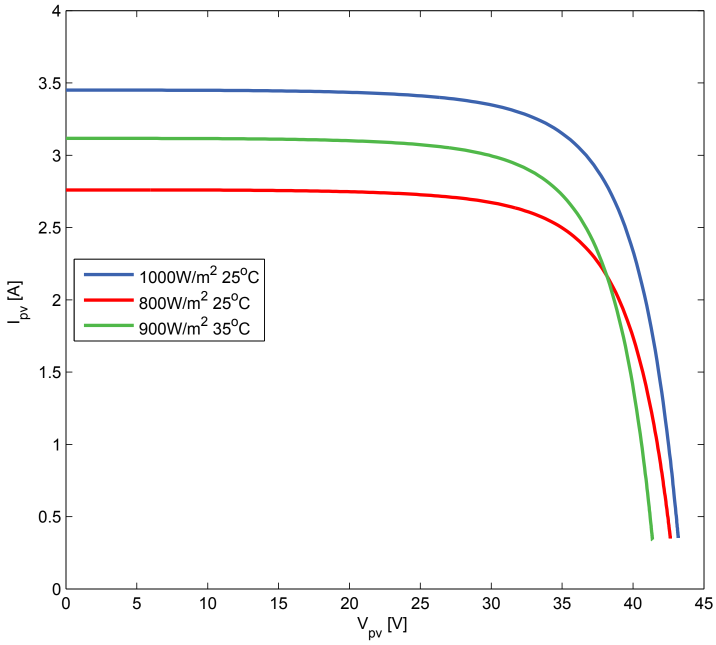

Figure 4-16: $i_{pv} - v_{pv}$ trajectories for different irradiance and temperature levels

predicted. One for the irradiance and temperature level of $900W/m^2$ and 35^oC and the second one of $800W/m^2$ and 25^oC respectively. The $100W/m^2$-25^oC curve along with the $800W/m^2$-25^oC curve, closely approach the voltage-current characteristic curve as shown in the SIEMENS SM 110-24 module's manual. The curves based on the technical data of the module can be seen in Figure 4-17 [28]. Additionally, the curve of $900W/m^2$-35^oC perfectly matches with the predicted curve shown in Figure 4-12b.

After many trials the $650W/m^2$-33^oC and $450W/m^2$-25^oC curves, shown also in Figure 4-12b could not be obtained. That can be a result of using the specific correction factors of Table 4-3, in the procedure explained earlier. It is clear that these data represent some PV technologies, by using the data of 7 specific PV modules, and are proposed as suitable for application in modules based in the same technologies. However, the proposed matching between modules with the same technology but with different technical characteristics might not be 100% correct. We should also keep in mind that the PV technology has made a significant progress through the last years, thus the data in Table 4-3 should be updated in order to follow the developments. In addition, in Marion et al.[30] it is stated that the reference I-V curve should be under conditions of irradiance and temperature close to the wanted ones. For our simulations the reference curve is the one based on the data referred to STC of the chosen PV module. The $650W/m^2$-33^oC and $450W/m^2$-25^oC curves can be considered not to be close to the initial data, a fact that might affect the outcome of the simulations. For all these reasons, future in-depth work has to be done, regarding the proposed PV generator model, with respect to the irradiance and temperature effect.

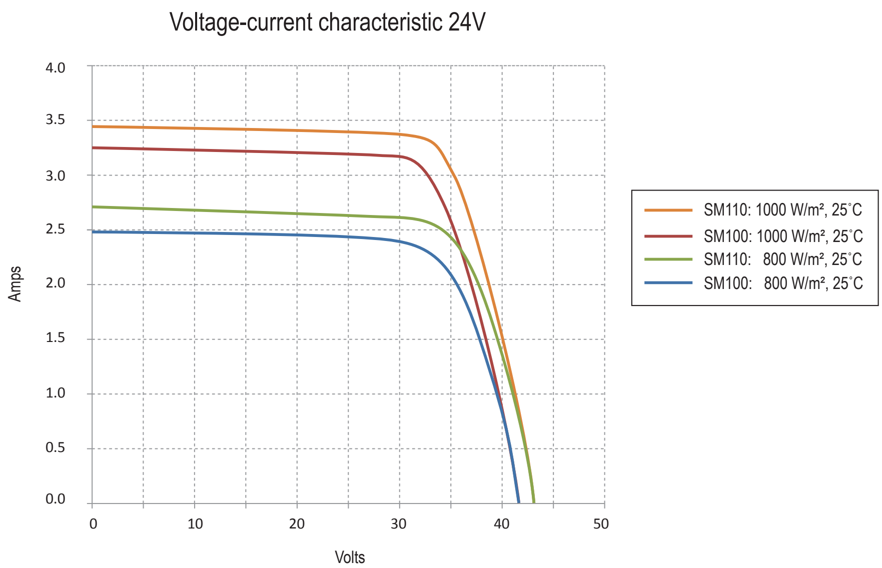

Figure 4-17: Voltage-current characteristics of the SIEMENS SM 100-24 PV module

Chapter 5

Modelling of a single-phase grid-connected PV system

In this chapter, the way in which the EMTP-based model of the PV generator can be connected with grid-connected systems in the general theoretical framework will be described. This will be done in terms of modelling a single-phase grid-connected photovoltaic (PV) system. Nowadays, grid-connected PV systems are an emerging technology. A valuable insight into the electrical behaviour of this kind of systems can be obtained through analytical simulation studies. In this case, existing simulation software packages are already available and quite reliable. For a large category of studies, such as the modelling of the power converter, most of them are well applicable. However, if someone wants to focus on the power system analysis level, the existing software packages can not simultaneously handle, in a computationally effective way, all the distinctive features of the grid-connected PV systems [31]. Due to the fact that, once more, in such studies a DC voltage source is mainly used instead of the PV generator, verifies the problem.

In the following sections, each one of the basic building blocks of a single-phase grid-connected PV system will be presented and the particularities with respect to modelling will be discussed. Next, appropriate models will be developed in ATPDraw and will be combined with the ENRC of the PV generator. The validity of the approach chosen, will be verified by comparing the simulation results with published measurements. A case study will be also performed in order to obtain current and voltage waveforms and finally harmonic distortion levels.

5-1 System configuration

In this project it was decided to use a simplified configuration of a single-phase PV system; a system comprising out of the PV source connected through a DC/AC inverter to the utility grid. The configuration of the inverter chosen is the central inverter mainly due to its simplicity. Of course, the possibility of designing the system as a unit was an important reason that lead towards this direction, since it offers the freedom to incorporate the MPPT controller in the inverter in a later stage. The system has been initially built, implemented and tested in Phoenix, Arizona, with the results presented and explained in McNeil et al.[32] and the same configuration has also been used for simulation studies in Theocharis et al.[4]. To specify, the system is composed of the PV generator, a DC filter, a DC/AC inverter, an isolation transformer and the utility grid. The PV generator model is the one described in Chapter 4, the transformer is referred to the PV side and is represented by a linear equivalent inductance L_{tr}/α_{tr}^2 for both primary and secondary sides and a simplified representation of a single-phase bridge inverter is used. In conclusion, this functional model of a line-commutated PV system has been chosen, since it can be easily incorporated into a transient stability program for dynamic analysis.

5-1-1 Single-phase bridge inverter

One important application of the PV based generation, is to feed the generated power (DC) into the utility grid (AC). For that reason, the last years PWM inverters are used, based on gate commutated devices such as IGBT, MOSFET and GTO. However, these devices suffer from high switching losses and their power handling capability and reliability are low, compared to thyristor/Silicon-Controlled Rectifier (SCR) [33]. For applications in which DC voltage has to be controlled, thyristors are mainly used, where conduction happens not only when exceeding threshold voltage in case of forward biased, but also when a triggering signal is applied at the gate [34].

In the case of a fully controlled single-phase bridge converter two mode operations can take place; rectification or inversion mode. Inversion mode is equivalent to a firing angle α between 90^o and 180^o, while rectification mode is said to happen when the firing angle is between 0^o and 90^o. The firing angle is the interval in electrical angular measure, through which the firing pulse of the switching device is delayed by phase control, compared to natural operation that would exist without controller elements [35]. Thus, the same converter can operate both as a rectifier and an inverter, depending on the value of α and the polarity of the DC source. In the case of the inversion mode, the line voltage is used for commutation, and is therefore called line-commutated inverter [34]. Basically, a line-commutated inverter is a phase-controlled inverter. Most commonly, the firing angle is varied up to 165^o, in order to facilitate the inversion mode for SCR. However, the most important drawback of the conventional line-commutated inverter is the quite high value of Total Harmonic Distortion (THD), 48.3% for square wave line current [33].

So, an appropriate presentation of a line-commutated single-phase bridge inverter has been used, where all the switching devices had been taken into consideration as ideal switches. An ideal switch is a device with zero resistance when closed and with infinite resistance when opened. A scheme for a single-phase bridge inverter can be seen in Figure 5-1. A line-commutated inverter is based on the principle of natural commutation process. When the current in the switching device goes through zero, the device is turned off [35]. Now, according to digital simulations, two operation modes are considered for this inverter, when none or two switches are conducting. In every timestep of the simulation the mode of the operation has to be tracked. This implies that in each timestep the current of any closed switch and the voltage of any open switch are checked. In the case where the current approaches zero value, the corresponding switch is considered turned off for the next timestep. Where, in the case

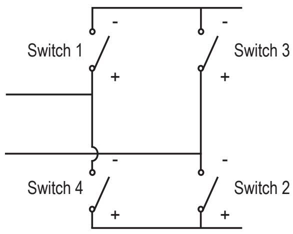

Figure 5-1: A line-commutated single-phase bridge inverter modelled with ideal switches

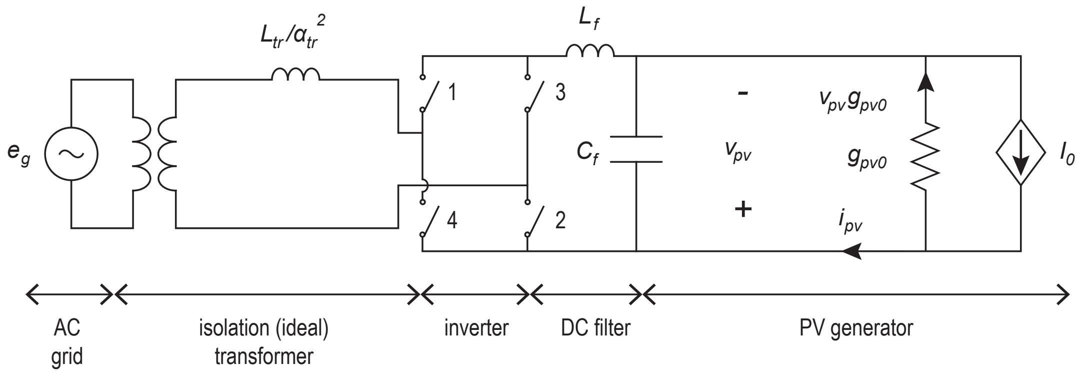

Figure 5-2: A typical configuration of single-phase grid-connected PV system

that the voltage is positive and the angle of the voltage approaches the selected firing angle, the corresponding switch starts conducting [29].

The main components of the PV system that have been mentioned previously, with the analytical representation of the ENRC of the PV generator and of the line-commutated inverter are shown in a system model presented in Figure 5-2, as introduced also in Theocharis et al.[29]. An example of the operation mode, in which switches 1,2 are conducting and $3, 4$ are not, is shown in Figure 5-3.

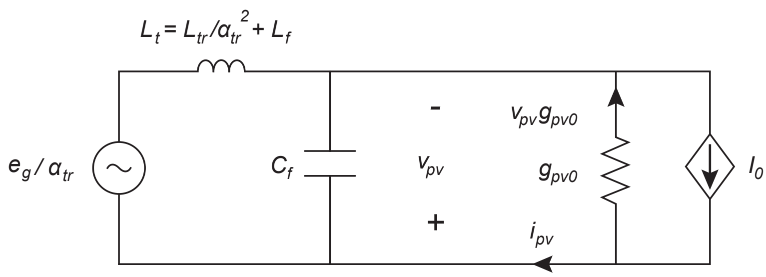

Figure 5-3: System topology when $1, 2$ are closed and $3, 4$ are open

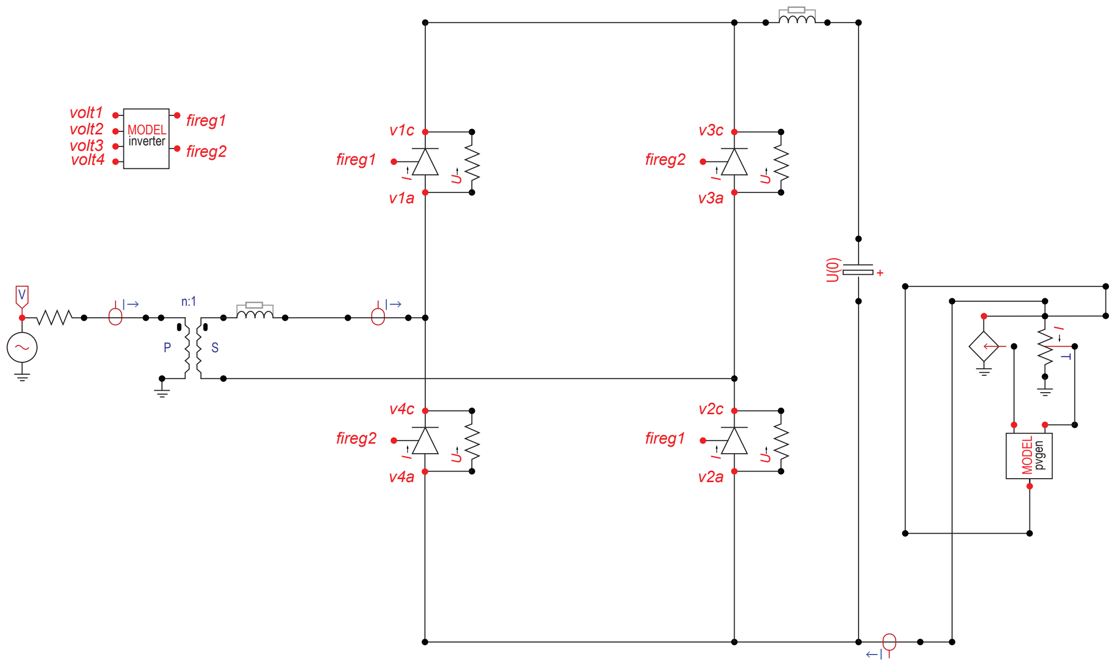

Figure 5-4: Single-phase grid-connected PV system simulated with ATP/MODELS

5-2 System and component models in EMTP

In order to start the simulation of the EMTP-based system, all the components included have to be designed. The diagram of the test system used can be shown in Figure 5-4.

5-2-1 PV generator model

The PV generator has the same structure as showed in Chapter 4 and will not be further explained in this section.

5-2-2 Filter/Inverter models

The filter consists simply of an inductance and a capacitor. The filter connecting the generator to the inverter serves to smooth the DC harmonics as well as to limit the rate of change of DC current. As for the inverter, it is just two pairs of thyristors, conducting based on the line-commutated inverter scheme presented before. Specifically, for the ATP model the TACS-controlled TYPE 11 switches were chosen to act as thyristors, while a MODELS was used for the control of the firing of the thyristors. The main idea behind the inverter's simulation is to measure the voltage difference across the thyristors and give it as input to the MODELS, which in turn will give the firing signals as an output, which will control the TACS thyristors. As it was mentioned before there are two conduction modes of this inverter, so the control strategy behind it is that thyristor pair 1,2 is triggered simultaneously at a switching angle of α, while the pair 3,4 is triggered at a delay of π radians in each cycle. The

Table 5-1: Data for the single-phase grid-connected PV system [32]

AC Grid	
	$Frequency = 60Hz$
	$V_{rms} = 240V$
Transformer	
	$L_{tr} = 320\mu H$
	$\alpha_{tr} = 1$
DC Filter	
	$L_f = 25mH$
	$C_f = 3.3mF$
PV Generator	
	$v_{pv} = 190V$
	$r_s = 2.15m\Omega$
	$I_{ph} = 23.562A, G = 0.55kW/m^2$
	$I_{ph} = 17.136A, G = 0.40kW/m^2$
	$I_D = 339.5\mu A$
	$W = 0.54932V^{-1}$

TYPE 11 switch in case of thyristor mode starts conducting if the voltage across it exceeds an ignition voltage level, which in this case is set to be zero and stops conducting if the current through it is approaching zero. In addition, the thyristors are assumed to start/stop conducting immediately, a fact determined by a switching function on the MODELS code. The resistances put in parallel to the thyristors are needed for the numerical stability of the system.

5-2-3 Isolation transformer/utility grid models

The isolation transformer used is an ideal TYPE 18 transformer with unit ratio and includes only an equivalent inductance for both primary and secondary sides. As for the utility grid, it is represented by an ideal AC voltage source.

5-3 Application and results

The data used in the simulated system, explained above, can be seen in Table 5-1 and were obtained from McNeil et al.[32] and also used in Theocharis et al.[4]. So, based on the data, the performance of the system will be examined for two irradiance levels, $0.40kW/m^2$ and $0.55kW/m^2$. One can realise that the data given in Table 5-1 do not match with the model of the PV generator built, which takes as inputs the V_{oc}, I_{sc}, I_{mpp} and V_{mpp} of the generator. For that reason the equations characterizing the single-diode equivalent PV model, as shown in García et al.[36], were used in such a way that the values needed for the model used in this project could be obtained. The equations are similar to the ones explained in Chapter 2. More specifically, the mathematical equation describing the PV current under irradiance G, and temperature T_α is:

$$i_{pv} = I_{ph} - I_D \left[e^{W(v_{pv} + i_{pv} r_s)} - 1 \right] \tag{5-1}$$

Table 5-2: Data for the PV generator for different irradiance levels

PV Generator Data	
$G = 0.40kW/m^2$	
	$V_{oc} = 197V$
	$I_{sc} = 17A$
	$V_{mpp} = 158V$
	$I_{mpp} = 15A$
$G = 0.55kW/m^2$	
	$V_{oc} = 202V$
	$I_{sc} = 23A$
	$V_{mpp} = 162V$
	$I_{mpp} = 21A$

where, I_{ph} is the light-generated current and I_D is the diode saturation current. W is a term given by the following equation:

$$W = \frac{q}{wKT_\alpha} \tag{5-2}$$

where, q is the electron charge, w us a curve fitting constant and K is the Boltzmann's constant. By rearranging the terms of equation (5-1) a relation between i_{pv} and v_{pv} can be reached, from which after some simulation trials the needed data for the EMTP-based model of the PV generator were obtained, using also the given values of the generator found on Table 5-1. The new data can be seen in Table 5-2. The timestep of the simulations has been set at $\Delta t = 10^{-7}s$. In order for both irradiance levels the PV voltage to settle at about 190V, suitable calculations of the firing angle of the inverter have been made. For the irradiance level of $0.40kW/m^2$ the firing angle was found to be $\alpha = 168^o$, where for $0.55kW/m^2$ was $\alpha = 150.5^o$. The result can be seen in Figure 5-5. As can be noticed from Figure 5-5, when the irradiance level changes from $0.55kW/m^2$ to $0.40kW/m^2$ the system operates under non-continuous conduction mode, verified also in Figure 5-6. This happens as a result of the decrease in the PV generator current, which can be seen in Figure 5-7 along with the minimum value of the current observed at time moment t_B.

In Figure 5-8 the trajectory of the operating point on the $i_{pv} - v_{pv}$ plane is presented for the period $[0, t_B]$, where t_B is the moment at which the minimum value of i_{pv} is detected. The point A corresponds to $t_A = 0s$ while the point B corresponds to t_B, where the minimum value of the current i_{pv} is observed, exactly as in Figure 5-7. As can be seen, the predicted curves using the ENRC model of the PV generator match the $i_{pv} - v_{pv}$ curves given by the PV's manufacturer, that were calculated using equation (5-1). A small mismatch can be observed, since the aforementioned procedure is an approximation and can not be accurate used for extrapolating equation (5-1) to the manufacturer's curves. Despite the small limitations, it can be concluded that the linearised approximation of the PV generator is in good agreement with the nonlinear model, described by equation (5-1). Figure 5-5, Figure 5-6, Figure 5-7, Figure 5-8 are also in good agreement with the corresponding figures presented in Theocharis et al.[4], a fact that further validates the EMTP-based model used in this section.

In Figure 5-9 the measured and predicted values of the harmonic content of the injected current i_{ac} into the utility grid are shown. The measured values where retrieved from McNeil

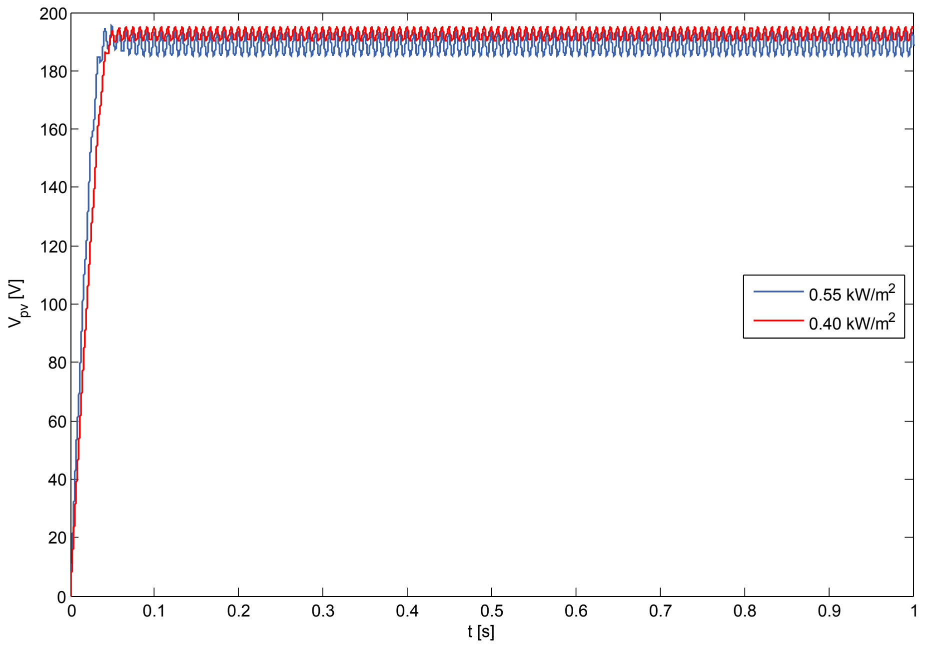

Figure 5-5: The voltage v_{pv} of the PV generator for irradiance levels of $0.40kW/m^2$ and $0.55kW/m^2$

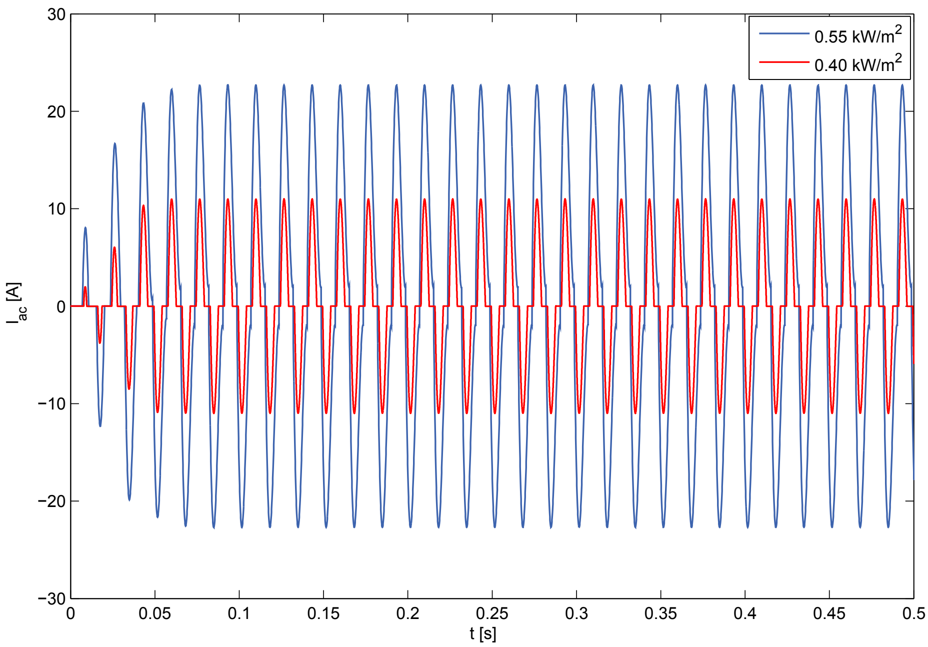

Figure 5-6: The current injected into the utility grid for irradiance levels of $0.40kW/m^2$ and $0.55kW/m^2$

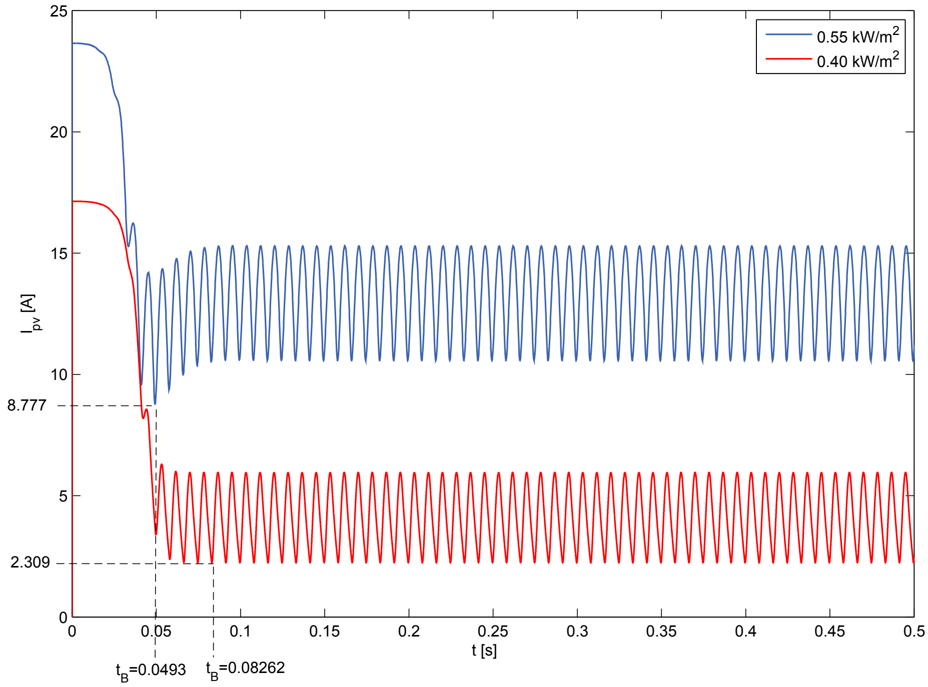

Figure 5-7: The current i_{pv} of the PV generator for irradiance levels of $0.40kW/m^2$ and $0.55kW/m^2$

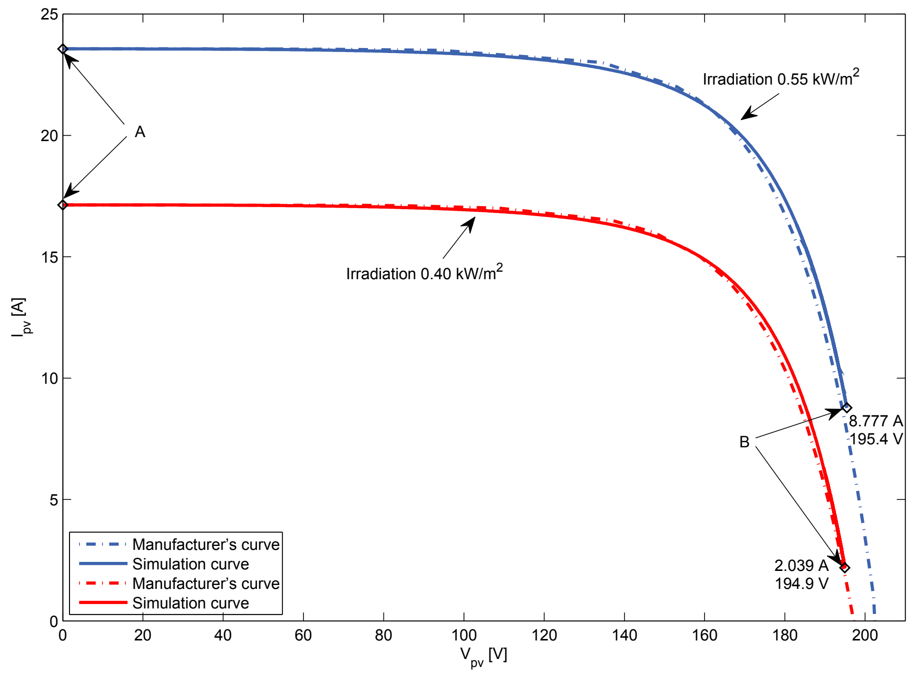

Figure 5-8: The trajectory point of the PV generator for the time period $(0, t_B)$ for irradiance levels of $0.40kW/m^2$ and $0.55kW/m^2$

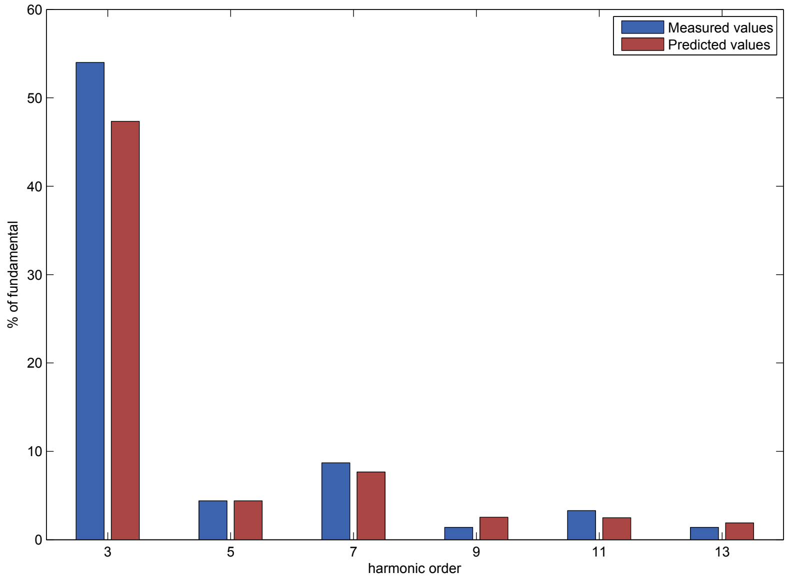

(a) Harmonic content for $0.40kW/m^2$

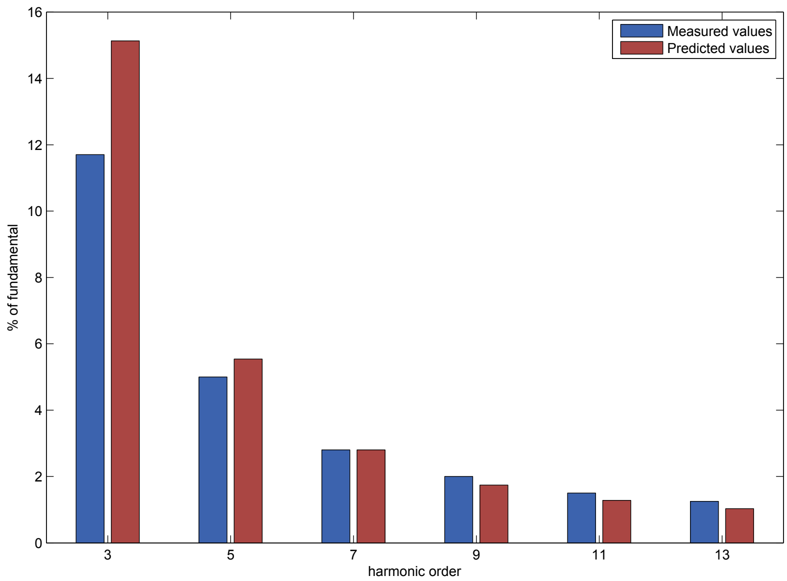

(b) Harmonic content for $0.55kW/m^2$

Figure 5-9: Harmonic content of the injected current for two levels of irradiance et al.[32] and were also used in Theocharis et al.[4]. As it can be observed, the harmonic content for both irradiance levels is extremely high. In both measured and predicted spectra the dominance of the third harmonic is clear and for the case of irradiance level of $0.40kW/m^2$ the spectra show a ripple, in which the seventh harmonic is larger than the fifth harmonic. For $0.40kW/m^2$ the Total Harmonic Distortion (THD) of the injected current to the AC grid is 0.47, while for $0.55kW/m^2$ the THD is about 0.15. This is mainly due to the fact that the inverter operates in non-continuous conduction mode. The predicted values are in a good agreement with the predicted values as presented in Theocharis et al.[4]. More specifically, comparing the results of the dominant third harmonic, the error between the measured and predicted values in Theocharis et al.[4] is about 22.7% for $0.55kW/m^2$ and 12.68% for $0.40kW/m^2$, while using the EMTP-based model the differences are almost the same for both irradiance levels. These errors are observed since the inverter is considered to be ideal and the transformer to be linear, for simplicity reasons as initially explained. Of course, a better agreement, between the measured and predicted values, can be achieved if more precise models for the inverter and the transformer are used.

The system designed based on the Table 5-1 and shown also in McNeil et al.[32] and Theocharis et al.[4] is a simplified system that does not correlate with a commercial grid-connected PV system, since both the harmonic content of the injected current into the utility grid and the fluctuation of the current of the PV generator are very high. A study regarding the performance of the system has been conducted in Theocharis et al.[4] for variable values of the inductor L_f size, the capacitor C_f size and the PV voltage v_{pv}. Along with a sensitivity investigation of the system, conducted in McNeil et al.[32], the previous study showed that the capacitor size does not affect the THD of the injected current, since the capacitor affects only voltage waveforms. As for the inductor size, the influence on the THD is remarkable. For the irradiance case of $0.55kW/m^2$ the THD can be significantly reduced by increasing the inductor, since the inverter goes from below to beyond continuous conduction mode and the current wave becomes more sinusoidal against the tendency to become a square wave [32]. This increase will also increase the power factor. So, in order to improve the THD and the power factor a variable inductance can be used in the filter, depending on the irradiance level. The idea behind this is to maintain the inverter as close to the continuous mode as possible [32]. As for the fluctuation of the PV generator current i_{pv}, it is affected by the inductor's current but mainly it is affected by the voltage of the PV generator v_{pv}, which is the same with the capacitor's voltage. Simulation results, shown in Theocharis et al.[4], prove that for an inductor L_f sized between $10mH$ and $300mH$ with a capacitor size $C_f = 3.3mF$ and $v_{pv} = 190V$ the big fluctuation of the current i_{pv} can be avoided. More specifically, the i_{pv} fluctuation can be reduced by reducing the fluctuation of the voltage v_{pv}, through applying an appropriate capacitor C_f size. After simulation trials, by using various capacitor sizes, it has been concluded that above $55mF$ the fluctuation is insignificant. In Figure 5-10 the fluctuation of the current i_{pv} can be seen, for three different sizes of the capacitor C_f. From this graph it is clear that while varying the capacitor size between $2mF$ and $340mF$, the current fluctuation becomes negligible for sizes above $55mF$. The results of simulating the same system under irradiance of $0.40kW/m^2$, using the $55mF$ capacitor and an inductor of $25mH$, with an appropriate firing angle that corresponds to a PV generator's voltage of $v_{pv} = 190V$, can be seen in Figure 5-11. It is clear, that the voltage of the PV generator can be considered typically constant, so indeed the fluctuation of the i_{pv} current is negligible.

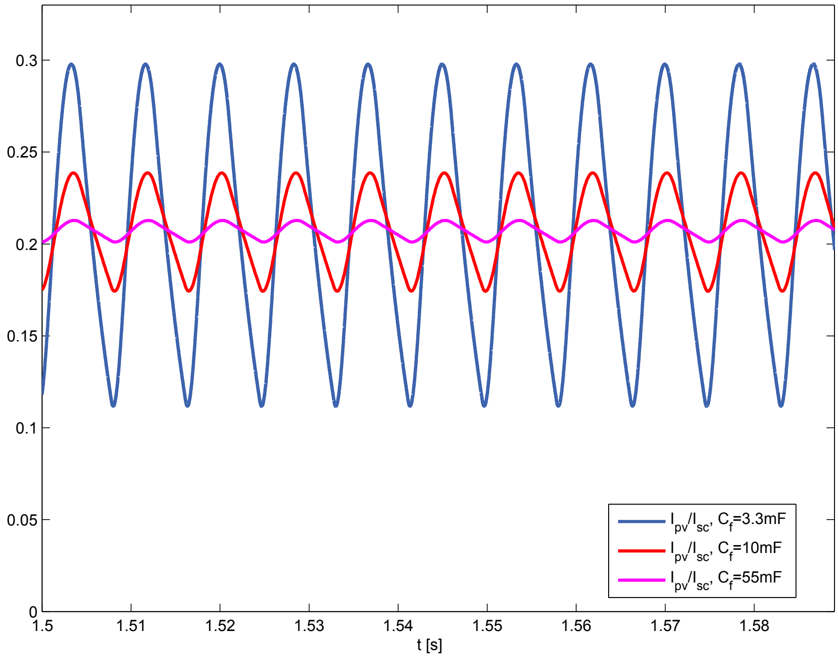

Figure 5-10: PV generator current i_{pv} for different capacitor C_f sizes, between $2mF$ and $340mF$

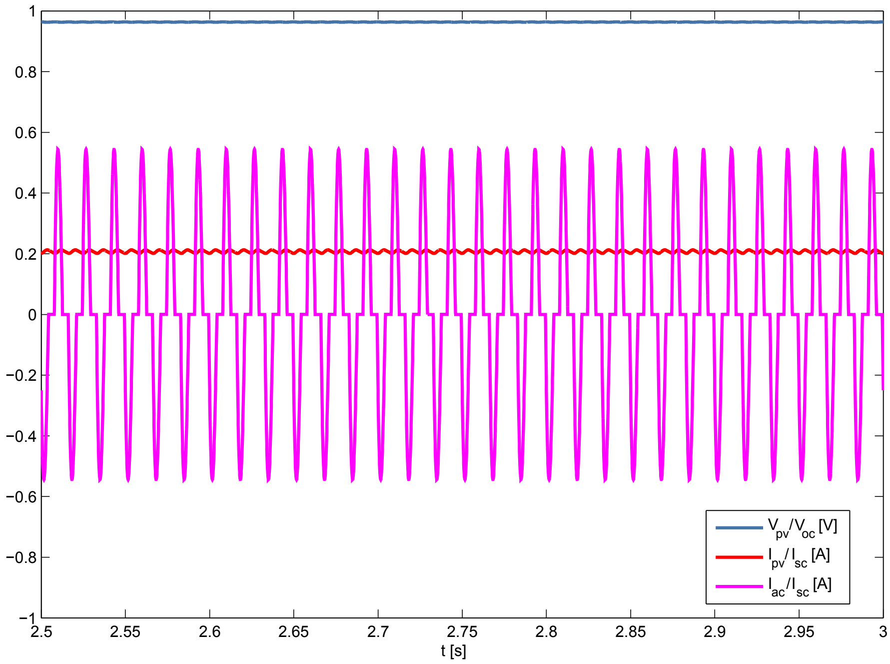

Figure 5-11: Simulation results for the single-phase grid-connected system, using a capacitor $55mF$ for irradiance level of $0.40kW/m^2$

5-4 Maximum Power Point Tracking (MPPT)

As shown in previous sections, the output current and voltage characteristics prove the non-linear nature of the PV generator. For a particular cell temperature and solar irradiance there is only one optimal operating point, called the maximum power point (MPP). Under temperature and irradiance variations the MPP would differ. So, the output of the PV generator is seldom maximum and the operating point is not optimal. Thus, in order to compensate this characteristic exhibited by the PV generator, a MPPT controller has to be incorporated, to force the system to always operate at the maximum power point and improve the photovoltaic generation system's efficiency. In this section, a control method for the MPPT, of the photovoltaic system introduced in the previous section, will be presented. The steps of designing the controller will be explained together with its simulation. The simulation results will then be discussed and compared to the ones obtained by operating the system without the MPPT but for maximum power operation.

5-4-1 MPPT Algorithm

As stated above the characteristics of a PV system vary with respect to the temperature and solar irradiance. Thus, the MPPT controller is responsible to track the new modified maximum power point in every temperature and irradiance variation. In this project, a method based on the slope of the power-voltage (p-v) curve has been developed, that constantly tracks the MPP through iterative checks of the output current and voltage of the PV generator. The MPPT can determine on which side of the power-voltage characteristic the current operating point is, in that way the current injection is indirectly controlled. In Figure 5-12 it is clear that by analysing the power-voltage derivative one can easily determine whether the PV generator is operating at the MPPT or far from it since:

- $\frac{dp}{dv} > 0$ for $v_{pv} < V_{mpp}$
- $\frac{dp}{dv} = 0$ for $v_{pv} = V_{mpp}$
- $\frac{dp}{dv} < 0$ for $v_{pv} > V_{mpp}$

More analytically, when the operating point is moving from the left side towards the MPP the derivative is decreasing, while in the case that it is moving from the MPP towards the left side the derivative it is increasing. Accordingly, on the right hand side, while moving from the MPP to the right, the derivative is decreasing, while in the opposite direction is increasing. So, the method proposed on this project consists of climbing the operating point along the generator characteristic to its maximum. Based on equation (5-3)

$$V_0 = \frac{2V_m}{\pi} cos\alpha \tag{5-3}$$

and the linear relation between the voltage and the firing angle, the operating point v_{pv} is adjusted with every MPPT cycle though the adjustment of its firing angle, providing the one that corresponds to the maximum power point [34]. Furthermore, an extra feature in the algorithm is used for monitoring the maximum and minimum values of the power-voltage

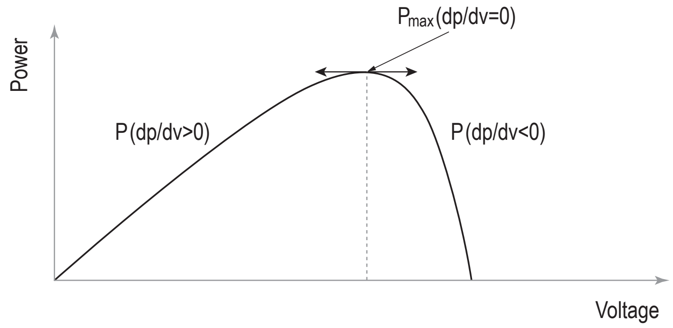

Figure 5-12: Operating point according to the sign of $\frac{dp}{dv}$ on the power characteristic

derivative oscillation on the PV side. Since a capacitor and inductance are used in the circuit, in the case that the operating point is close to MPP, the influence of the ripple of voltage and current are significant [37]. So, by simply detecting the voltage or current, the estimation of the change in the firing angle may be inaccurate. In order to overcome this problem, a method to control the change of the firing angle through power detection was chosen. When the system operates in the area around the MPP the power ripple of the PV side is minimised [37]. This characteristic can be used in order to detect in which part of the power-voltage characteristic the system operates. So, the power oscillation is of significant value, in order to find how close to MPP the current operating point is, and thus slow down the increment of the firing angle so that the MPP is not crossed. A flowchart, shown in Figure 5-13, presents the multilevel variable-step MPPT developed. It shows how the firing angle of the inverter voltage changes, so that the operating point remains as close to the MPP as possible.

The algorithm uses the output generator voltage v_{pv} and the output current i_{pv} at the time instant k and $k-1$ as the input values and gives the firing angle of the inverter voltage that corresponds to the desired MPPT. As can be seen in the flowchart, v_{pv} and i_{pv} are used to calculate the current generator output power $p_{pv}(k)$. This value is then used to determine the difference between $p_{pv}(k)$ and the value obtained from the last measurement $p_{pv}(k-1)$. Respectively, the difference between $v_{pv}(k)$ and $v_{pv}(k-1)$ is found. The derivative of this differences is then calculated and declared as D. Thus, the MPP can be tracked by comparing the derivative of the power and voltage instantaneous difference and so judge whether the system works at the MPP or at the left or the right side of the power-voltage angle. Additionally, by analysing the derivative the operating point can be tested and checked to determine if the generator is operating at its MPP or how far from it. The measure in the derivative oscillation on the PV side is used to qualify the increment size, denoted as *incr*, which determines the movement toward the MPP and ensures that the firing angle will rapidly converge into the vicinity around the MPP. As soon as the operating point is close to the MPP, the derivative should ideally be zero, although in a more pragmatic approach should not exceed a threshold limit, as shown in Figure 5-14. If the derivative is above the threshold limit, an adjustment has to occur by increasing the voltage, thus by increasing the firing angle with the appropriate increment size. In the case that the derivative is below the limit the adjustment has to occur by decreasing the voltage correspondingly. However, this might cause a power loss which also depends on the increment size of each adjustment. If the

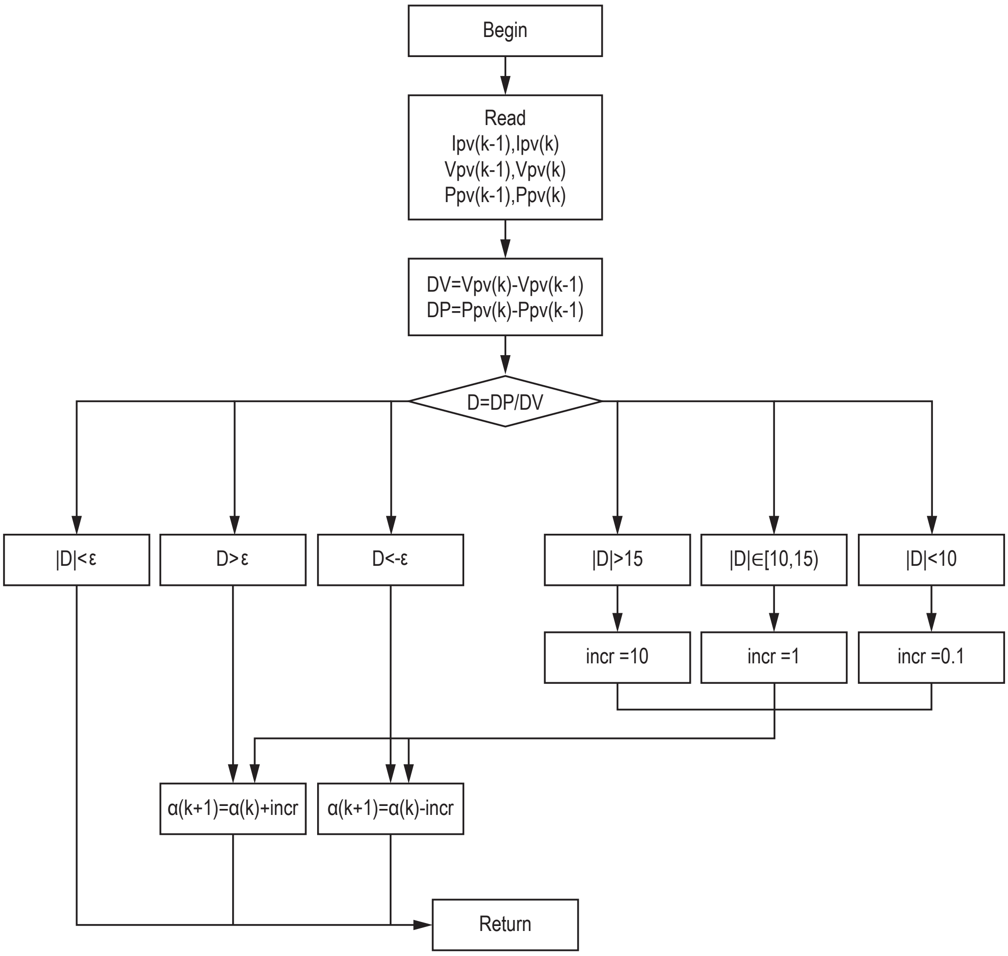

Figure 5-13: Flowchart of the MPPT algorithm

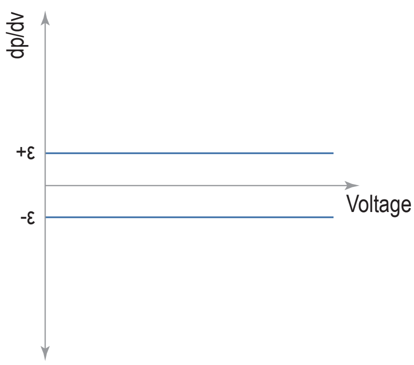

Figure 5-14: Power-voltage derivative oscillation limits

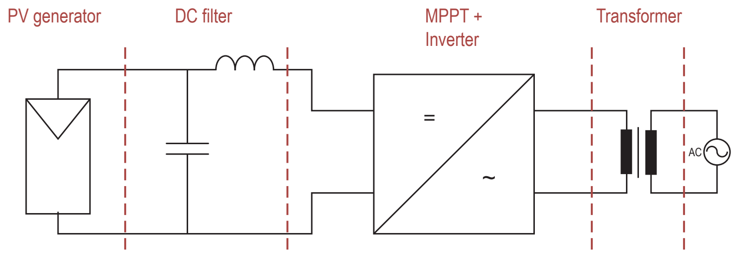

Figure 5-15: System configuration of a single-phase grid-connected PV system with MPP tracker

operating point is very far from the threshold limits of the derivative the increment step is big and varies regarding how far from the limits it is. The value of the increment size is system dependent and had to be determined experimentally. The value of the oscillation limit $\pm\varepsilon$ is system dependent too and had to be determined regarding the frequency of the system and the timestep of the digital simulation.

5-5 System and component models in EMTP

The system configuration in the case with the MPPT remained the same, as the one presented in Figure 5-2. The slight difference in this case is that the MPPT algorithm has been embedded in the control of the line-commutated inverter. The configuration of the single-phase grid-connected system with MPP tracker can be seen in Figure 5-15. Regarding the implementation of the system in ATP nothing has changed and the same one as shown in Figure 5-4 was used. Additionally, the MPPT algorithm, as presented before, has been added in the inverter MODEL and the TACS device, DEVICE66, has been added in order to obtain rms characteristics of the measured values.

5-6 Application and results

Although the PV system analysed above has been designed for specific values of V_{oc}, I_{sc}, V_{mpp}, I_{mpp}, that correspond to unique values of irradiance and temperature one can claim that the use of the MPPT is not required. Although, the use of the MPPT is a good proof that the system can be successfully adjusted in new data and above all that it can be easily expanded in a more complete system, that takes into consideration irradiance and temperature variations. In order to verify the performance of the PV system, for each case of irradiance level mentioned previously, the simulation results using different initial values for the firing angle α will be presented. The validation will follow by comparing the results with the ones obtained by simulating the PV system without the MPPT and a firing angle equal to the one corresponding to the maximum power.

The EMTP-based PV system, shown in Figure 5-4, was used once more for the following simulations, although with the MPPT algorithm added in the inverter control. The corresponding data used are the ones used in the prototype system of the same configuration,

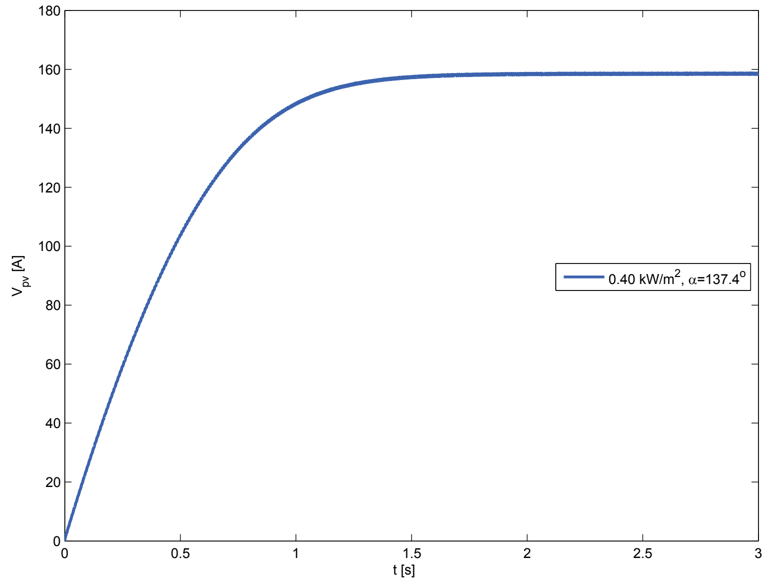

Figure 5-16: PV generator's voltage v_{pv} for $\alpha = 137.4^o$ and irradiance level $0.40kW/m^2$

shown in Table 5-1 and Table 5-2, however with a capacitor $C_f = 55mF$, for irradiance levels of $0.40kW/m^2$ and $0.55kW/m^2$ and different initial firing angle values. The timestep of the simulations was chosen to be $\Delta t = 10^{-6}s$. In addition, the MPPT algorithm is not energised from $t > 0s$ of the simulation and is updated every 5 cycles, in order to provide the system some stability.

5-6-1 Simulation results with MPPT for $0.40kW/m^2$ irradiance level

As explained before, the first step in order to prove the validity of the proposed MPPT algorithm is to compare the simulation results with the ones obtained from the system without using the MPPT and for an appropriate firing angle value, that corresponds to the maximum power of the system. Hence, after running various simulations and numerical calculations, the firing angle corresponding to the maximum PV generator's power P_{max} of the system was detected. Following, the system mentioned above, for irradiance level $0.40kW/m^2$ and a firing angle $\alpha = 137.4^o$ corresponding to the maximum power, is simulated. In Figure 5-16 the PV generator's voltage v_{pv} is presented. As it can be seen the maximum voltage value obtained from this simulation is about $V_{max} = 158.3V$. In Figure 5-17 the PV generator's current i_{pv} can be seen, the maximum value in this case is about $I_{max} = 15A$. In Figure 5-18 the PV generator's power, that corresponds to a firing angle $\alpha = 137.4^o$, is shown. The maximum value is about $P_{max} = 2384W$. The aforementioned digital simulation results are in very good agreement with the values collected from the numerical calculations. As known, the value of the maximum PV power P_{max} should be equal to $P_{max} = V_{max} * I_{max}$.

The next step is to run simulations for different initial values of the firing angle, smaller and greater than the one corresponding to the MPP, in order to check the system's behaviour and

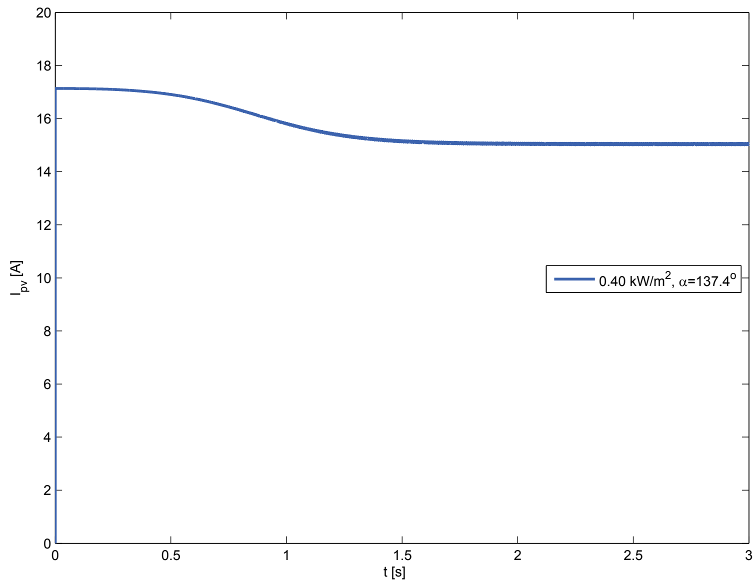

Figure 5-17: PV generator's current i_{pv} for $\alpha = 137.4^o$ and irradiance level $0.40kW/m^2$

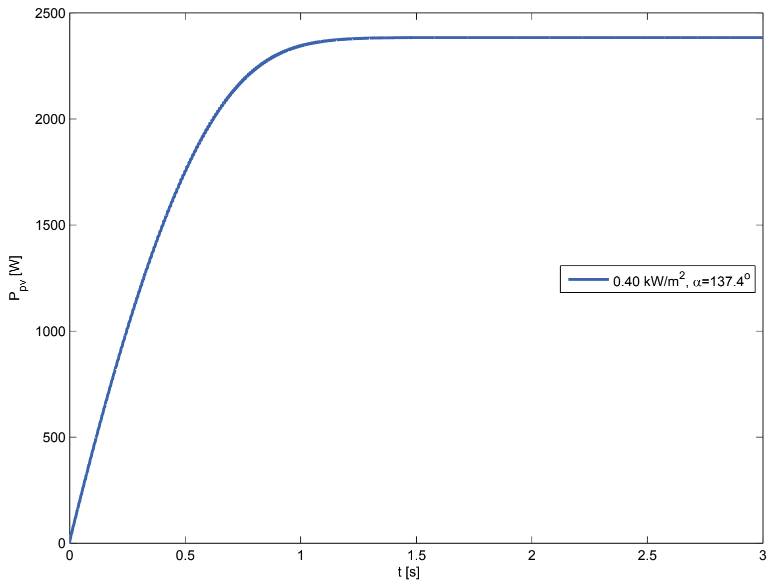

Figure 5-18: PV generator's power p_{pv} for $\alpha = 137.4^o$ and irradiance level $0.40kW/m^2$

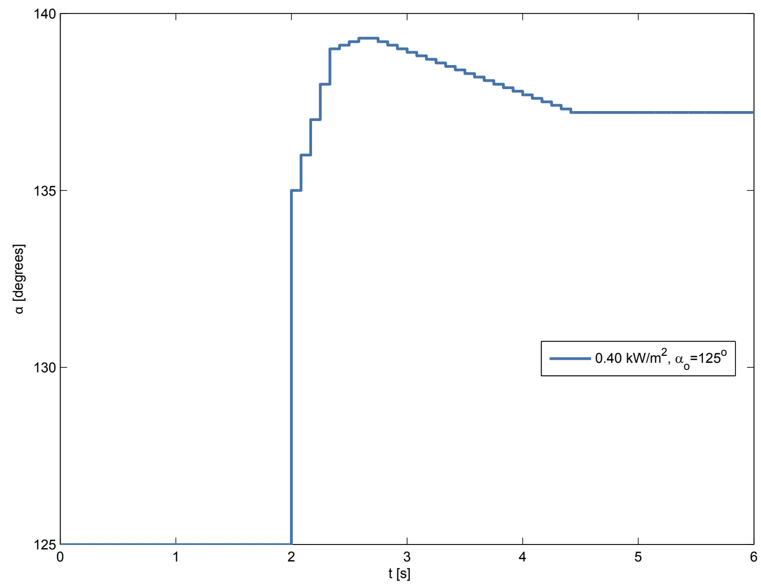

Figure 5-19: Firing angle tracking for $\alpha_o = 125^o$ and irradiance level $0.40kW/m^2$

the effectiveness to reach the desired MPP. For that reason the system configuration, explained in Figure 5-15, is used along with the MPPT algorithm, as presented in Figure 5-13.

The first set of simulation results with respect to an initial firing angle $\alpha_o = 125^o$. In Figure 5-19 the optimal firing angle tracking in respect with time is presented. As it can be seen the tracking changes accordingly to the MPPT algorithm with changes of 0.1, 1 and 10 degrees for every iteration, depending on how far of the MPP the current operating point is. The optimal firing angle value of the inverter voltage, that corresponds to the maximum PV power P_{max}, tracked by the system simulation is $\alpha = 137.4^o$, which is exactly the value that was expected by the previous simulations and calculations. In Figure 5-20 the PV generator's voltage v_{pv} can be seen. The maximum value obtained when the system reaches the steady state, after almost $t = 4.45s$, is about $V_{mpp} = 158V$, a value that is in very good agreement with the one obtained using the same system without the MPPT for optimum firing angle. Accordingly to the v_{pv} changes, the PV generator's current i_{pv} simulation results can be seen in Figure 5-21. It is obvious that the current is decreasing in the time periods that the voltage is increasing and accordingly is reaching the steady state after almost $t = 4.45s$. The maximum value obtained after this moment is about $I_{mpp} = 15.09A$, value again in very good agreement with the one obtained from the same system without the MPPT, running for maximum power. Combining the data of the PV generator's voltage v_{pv} and current i_{pv}, the PV generator's power curve was obtained and shown in Figure 5-22. The maximum value in this case was found at $P_{max} = 2384.01W$, as expected. The rms value of the current injected into the utility grid i_{acrms}, is displayed in Figure 5-23. The big fluctuations of the graphs, seen for $t > 2s$ that the MPPT is energised, are due to the fact that the system is initially found far from the MPPT. From the graphs it is clear that before $t = 2s$ the system is trying to approach a steady state but with the MPPT energised a period for calculating the new values is passing until the system settles to the optimal steady state.

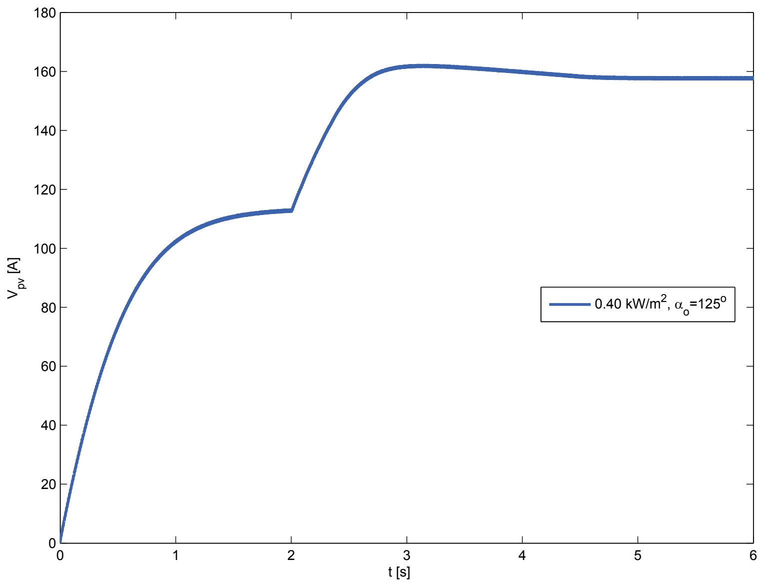

Figure 5-20: The PV generator's voltage v_{pv}, for $\alpha_o = 125^o$ and irradiance level $0.40kW/m^2$

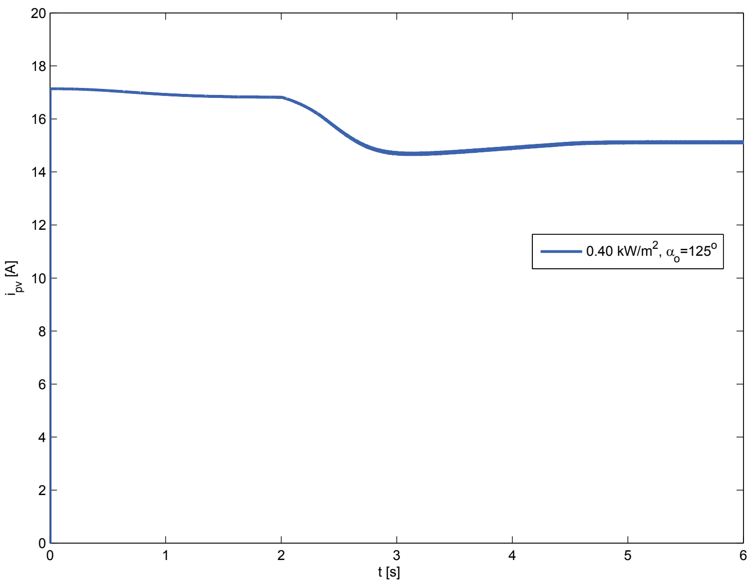

Figure 5-21: The PV generator's current i_{pv}, for $\alpha_o = 125^o$ and irradiance level $0.40kW/m^2$

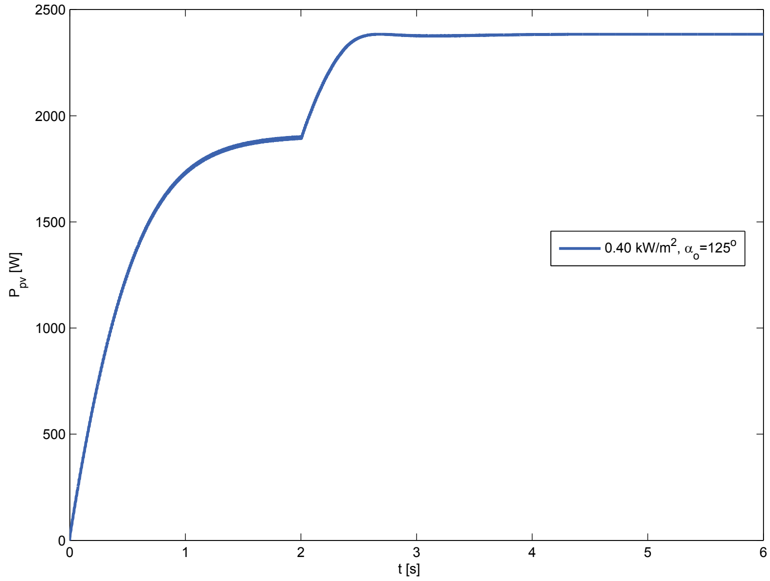

Figure 5-22: The PV generator power's p_{pv}, for $\alpha_o = 125^o$ and irradiance level $0.40kW/m^2$

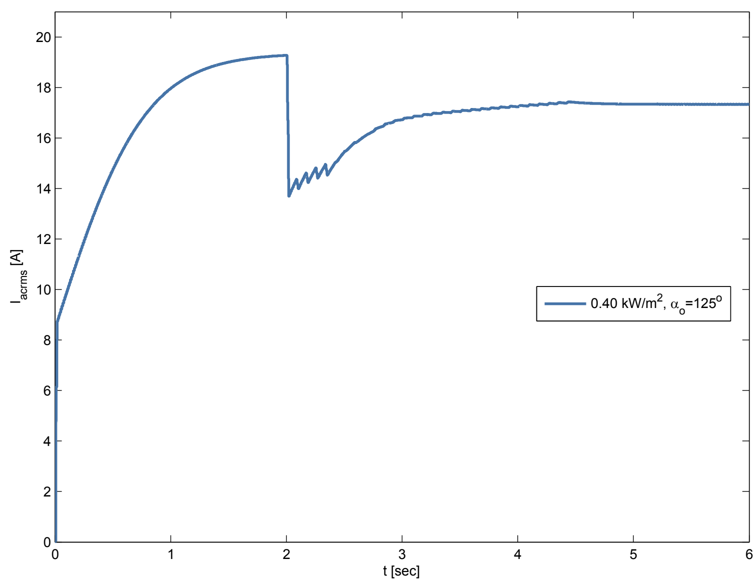

Figure 5-23: The current (rms) injected into the utility grid i_{ac}, for $\alpha_o = 125^o$ and irradiance level $0.40kW/m^2$

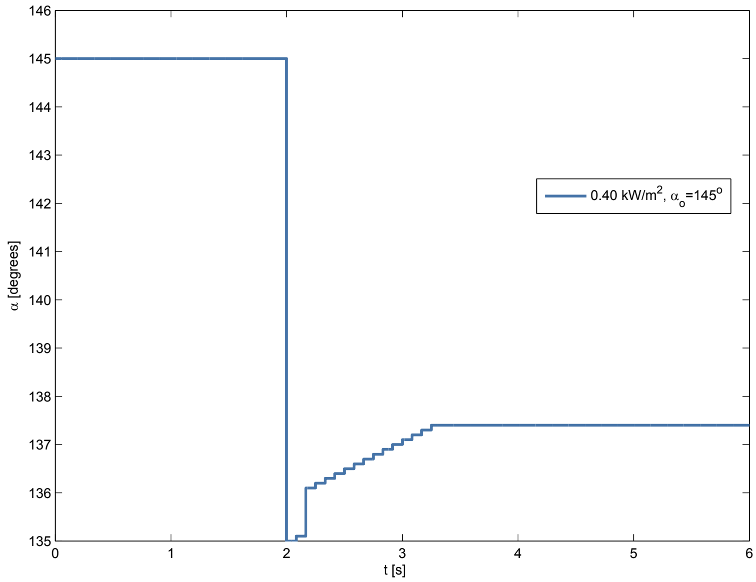

Figure 5-24: Firing angle tracking for $\alpha_o = 145^o$ and irradiance level $0.40kW/m^2$

The next step is to approach the MPP with an initial firing angle greater than the one expected. So, the value is set at $\alpha_o = 145^o$. In Figure 5-24 the optimal firing angle tracking with respect to time is presented for this case. The tracking is following precisely the MPPT algorithm. The optimal firing angle, that corresponds to the maximum PV power P_{max}, tracked by the system is found at $\alpha = 137.4^o$, once more the value as expected. In Figure 5-25 the PV generator's voltage v_{pv} can be seen. The maximum value obtained when the system reaches the steady state, after almost $t = 3.5s$, is about $V_{mpp} = 158.4V$, once more value that is in very good agreement with the one obtained from the same system without the MPPT and for maximum power. Following, the PV generator's current i_{pv} curve can be seen in Figure 5-26. The maximum value, obtained after this point, is about $I_{mpp} = 15.05A$, a value really close to the one obtained from the same system without the MPPT. The PV generator's power curve is shown in Figure 5-27. The maximum value in this case is found to be $P_{max} = 2383.95W$, a value which agrees with the one expected. The rms value of the current injected into the utility grid i_{acrms}, is displayed for this case in Figure 5-28.

Here, the MPPT algorithm is energised for $t > 2s$ as well and the firing angle drops 10 degrees exactly after the MPP starts the tracking. That means that the system is initially found operating at a point far from the MPPT. This causes the spikes seen in the graphs, especially in Figure 5-27 and in Figure 5-28 at the time instant after $t = 2s$.

5-6-2 Simulation results with MPPT for $0.55kW/m^2$ irradiance level

Following the steps explained in the previous section, for the irradiance level of $0.55kW/m^2$ the firing angle corresponding to the maximum PV generator power P_{max} of the system is calculated, after running various simulations and numerical calculations. Thus, the same system as explained previously, for irradiance level $0.55kW/m^2$ and an optimum firing angle

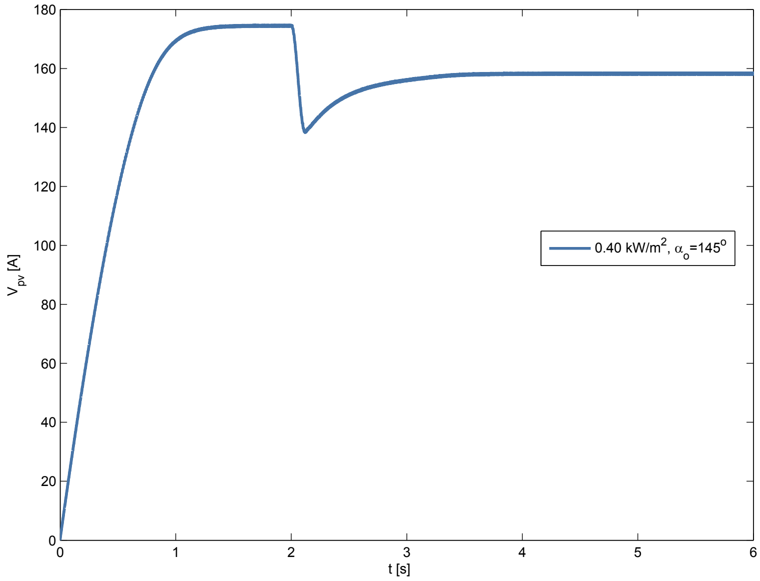

Figure 5-25: The PV generator voltage v_{pv}, for $\alpha_o = 145^o$ and irradiance level $0.40kW/m^2$

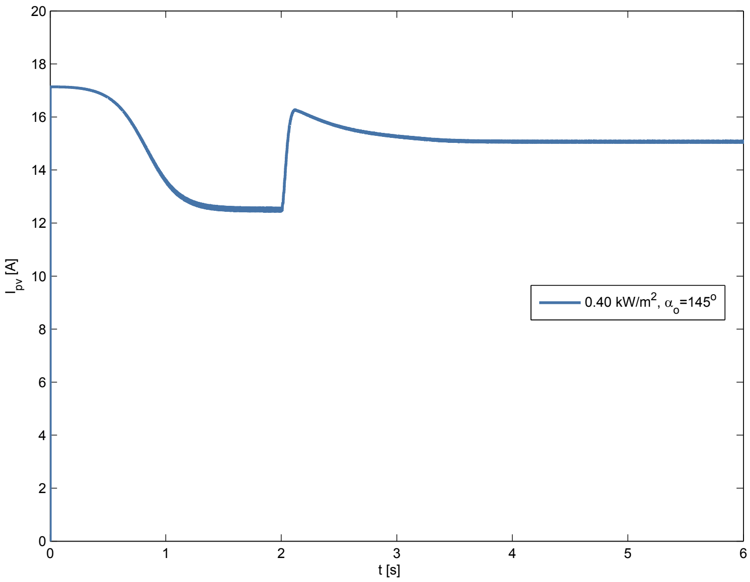

Figure 5-26: The PV generator's current i_{pv}, for $\alpha_o = 145^o$ and irradiance level $0.40kW/m^2$

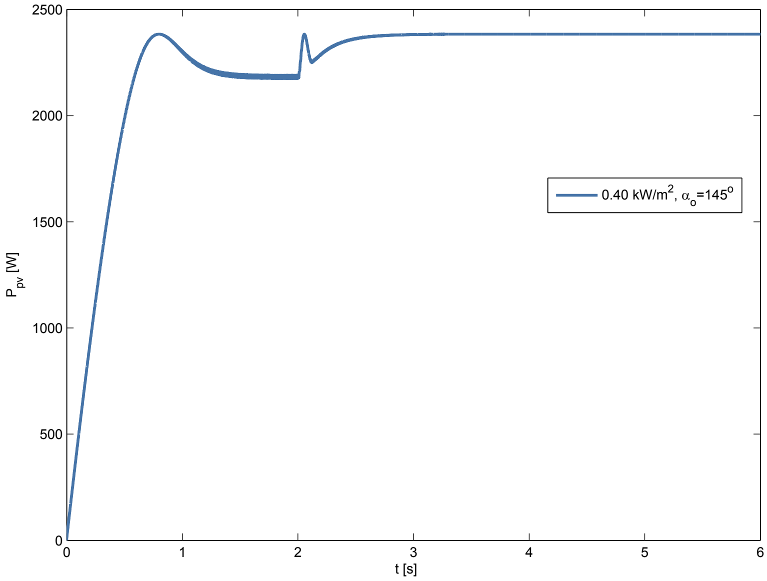

Figure 5-27: The PV generator's power p_{pv}, for $\alpha_o = 145^o$ and irradiance level $0.40kW/m^2$

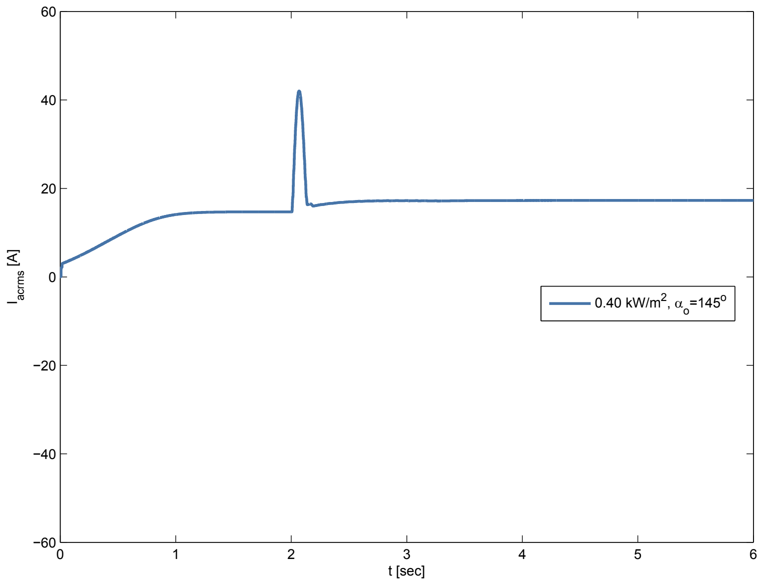

Figure 5-28: The current (rms) injected into the utility grid i_{ac}, for $\alpha_o = 145^o$ and irradiance level $0.40kW/m^2$

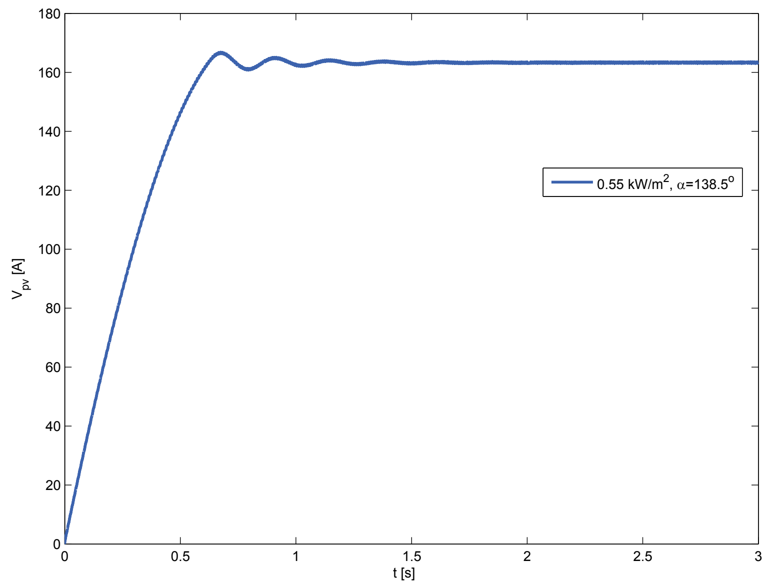

Figure 5-29: PV generator's voltage v_{pv} for $\alpha = 138.5^o$ and irradiance level $0.55kW/m^2$

$\alpha = 138.5^o$, is simulated. In Figure 5-29 the PV generator's voltage v_{pv} curve is shown. As it can be seen the maximum voltage value obtained from this simulation is about $V_{max} = 163.51V$. In Figure 5-30 the PV generator's current i_{pv} is presented, where the maximum value was detected at about $I_{max} = 20.82A$. In Figure 5-31 the PV generator's power, that corresponds to a firing angle $\alpha = 138.5^o$, is shown. As can be seen the maximum value is $P_{max} = 3405.4W$. All the above simulation results are in excellent agreement with the numerical calculations computed initially.

The next step to follow, with the same settings, is to run simulations for different initial values of the firing angle, smaller and greater than the one corresponding to the MPP, in order to check the system's performance. The same system configuration, explained in Figure 5-15, is used once more.

The first set of simulation results is obtained by setting an initial firing angle $\alpha_o = 130^o$. In Figure 5-32 the optimal firing angle tracking is presented. As it can be seen, also in this set of simulations, the tracking is strongly following the MPPT algorithm with changes of 0.1, 1 and 10 degrees for every iteration, depending on how far of the MPP the current operating point is. The optimal firing angle value of the inverter voltage, that corresponds to the maximum PV power P_{max}, tracked by the system simulation is $\alpha = 138.5^o$, which is exactly the value that was expected by the previous simulations and calculations. In Figure 5-33 the PV generator's voltage v_{pv} can be seen. The maximum value obtained when the system reaches the steady state, after almost $t = 3.55s$, is about $V_{mpp} = 163.52V$, a value that is in very good agreement with the one obtained from the same system without the MPPT for maximum power, as explained at the beginning of the section. Respectively, the PV generator's current i_{pv} simulation results are presented in Figure 5-34. It is clear that the current is decreasing in the time periods that the voltage is increasing and accordingly is reaching the steady state almost after $t = 3.55s$. The maximum value obtained after this

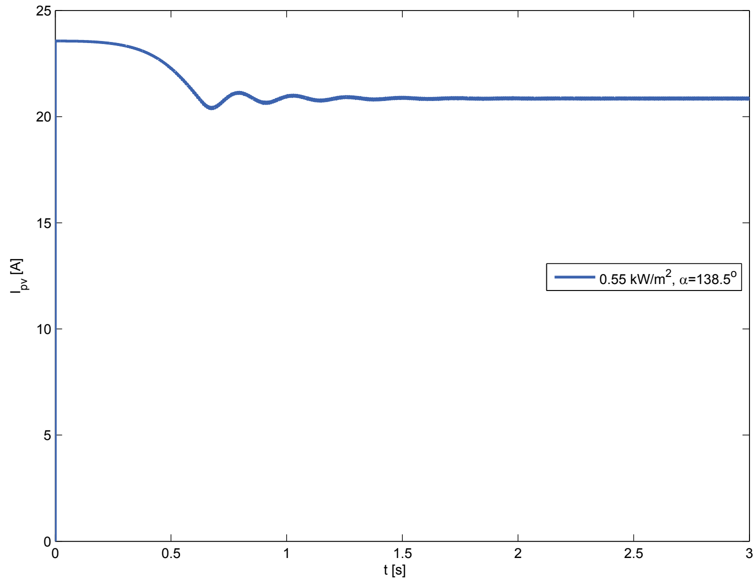

Figure 5-30: PV generator's current i_{pv} for $\alpha = 138.5^o$ and irradiance level $0.55kW/m^2$

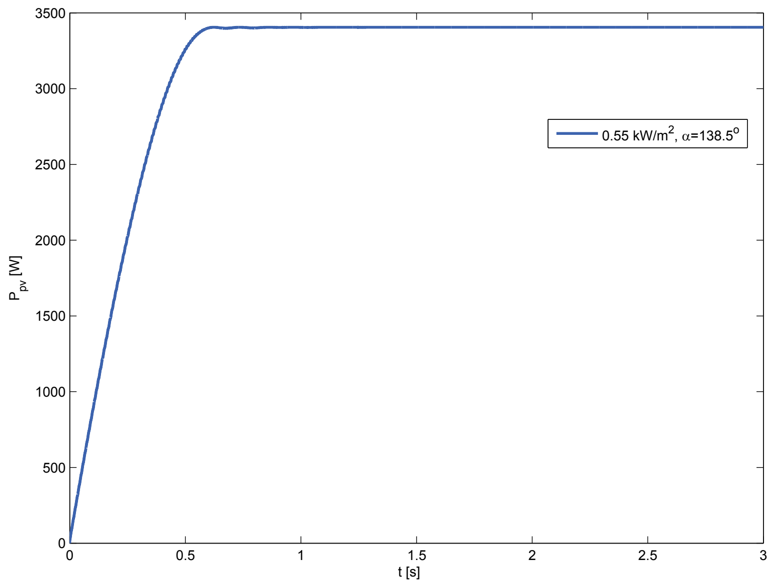

Figure 5-31: PV generator's power p_{pv} for $\alpha = 138.5^o$ and irradiance level $0.55kW/m^2$

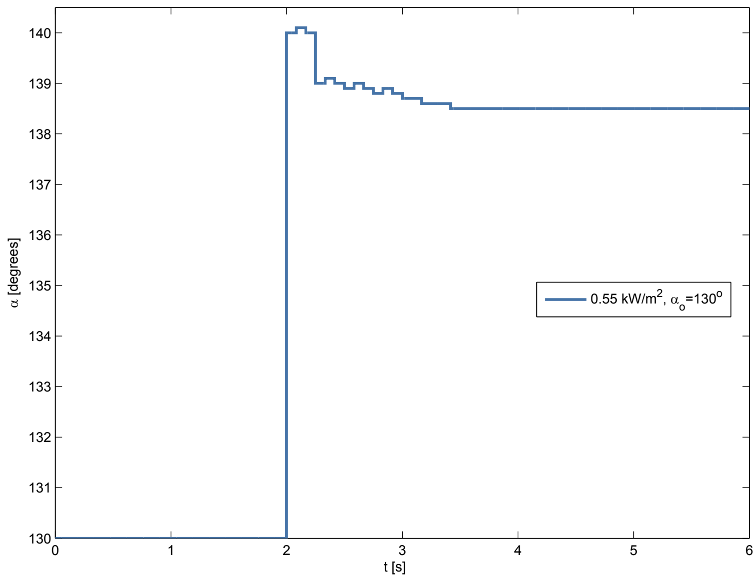

Figure 5-32: Firing angle tracking for $\alpha_o = 130^o$ and irradiance level $0.55kW/m^2$

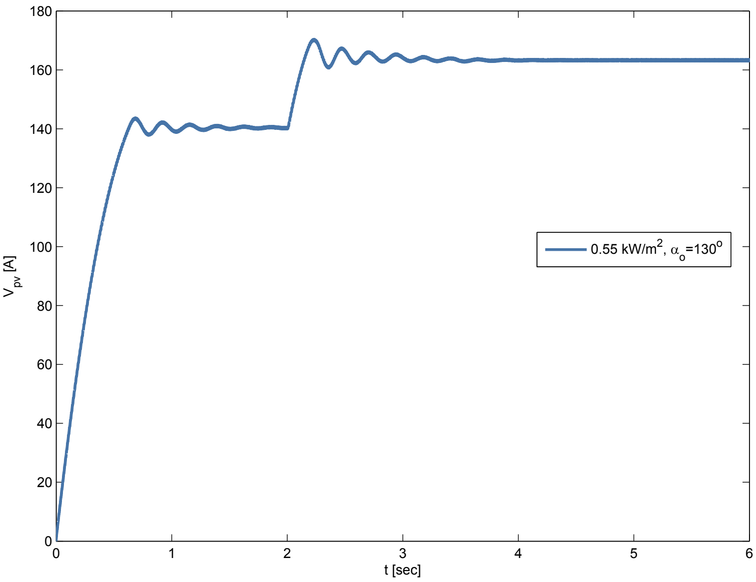

Figure 5-33: The PV generator's voltage v_{pv}, for $\alpha_o = 130^o$ and irradiance level $0.55kW/m^2$

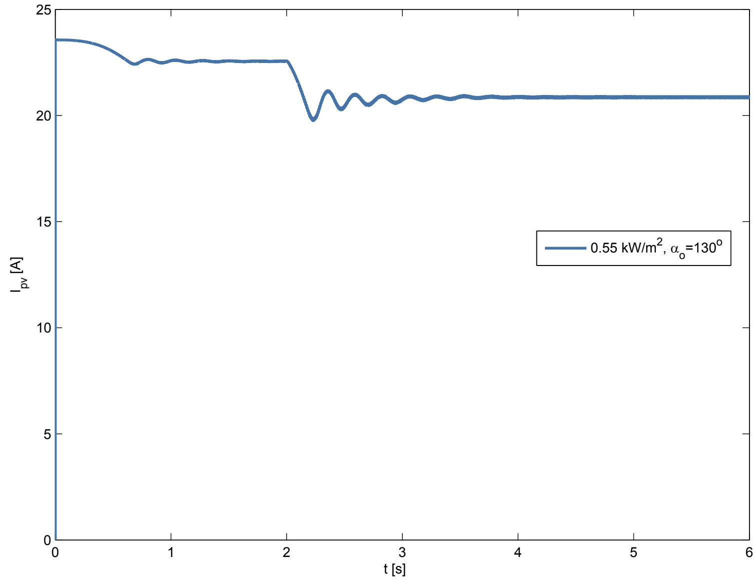

Figure 5-34: The PV generator's current i_{pv}, for $\alpha_o = 130^o$ and irradiance level $0.55kW/m^2$

moment is about $I_{mpp} = 20.82A$, a value in excellent agreement with the one explained at the beginning of the section. Subsequently, the PV generator's power curve is obtained and shown in Figure 5-35. The maximum value in this case is found at $P_{max} = 3405.5W$, as expected. The rms value of the current injected into the utility grid i_{acrms}, is displayed in Figure 5-36. In this simulation, the MPPT algorithm is again energised for $t > 2s$ and the firing angle increases 10 degrees exactly after the MPP starts tracking. So, the system is initially found operating at a point far from the MPPT, which causes the big spike seen in Figure 5-36 at the time instant exactly after $t = 2s$. In addition, for this simulation case the transient regime is longer while the system is trying to settle in a steady state, for the period of time prior to the MPPT energisation, compared to the simulation cases of the previous section. During this period only the inverter controller is active controlling the firing angle. As it is known, every controller parameter is tuned for one range of values, which in this case is the PV generator's power. When the same controller is used for another range of values it may lead to some overshoot or damping and the settling time may increase or decrease slightly, compared to the PV power for which it is tuned. In conclusion, the inverter controller is tuned for the values corresponding to the previous section, causing this transient response prior to the MPPT energisation.

Similarly to the case shown above, the following action is to approach the MPP with an initial firing angle greater than the one expected. So, the value is set at $\alpha_o = 150^o$. In Figure 5-37 the optimal firing angle tracking in respect with time is presented for this case. The tracking is following precisely the MPPT algorithm. The optimal firing angle, that corresponds to the maximum PV power P_{max}, tracked by the system is found at $\alpha = 138.5^o$, as expected. The demonstration of the PV generator's voltage v_{pv} can be found in Figure 5-38. The maximum power point, obtained when the system settles in the steady state almost after $t = 3.55s$ of transient regime, is tracked at $V_{mpp} = 163.6V$ voltage, once more value that is in very good

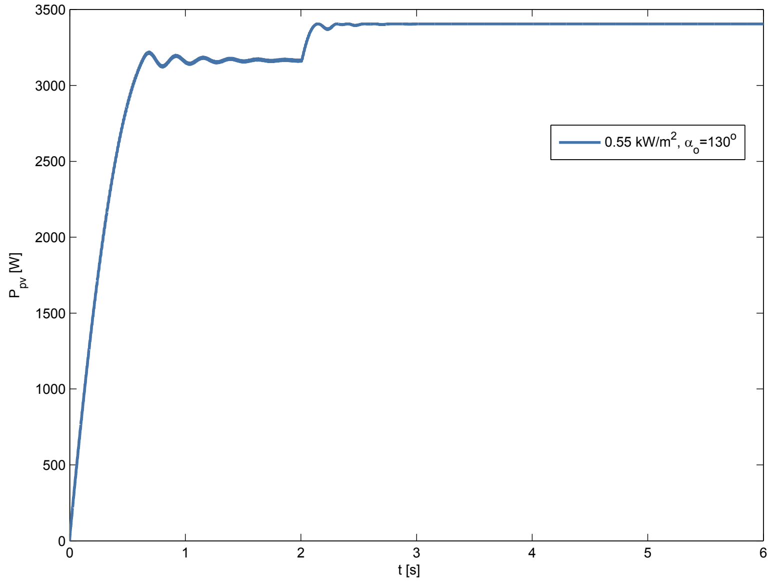

Figure 5-35: The PV generator's power p_{pv}, for $\alpha_o = 130^o$ and irradiance level $0.55kW/m^2$

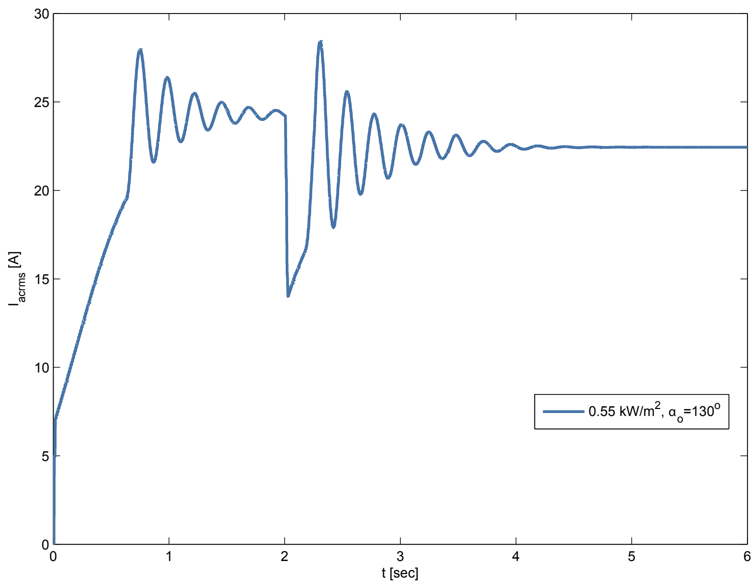

Figure 5-36: The current (rms) injected into the utility grid i_{ac}, for $\alpha_o = 130^o$ and irradiance level $0.55kW/m^2$

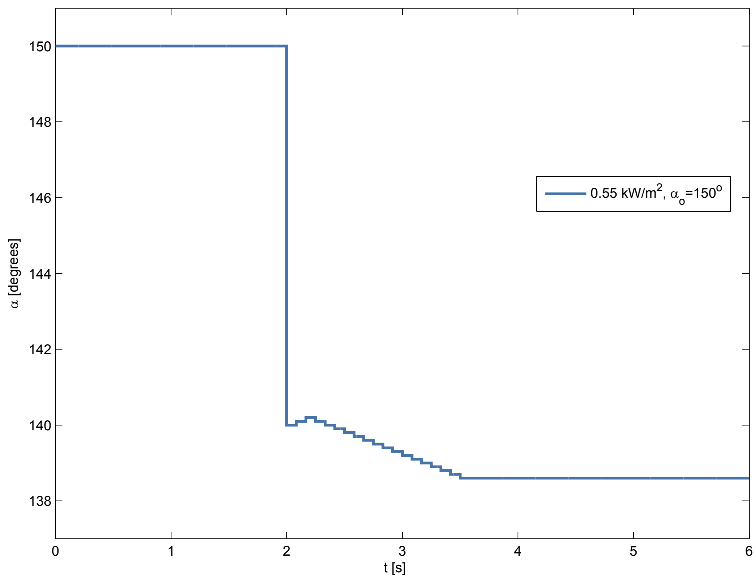

Figure 5-37: Firing angle tracking for $\alpha_o = 150^o$ and irradiance level $0.55kW/m^2$

agreement with the one obtained using the same system without the MPPT for maximum power. The PV generator's current i_{pv} curve is shown in Figure 5-39. The maximum value, at which the MPP is tracked after the transient regime, is about $I_{mpp} = 20.79A$. The PV generator's power curve is presented in Figure 5-40. The maximum value in this case is found $P_{max} = 3405.48W$, value in accord with the one expected. The rms value of the current injected into the utility grid i_{acrms}, is displayed for this case in Figure 5-41. The conclusions of this simulation are quite similar to the above mentioned case. The MPPT algorithm is again energised for $t > 2s$ and the firing angle abruptly decreases exactly after the MPP starts the tracking. So, the system is initially found operating at a point far from the MPPT and this causes the big spike clearly seen in Figure 5-41 at the time instant exactly after $t = 2s$.

After running all simulations, explained in the previous sections, we can conclude that the system responds to the changes of the firing angle successfully. It can predict, with a quite good accuracy, the value that corresponds to the maximum PV power. All the simulation results, as previously mentioned, coincide with the results of the numerical calculations but also are really close to the V_{oc}, I_{sc}, V_{mpp}, I_{mpp} values given as data for each simulated PV generator. Small differences might occur due to numerical errors at the simulations, which associate directly with the value of the chosen timestep. In addition, the MPPT algorithm is built in a way that it can track the optimal operating point that is within between accepted limits. So, the predicted values can not always be in full agreement with the given data and a small error is expected. It has to be mentioned again that the implementation of the MPPT in this system can prove that the user can have great controllability of the system and the operating point for every time instant can be detected on the $i_{pv} - v_{pv}$ and $p_{pv} - v_{pv}$ curves, regardless of the circumstances.

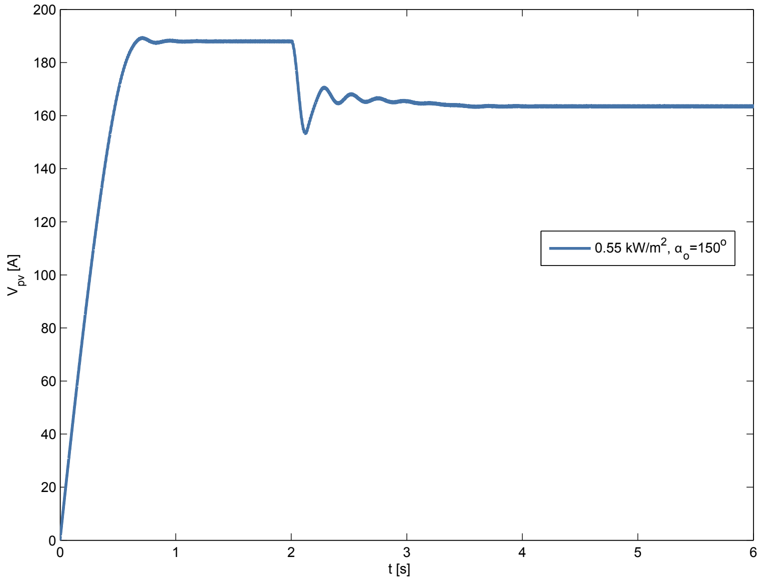

Figure 5-38: The PV generator's voltage v_{pv}, for $\alpha_o = 150^o$ and irradiance level $0.55kW/m^2$

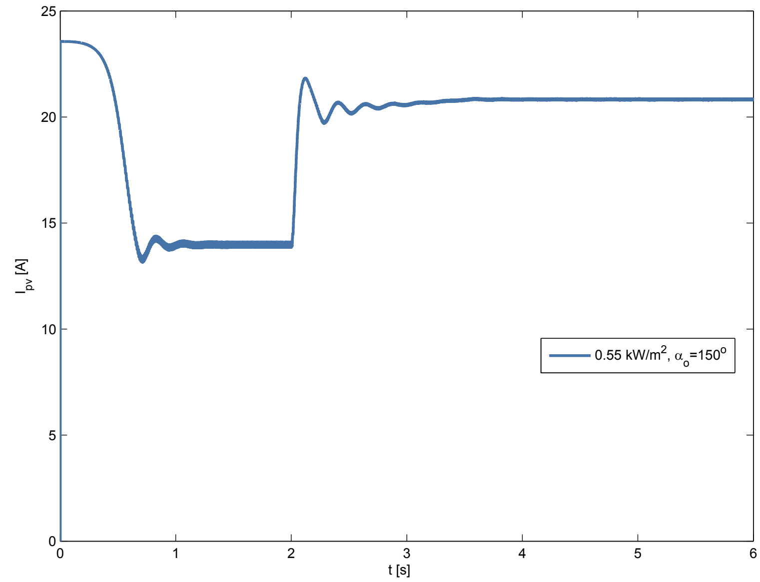

Figure 5-39: The PV generator's current i_{pv}, for $\alpha_o = 150^o$ and irradiance level $0.55kW/m^2$

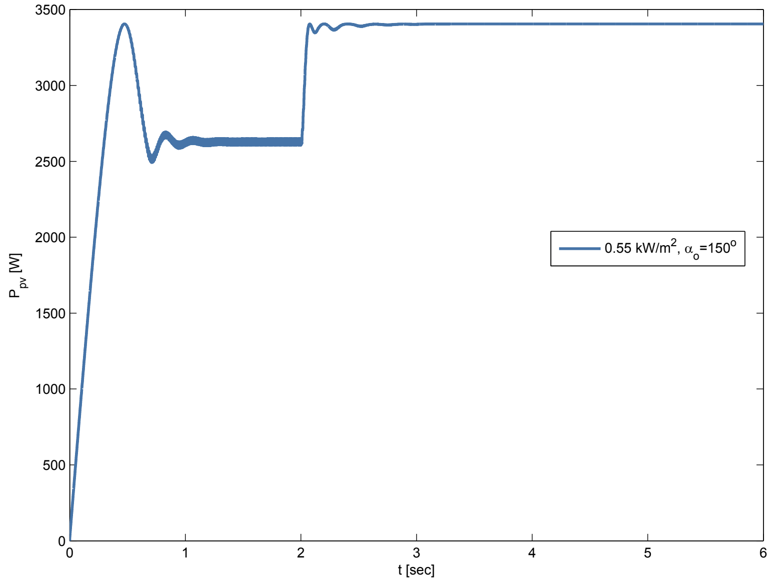

Figure 5-40: The PV generator's power p_{pv}, for $\alpha_o = 150^o$ and irradiance level $0.55kW/m^2$

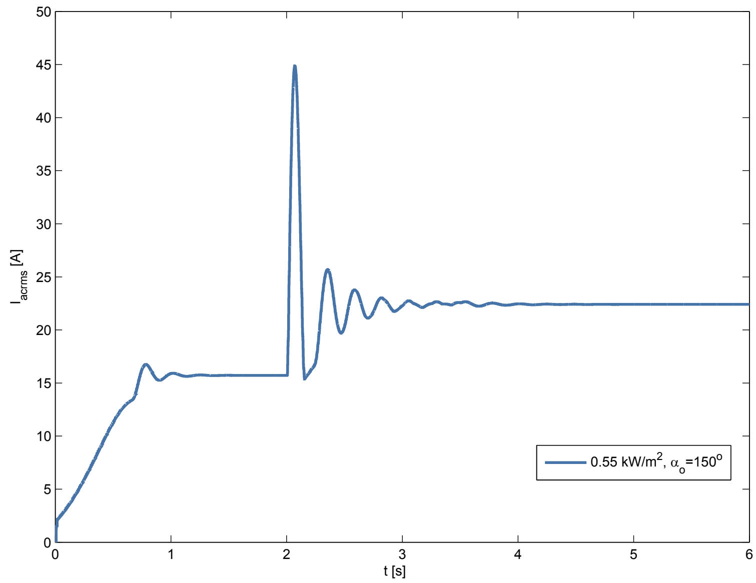

Figure 5-41: The current (rms) injected into the utility grid i_{ac}, for $\alpha_o = 150^o$ and irradiance level $0.55kW/m^2$

5-7 Model optimisation

As we saw in previous sections, the characteristics of the PV generator depend on the variations of the cell temperature T_c and irradiance G, which actually affect the I_{sc}, the V_{oc} and consequently change the power p_{pv} of the generator. As explained before, in order to optimise the ENRC based PV generator model and take into consideration the irradiance and temperature effect, four new equations had to be added in the generator model. Equations (4-24), (4-25), (4-26) and (4-27) were used, so that the new data of the PV generator could be determined for any irradiance and temperature change. In this section, the proposed MPPT method and the optimisation scheme of the PV generator will be investigated and verified under rapid variations of the solar array temperature and the solar irradiance.

5-7-1 Simulation and results

For the ATP simulation the system, shown in Figure 5-4, was chosen for the reference irradiance level of $0.40kW/m^2$ and an initial firing angle of $\alpha_o = 110^o$. The data from Table 5-2 we taken as reference values, since the data for STC were not available in McNeil et al.[32], where the same system was initially used and presented. For defining the irradiance and temperature factors and functions that are needed for the equations shown above, the table given in Marion et al.[30] was again used, with the data corresponding to the specific PV generator highlighted as also shown in Table 4-3. The system was simulated for a frequency $f_r = 60Hz$ and a timestep $\Delta t = 10^{-6}s$. The approach used in order to demonstrate the performance of the system was to make a choice box in the PV generator model, as can be seen in Figure 5-42. The choice box, called "Scenario", corresponds to 4 possible choices:

- Scenario=1 $\longrightarrow$ No variations
- Scenario=2 $\longrightarrow$ Irradiance variations
- Scenario=3 $\longrightarrow$ Temperature variations
- Scenario=4 $\longrightarrow$ Irradiance and temperature variations

To examine the performance of the system all four scenarios were simulated and the results will be presented and explained in the following section for each case. However, scenario 1 will not be demonstrated, since it coincides with the results presented in previous sections.

Scenario 2

With increasing irradiance, the current I_{sc} increases almost linearly, while the voltage V_{oc} slightly increases and thus the MPP varies [7]. When MPP changes due to irradiance variations, the MPP tracking in dynamic conditions is then analysed using staircase or trapezoidal irradiance profiles. In most of the cases, trapezoidal irradiance profiles are used to test the inverter in dynamic irradiance conditions [38]. Figure 5-43 shows the trapezoidal irradiance profile, chosen in this case. The output power, voltage, current and firing angle trajectories are shown in Figure 5-44. For this simulation the MPPT was energised for $t > 0s$. The tran-

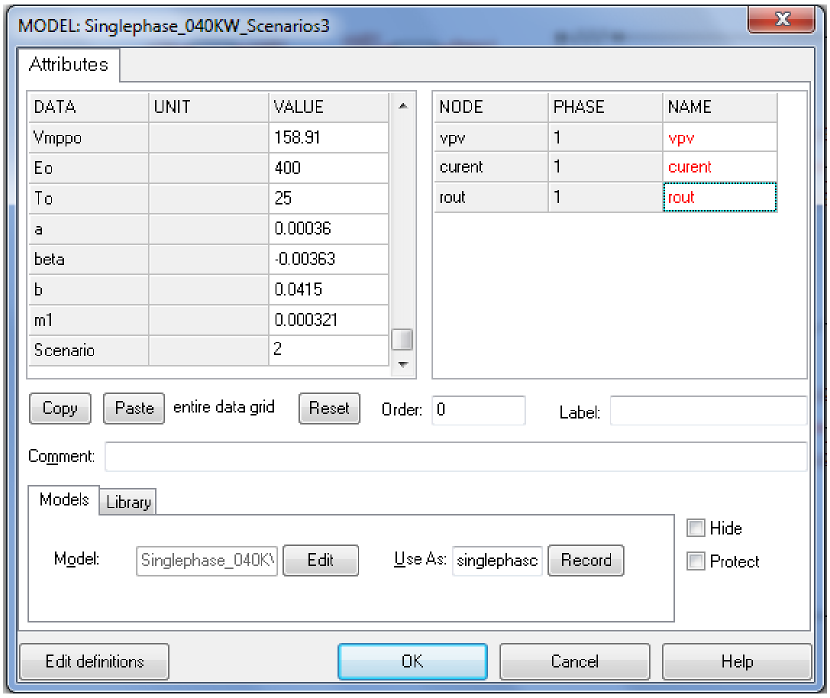

Figure 5-42: The choice box in the PV generator model

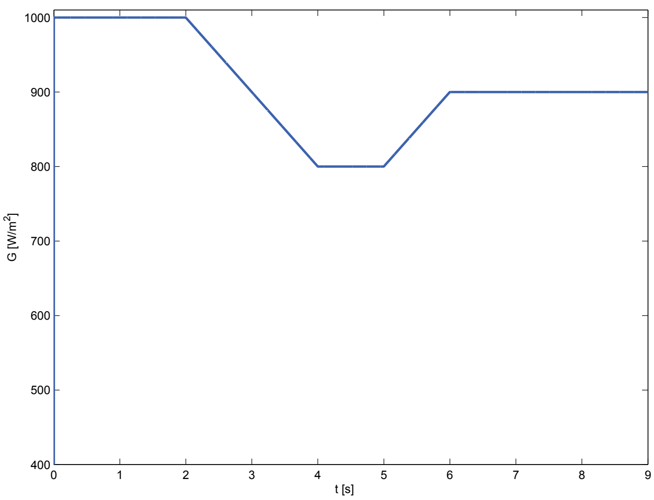

Figure 5-43: Trapezoidal irradiance profile for the dynamic MPPT efficiency test

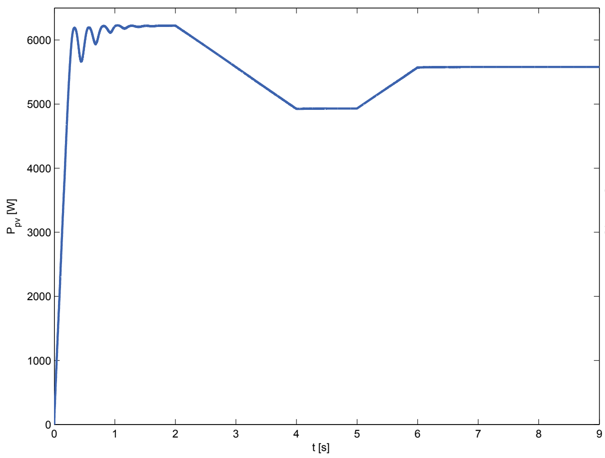

(a) PV generator power P_{pv}

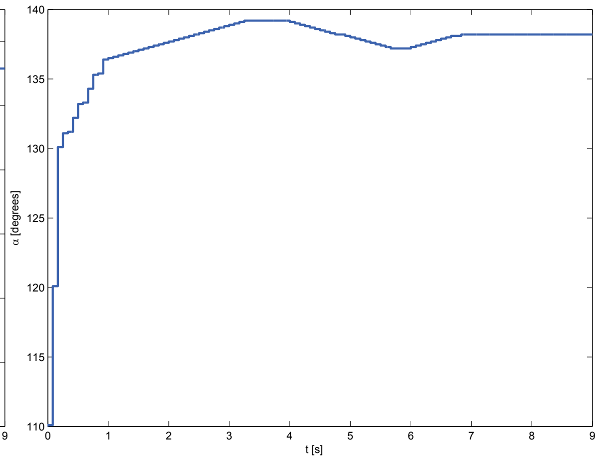

(b) Firing angle α

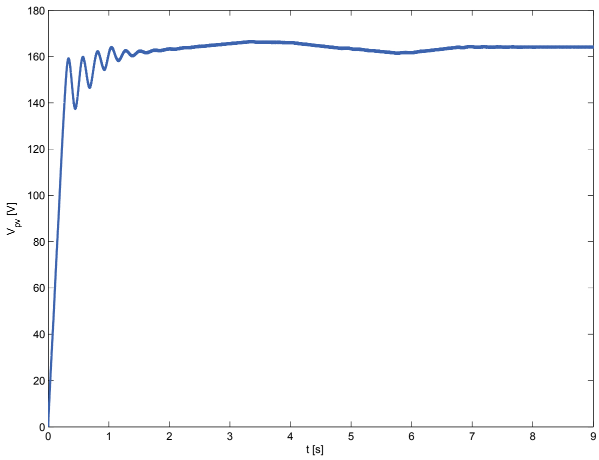

(c) PV generator voltage V_{pv}

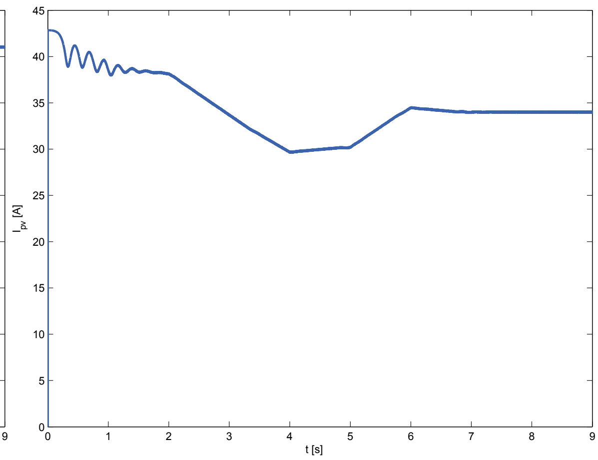

(d) PV generator current I_{pv}

Figure 5-44: Trapezoidal irradiance profile test results sient response of the system, clearly shown in the first seconds of the simulation, is mainly due to numerical instability, since the system data have to change directly regarding the abrupt irradiance change from $0.40kW/m^2$ to $1kW/m^2$. The system values at the steady state are found about $v_{pv} = 164.3V$, $i_{pv} = 34A$, $p_{pv} = 5579.5W$ while the firing angle settles in about $\alpha = 138.2^o$.

In order to validate this performance one has to carefully examine the efficiency of a PV module and how this is defined. In general, the conversion efficiency of a PV module is the proportion of the sunlight energy, that is received and is converted to electrical energy. More specifically, is the ratio between the module's output and incident light power [7]:

$$\eta = \frac{P_{out}}{P_{in}} = \frac{V_{pv} \cdot I_{pv}}{A_{pv} \cdot G} \tag{5-4}$$

where A_{pv} is the solar module surface and G the irradiance.

To be more accurate the "true" efficiency of the panel is the multiplication of several factors, such as the junction temperature increase, the power losses by Joule effect in the cables, the factor due to losses in the inverter and the factor related to the MPPT. Only one of the factors is the efficiency presented in equation (5-4) and is the one best suited in this system, since for simplicity reasons the rest of the factors were omitted in this project.

However, in the case examined in this project the surface of the PV generator remains the same through the whole simulation and the efficiency of the generator is considered to be constant. Thus, from equation (5-4) and the system characteristics, it is now clear that the power output p_{pv} of the generator is expected to be proportional to the irradiance G. This is actually proved and presented in Figure 5-44. So, in the case of a trapezoidal irradiance variation, that can occur in the case that the sun is temporarily shadowed, the MPPT tracking is working properly. This validates the good design of the MPPT algorithm and of course the optimisation scheme proposed.

Scenario 3

While running simulations for this case, the system has to adapt in temperature variations. With an increase in temperature the rate of photon generation increases, hence the reverse saturation current increases and this causes a decrease in the band gap. As a result, PV current slightly changes while this leads to major changes in the voltage. Temperature in total affects negativity the solar cell performance [7]. Figure 5-45 shows the temperature profile, chosen in this case. The digital simulation results are shown in Figure 5-46. For this simulation the MPPT was active for $t > 1s$. At the steady state the system roughly settles at $v_{pv} = 160.7V$, $i_{pv} = 15.09A$, $p_{pv} = 2422.9W$ and the optimal firing angle at $\alpha = 138^o$. As it can be seen in the graphs, the settling to the steady state regime, follows the incremental change of the firing angle towards its final value.

In order to validate the performance of the system, while simulating the given temperature profile, numerical calculations have been simulated also in Matlab using equations (4-24), (4-25), (4-26) and (4-27), so that the results could be compared. The outcome of the comparison shows clearly that the digital EMTP-based simulations can successfully deliver the results expected from the numerical calculations. Unfortunately, the results could not be evaluated

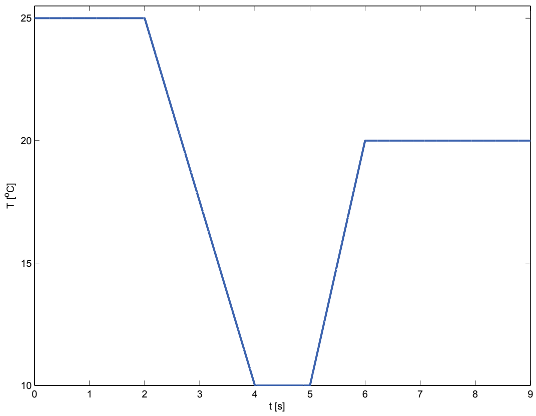

Figure 5-45: Temperature profile for the dynamic MPPT efficiency test

using the temperature coefficients for power, V_{oc} and I_{sc} normally given in the PV datasheet. The PV datasheet for this case was not available and the results were not comparable with the coefficients of the most recently used PV's, since the data used for this system and found also in McNeil et al.[32] can be considered outdated.

To conclude, from the graphs presented in this case it can be confirmed that the effect of the temperature variation in the PV output voltage is quite significant. In addition the results show excellent agreement with the numerical calculation results. So, also in the case of temperature variation the MPPT tracking is working properly. This validates the good design of the MPPT algorithm and of course the optimisation scheme proposed in this case.

Scenario 4

The choice 4 of the scenario box corresponds to both irradiance and temperature variations. In this case, the profiles used in the previous sections and showed in Figure 5-43 and Figure 5-45 are again chosen.

The digital simulation results are shown in Figure 5-47. For this simulation the MPPT is activated for $t > 0s$, so the transient response of the system at the first seconds of the simulation is quite clear. The system values at the steady state were found roughly at about $v_{pv} = 167.1V$, $i_{pv} = 33.8A$, $p_{pv} = 5663.3W$ and the maximal firing angle at $\alpha = 139.4^o$.

As in the previous case, the validation of the digital simulations came from the good agreement with the results of numerical calculations in Matlab. Finally, from the graphs presented it can be confirmed that the effect of the irradiance variation effect plays a significant role compared to the temperature variation, since it is clear that the output current changes almost linearly with the change in the irradiance. So, also in the case of irradiance and temperature variation the MPPT tracking is working properly. This validates once more the MPPT algorithm and the optimisation scheme.

Since the value of the increment size in the MPPT algorithm is system dependent, in all the above mentioned cases had to be determined experimentally. The value of the oscillation

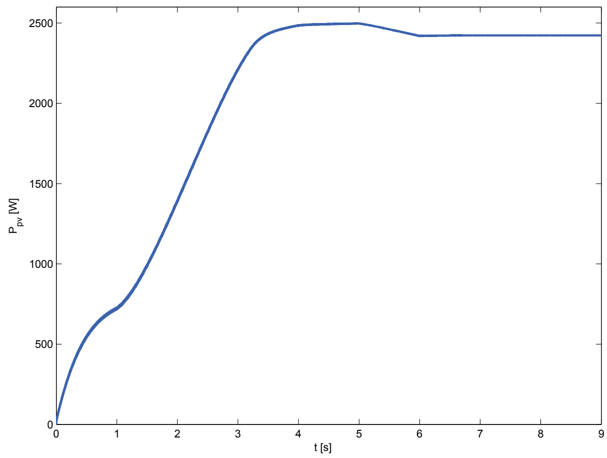

(a) PV generator power P_{pv}

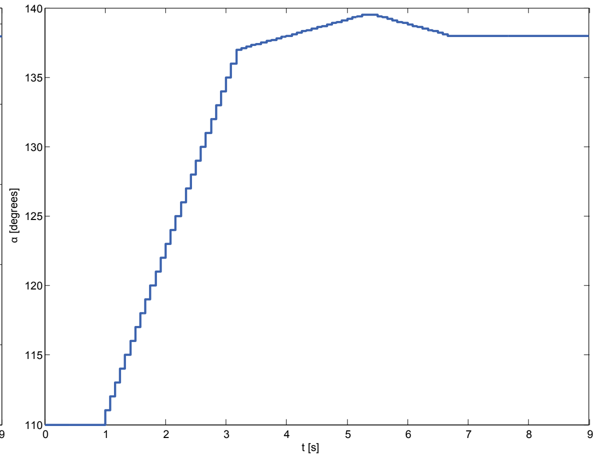

(b) Firing angle α

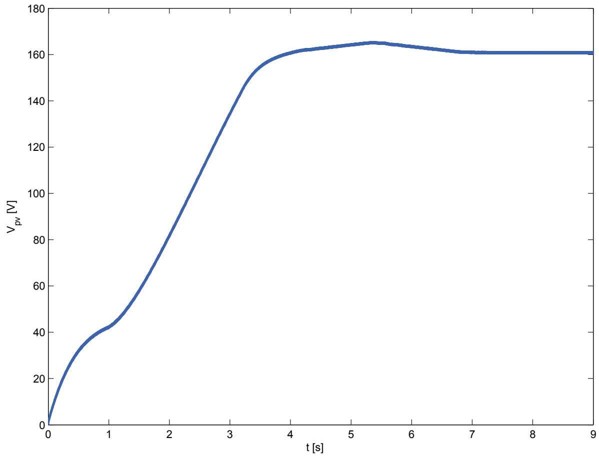

(c) PV generator voltage V_{pv}

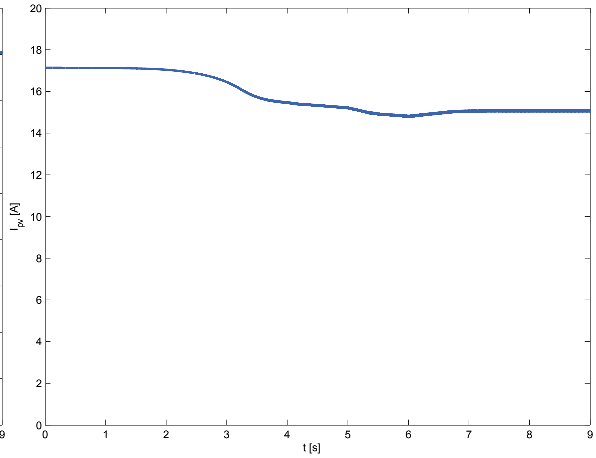

(d) PV generator current I_{pv}

Figure 5-46: Temperature profile test results

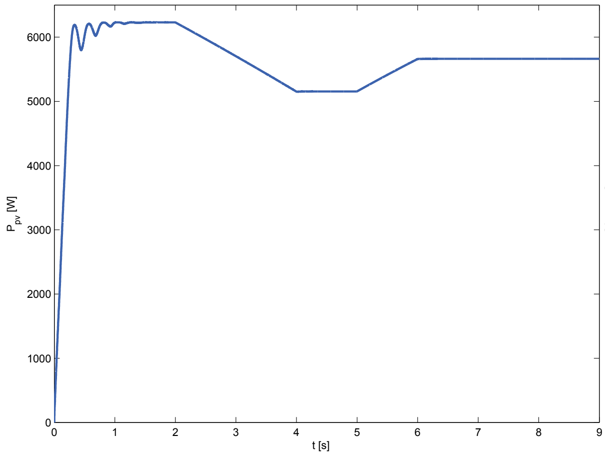

(a) PV generator power P_{pv}

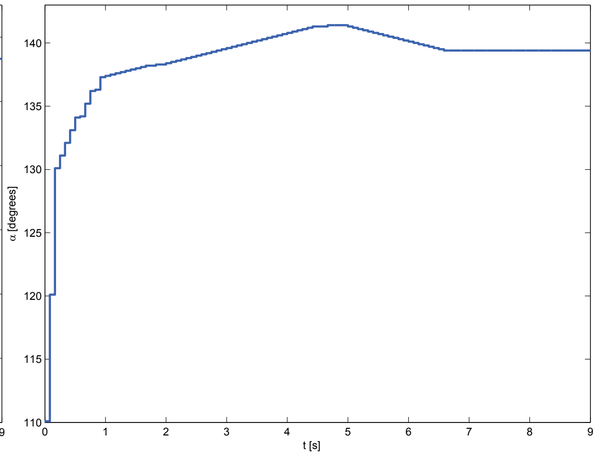

(b) Firing angle α

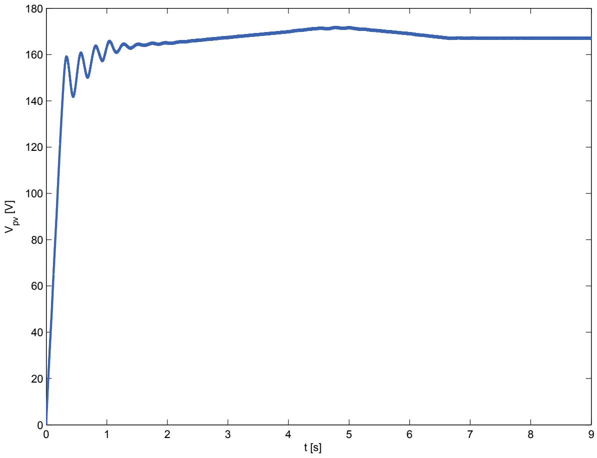

(c) PV generator voltage V_{pv}

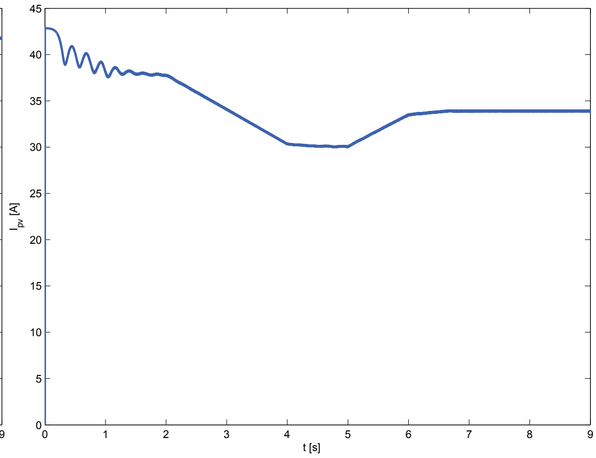

(d) PV generator current I_{pv}

Figure 5-47: Irradiance and temperature profile test results limits $\pm\varepsilon$ is also system dependent and had to be determined regarding the frequency of the system and the timestep of the digital simulation for each case.

At this point, one might object regarding how realistic the abrupt changes in irradiance and temperature are. For this reason, it should be made clear that the goal of this optimisation proposal was to prove the controllability and good design of the MPPT algorithm and the accuracy on delivering correct results of the proposed system.

Chapter 6

Case studies using hybrid PV/battery grid-connected system

As stated in Chapter 5, the implementation of PV distributed generation systems, such as PV's connected to the utility grid, has increased drastically in the last decades mainly due to the need of supplying the rising demand for electric power worldwide. However the disadvantage of PVs is their intermittent generation due to big changes in weather conditions. In order to overcome these disadvantages, energy storage elements can be used. Due to the mature technology battery energy storage systems are widely used to maintain the PV generation output stable and reliable, enhancing both steady and dynamic behaviours of the whole system [39]. Following this line, this chapter presents the way that the EMTP-based model of the PV generator, presented in previous chapters, can be associated with three-phase grid-connected systems and more specifically with a hybrid PV/battery three-phase grid-connected system. For simplicity reasons an established system, built and presented as part of the past graduation project Alberto[40], simulated using MATLAB/Simulink, is used so that the EMTP-based models can be tested and validated in a three-phase scenario. Another reason for choosing this system is that in general MATLAB/Simulink models are appropriate for studies regarding the performance of hybrid systems. In addition, dynamic operation and control system strategies can be easily incorporated in an existing model to facilitate studies on the overall performance of the system [39].

In the following sections the basic building blocks of a three-phase grid-connected PV system will be presented and analysed. Then, the models developed in MATLAB/Simulink will be combined with the EMTP-based models, explained previous chapters. In order to verify the proposed system four different case studies will be performed and the dynamic performance of the system will be tested and analysed.

6-1 System configuration

The configuration of the system can be seen in Figure 6-1. The system will operate in dispatch mode. This mode can be used in real life applications for purpose of power contract with

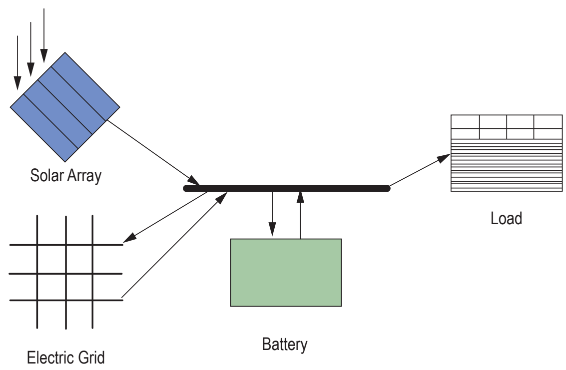

Figure 6-1: Hybrid PV/battery system configuration

utility [41]. In this mode power is used to compensate power mismatch between the PV array and the dispatched amount. In dispatch mode the battery might experience frequent shifts between charging and discharging mode [41]. As can be seen the battery energy storage can charge or discharge to help maintain the balance between the PV generation and loads demand. When the generation exceeds the demand the PV generation will charge the battery in order to store the excess power, while in case of PV generation shortage the battery will discharge and provide the stored power to supply the grid.

6-2 System and component models in MATLAB/Simulink

In this section all the components of the system, as modelled in the project shown in Alberto[40], will be introduced along with the modifications introduced in this project. The model of the system in Simulink can be seen in Figure 6-2.

6-2-1 PV generator and MPPT model

Since the core idea of this project is the EMTP-based model of the PV generator, the model that has been explained in the previous chapters is used for this study as well. The results extracted in an Excel file format are inserted to Simulink and combined with the rest of the system in terms of a function. In order to extract the values the single-phase grid-connected model with the MPPT, as analytically explained in the previous chapter, is used.

6-2-2 DC/DC boost converter model

The EMTP-model as simulated in the ATPDraw interface includes already the MPPT algorithm. For that reason the MPPT is omitted from the Simulink model of the PV array. As for the DC/DC converter the boost configuration has been chosen for its better dynamic performance. The configuration of the boost converter is the same as the one presented in Figure 3-7. The inductance of the converter is set at $0.85mH$, the input capacitance at $11.7mF$ and the output capacitance at $24mF$ [40]. The new Simulink model including the

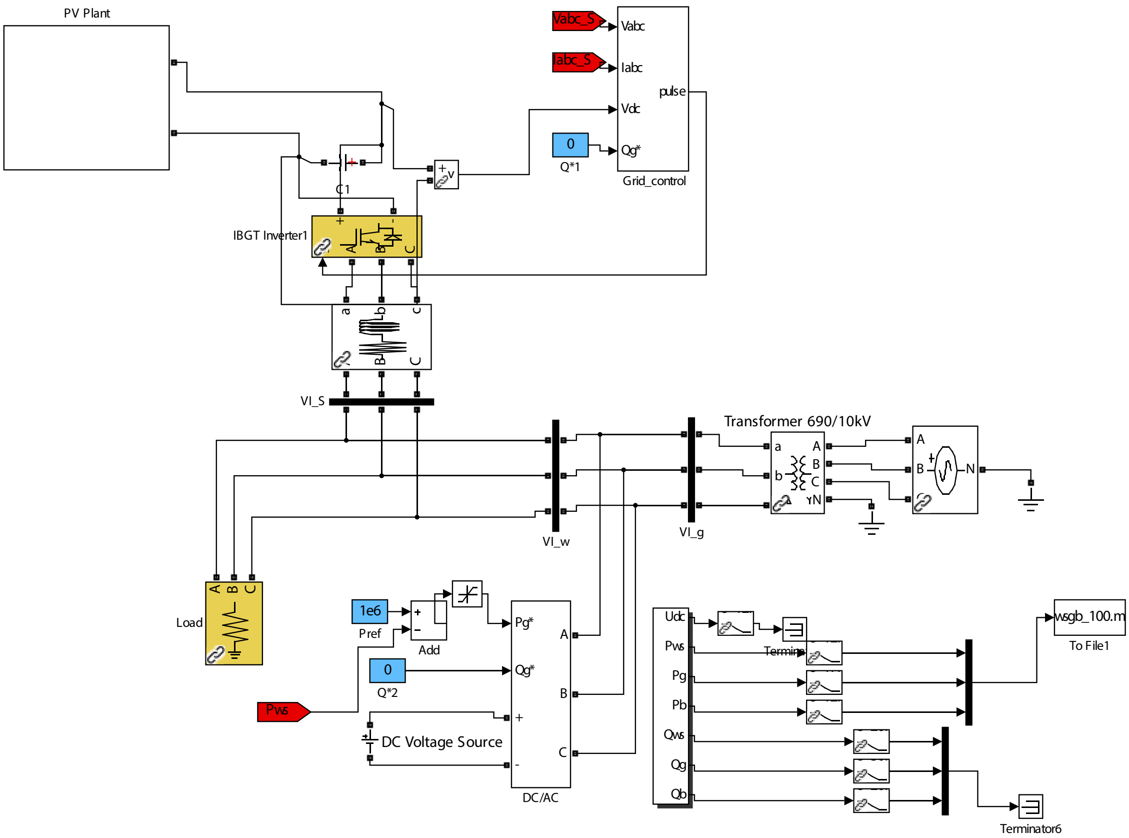

Figure 6-2: Three-phase grid-connected hybrid PV/battery system simulated with Simulink

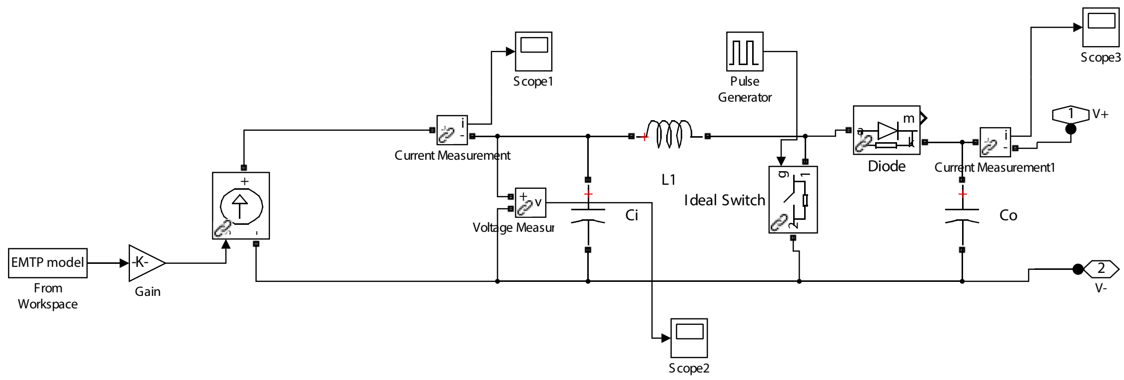

Figure 6-3: New PV model modelled in Simulink

function representing the EMTP-based PV and MPPT outputs along with the boost converter is shown in Figure 6-3. The input of the converter is the voltage output of the EMTP model, the boost converter will change this input into a DC voltage of different value depending also on the pulse that turns the converter bridge on and off. The desired duty cycle, necessary to boost the input voltage to the expected value and maintain it as constant as possible, was determined empirically and the pulses are given in the new model through a pulse generator.

6-2-3 DC/AC inverter model

The output of the PV generator model is connected to a DC/AC inverter with IGBTs, controlled using Space Vector Pulse Width Modulation (SVPWM). The inverter maintains the voltage at the DC side at about 2000V and controls the reactive power flow to the grid [40]. The d-axis (direct) reference current is actually determined by the DC voltage PI controller, to control the converter's output real power. The reactive power is maintained at zero by the control of the q-axis (quadrature) as explained and presented in Alberto[40].

6-2-4 Battery system/Load models

A three-phase parallel RLC load has been used in a Y grounded configuration. As for the battery system, even though most of them in literature are modelled accounting the battery's internal parameters, such as the internal resistances, capacitances and the State of Charge (SOC), in Alberto[40], where the system is simulated for a very short time period, the battery is considered to have very small variations so that the internal characteristics do not significantly influence the voltage and current of the battery. Based on this assumption the battery is modelled as a DC constant voltage source of 1500V and the power output is controlled by a DC/AC inverter, that is connected to the grid [40]. The system simulated in Alberto[40] is a 2MW/0.5MWh system based on the model of A123 company, composed by Li-Ion batteries. The system's response is in the range of 120ms. As for the controller of the system, it is designed to control the active and reactive power outputs of the system based on SVPWM, aligning the voltage vector with the d-axis and setting q-axis component to zero. That way, the d-axis current controls the active power, while the reactive power is controlled by the q-axis current. The reference active power is set at zero and the reference active power is described as the difference between the desired power that has to be injected to the grid and the difference between the solar power and the load [40]:

$$P_{batt} = P_{set} - (P_{solar} - P_{load}) \tag{6-1}$$

where P_{batt} is the battery's power, P_{set} is the desired power, P_{solar} is the power output of the PV system and P_{load} is the power consumed by the load.

6-2-5 Transformer/utility grid models

The PV generator and battery systems are both connected to the utility grid through a RL series branch of 0.5mH and 1mΩ. As for the transformer, a three-phase two winding 690V/10kV model is used. The grid in this case is represented by a 10kV line-to-line constant voltage source and constant frequency of 50Hz.

6-3 Simulation and results

Based on the above explained models and control methods four case studies, similar to the ones presented in Alberto[40], are studied in this project, so that a comparative study can be developed and the behaviour of the EMTP-based PV generator can be tested in a three-phase system scenario.

As explained before the EMTP-based model of the PV generator is used in order to extract the values and insert them into the Simulink model. So, for the case studies of this chapter the data of the PV generator, as used in Alberto[40] are used as inputs for the simulations in the ATP interface, namely the Solarex MSX 60 datasheet values under STC. This module consists out of 36 cells in series and its electrical characteristics can be seen in Table 6-1. For the simulations in Alberto[40] project a number of 800 series and 54 parallel modules were used in order to build a solar plant of about 2.3MW. The values of Table 6-1 are used accordingly to the specifications of each case study as inputs for the EMTP-based model, in order to extract the characteristic values of the PV array and insert them in the Simulink model. It is clear that for this study the PV generator is working as a PV array.

Table 6-1: Typical electrical characteristics of Solarex MSX 60 PV module [42]

Mamimum power (Pmax)	60W
Vmpp	17.1V
Impp	3.5A
Guaranteed minimum Pmax	58W
Isc	3.8A
Voc	21.1V

Table 6-2: Data for the three-phase grid connected PV array

Vmpp	923.4V
Impp	3040A
Isc	3040A
Voc	1139.4V

Case study 1

For the case study 1, by recalculating the values of the series and parallel modules and by using the data of Table 6-1, a PV array with an output power of about 3MW and constant atmospheric conditions is simulated. The load is set to be 1MW while the total power is set to dispatch 2MW to the grid. The results of the simulation running for $t = 6s$ can be seen in Figure 6-4. The results are in good agreement with the graph presented in Alberto[40]. The battery operates in charging mode when there is surplus generation and turns to discharging mode in case of generation shortage.

Case study 2

The number of modules is once more adjusted in order to result in a PV array power of about 2MW. The load power for this case study remains at 1MW and the design of the system is carried out for feeding 2MW power to the grid. The results of the simulation running again for $t = 6s$ can be seen in Figure 6-5. Once more the graph is in agreement with the corresponding graphs presented in Alberto[40]. In addition, it is clear that the system follows equation (6-1).

Case study 3

this simulation is running after increasing the load power to 3.5MW and maintaining the solar power at the same levels as explained in case study 1. The results of the simulation are presented in Figure 6-6. In this case, it is obvious that the assumption that the SOC of the battery will not be taken into account for such a small time interval, leads to the battery system not being able to absorb or provide power of more than 2MW. So, from the graphs we can see that when the load consumes more power than the PV array can deliver the demand of the grid cannot be met and the power drops, a case that can cause stability problems in real life situations.

From the simulation results of case study 3 it can be concluded that for this system to work properly a very good forecast of the load power and the weather conditions should be made, so that the active power requested from the battery system does not exceed the amount of power of 2MW. In addition, it has to be clear that the objective of these case studies is to keep the grid power constant, an approximation that does not correspond with real life conditions. Also, the grid has been simulated as a constant voltage source, which stands far from the reality where the voltage and the frequency of the system can vary significantly. The system can be improved, by modelling the battery system taking into account the SOC, and by controlling the voltage and frequency of the utility grid by regulating the active and reactive power injected by the battery system.

At this point it has to be clear that the transient regime lasting the first two seconds is mainly due to the fact that the MPPT in the EMTP-based model is energised for $t > 2s$. In addition, the transient response of the PV array shows similar behaviour as in the previous chapters. The initial mismatches are mainly due to the fact that the modelling of the EMTP-based PV generator starts the simulations for I_{sc} causing the voltage to start from zero and thus the power generation to start from zero. Due to the limitations of the Simulink system the initial mismatches can be seen in the graphs.

Case study 4

Assuming the case presented in scenario 2 in Section 5-7, where the solar irradiance changes, a new case study is investigated. As explained in previous chapters, the I-V characteristic of the PV array is dependent on the solar irradiance changes and changes with these variations. Accordingly the MPPT controller is following these variations in order to make the PV always generate the maximum power [39]. The profile of the irradiance is the same as the one presented in Figure 5-43. During the time period $t = 0-2s$ the irradiance level is $1000W/m^2$, for $t = 2-4s$ it decreases at $800W/m^2$, for $t = 4-5s$ it increases at $900W/m^2$ and from $t = 6s$ and on, the irradiance remains constant at $900W/m^2$. For this case study the load power is again set at 1MW. Figure 6-7 shows the active and reactive power flux .

With the power generated from the PV array not always equal to the power demands, the battery will charge and discharge to compensate this power unbalance. In this case the MPPT algorithm built in this project is energised for $t = 1s$ and as can be seen only for an irradiance level of $1000W/m^2$ the solar power can sufficiently cover the demand of the load and the grid. For the other two levels the battery system has to discharge and supply the power demanded.

As a conclusion for the aforementioned case studies it can be stated that the system shows good performance under dispatch operation. The battery operates in charging mode when there is surplus power and turns to discharging state when there is generation shortage. Battery's power generation or absorption equals the amount by which the PV generation is subtracted from the dispatched power.

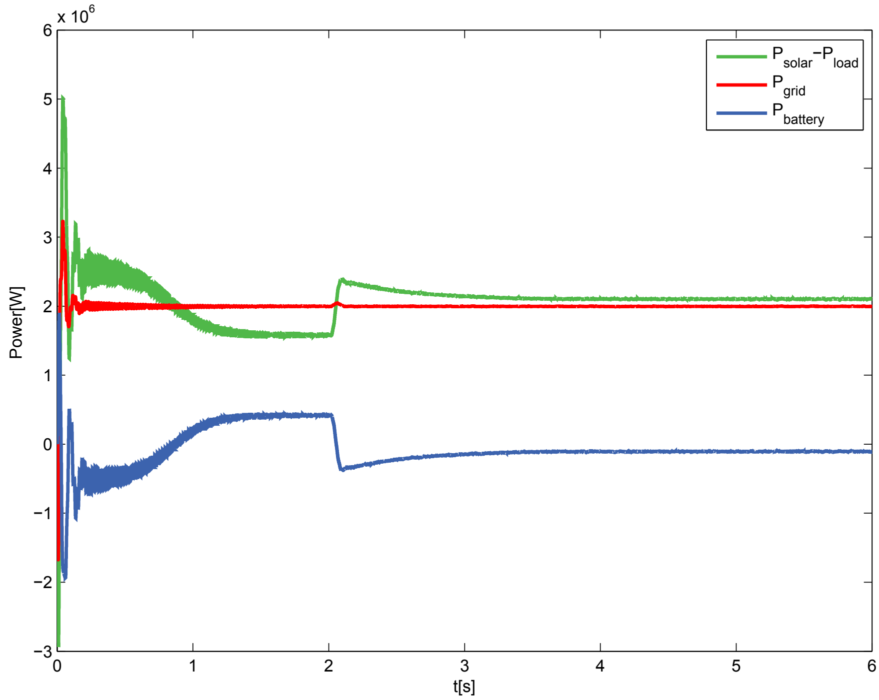

Figure 6-4: System power simulation results of case study 1

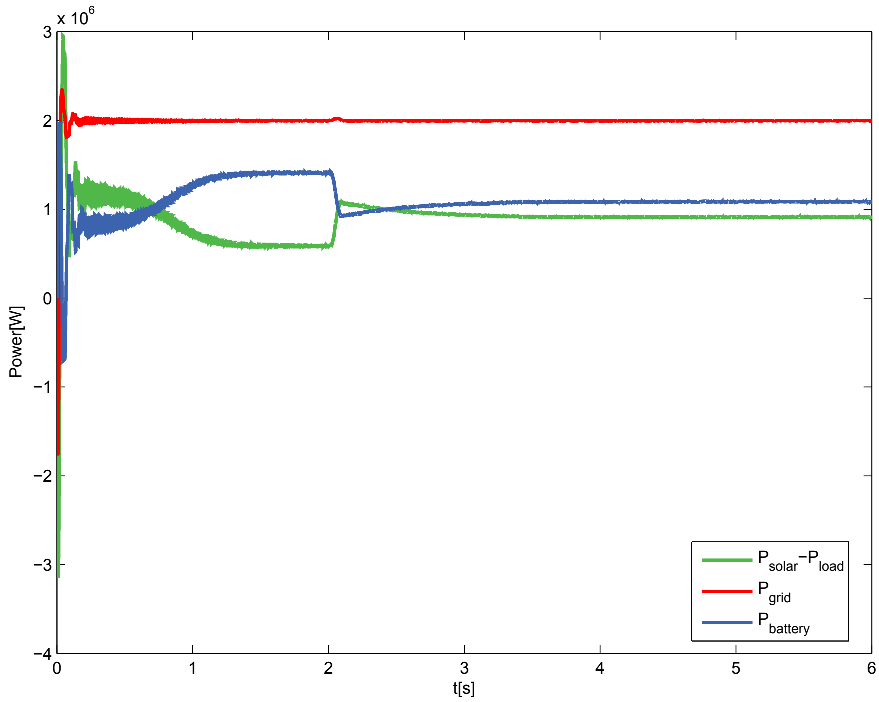

Figure 6-5: System power simulation results of case study 2

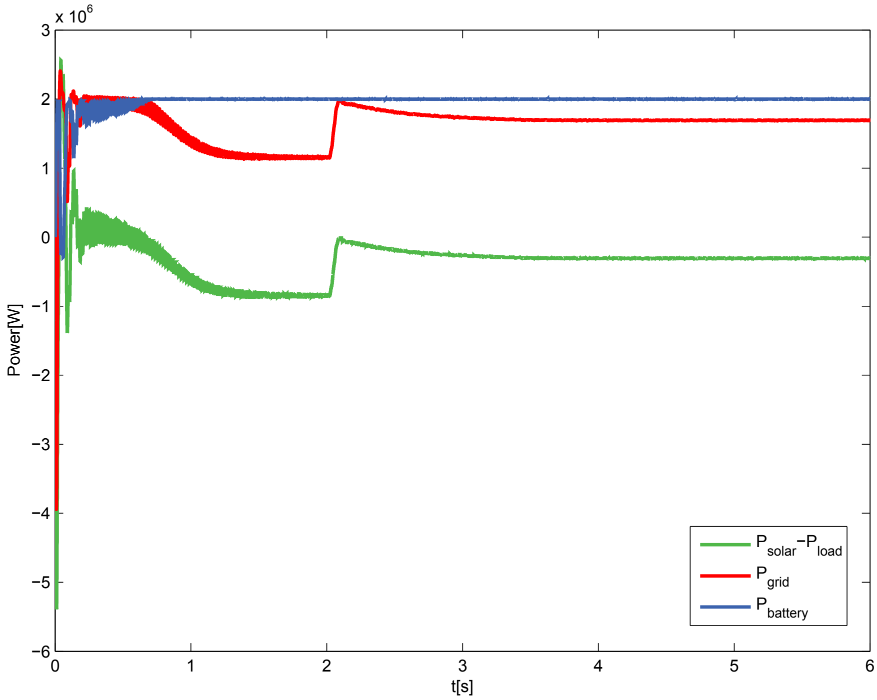

Figure 6-6: System power simulation results of case study 3

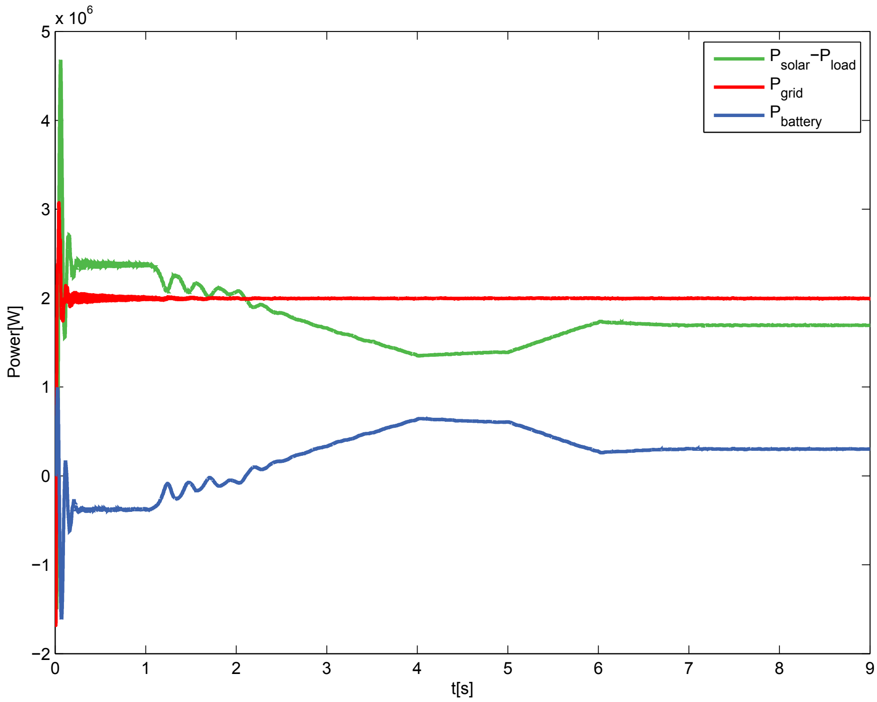

Figure 6-7: System power simulation results of case study 4

Chapter 7

Conclusions and future work

In this chapter the main conclusions extracted from this study, as well as recommendations for future researchers are presented.

7-1 Conclusions

As stated in the project objective, a PV generator EMTP-based model is proposed in this report based on the linearisation of the current-voltage characteristic. A nonlinear characteristic of current vs. voltage of a PV generator should be modelled by at least two exponential factors, to be simulated precisely. However electromagnetic transient programs cannot handle this nonlinearity. With the proposal in this project all the restrictions of using a PV model within an electromagnetic transient software can be overcome.

In order to study the dynamic behaviour of the proposed PV generator model first a study of circuits involving R,L,C elements has been implemented. The model successfully reproduces $i_{pv} - v_{pv}$ and $p_{pv} - v_{pv}$ curves and matches real module data under different scenarios. In the proposed model of the PV generator the values I_{sc}, V_{oc}, I_{mp}, V_{mp} can be conveniently inputted, when they are known under specific atmospheric conditions, while the model is also expandable in case of irradiance and temperature variations. However, the functionality of the optimisation scheme proposed has limitations and is not adjustable for every value of irradiance and temperature.

Following, the model is used for utility grid-connected studies. First a single-phase grid connected system is developed, with all the included elements analysed and modelled in EMTP, in order to gain valuable insights of the system's behaviour for further studies on a power analysis level. The model shows very good numerical stability and the predicted waveforms agree with measured ones. Additionally, a new MPPT algorithm is proposed, based on the specifications of the system, that after simulations shows also good dynamic behaviour. However, the modelling of the system does not correspond to a well designed commercial PV system, due to its high harmonic levels and the simple configuration chosen for the system's elements. In general though, the association of the PV generator model with the grid-connected system proved that the proposed model can be successfully used to analyse the characteristics and problems of distributed PV systems, but most of all is applicable to both slow and fast simulations.

As a next step, in order to validate the expandability and flexibility of the proposed PV generator model, an already established three-phase grid-connected hybrid PV/battery system, presented in a past graduation report, is used and combined with the EMTP-based models developed in this project. Four case studies are simulated. The results validate the PV generator model's behaviour in a three-phase scenario and a real life application approach system, without providing in-depth insights of the system's transient response and analysis in the power system level though.

In conclusion, in this project a new simple model for the representation of PV generators in a commercial electromagnetic transient program is proposed. It has the potential to be a useful tool for power engineers dealing with PV systems modelling, while working both as a PV module and an array depending on the system configuration. The model simplifies the representation of PV generators in EMTP, avoiding complex block-circuits with several elements and control commands, while additionally being suitable for implementation in other electromagnetic transient software packages.

7-2 Future work

During this project, there were topics found to be unanswered or left for further studies.

Improvements on the equations used to determine the parameters of the nonlinear PV generator model, like $k1$, $k2$, $k3$, $k4$, m should be made in order to increase the accuracy of the model. It is really important that these changes are not limiting the simplicity of the procedure.

The optimisation scheme, that is proposed so that the PV generator can change according to atmospheric condition variations, can also be improved and more appropriate equations should be derived, so that the PV generator adjusts better in every condition.

As for the model of the single-phase grid-connected PV system, it should also be improved, by developing a more concrete inverter and controller system. The results should be verified with modern commercial PV system outputs while the system's harmonics should be maintained at acceptable levels. Fault simulations and detailed transient analysis should be the next steps to be done.

Nowadays, the integration of solar energy in microgrids is becoming a main concern of the power system industry. At the same time, the modelling of renewable energy sources for large-scale power system integration simulation is becoming more and more important, therefore simulation tools will play a significant role during optimal design and intelligent management processes [43]. An extensive technical study is required in terms of the impact of these large-scale systems on the voltage stability, the power quality, the response to faults and short circuit contributions, etc. [44]. For these studies a complete three-phase PV solar system is required in an electromagnetic transient software environment such as EMTP. Hybrid systems should also be a future target, since their control strategies are quite different form the control in conventional systems [41]. The focus on these systems should be on the battery charging/discharging control and on the technique of using low-pass filters [41].

Appendix A

The Newton Raphson algorithm

Newton Raphson algorithm is a powerful technique for solving equations numerically. Like many other differential calculus, stands on the simple idea of linear approximation and it is based on a Taylor series expansion of the function f(x). More analytically, if the f(x) is expanded around a point α the function becomes:

$$f(x) \approx f(a) + (x-a)^T f^{'}(a) + \frac{1}{2}(x-a)^T f^{''}(a)(x-a) \tag{A-1}$$

where $f^{'}(\cdot)$ is the gradient vector and $f^{''}(\cdot)$ is the hessian matrix of second derivatives. This creates quadratic approximation for f. In order to maximize this quadratic function the following equation must be solved:

$$\frac{d}{dx} f(a) + (x-a)^T f^{'}(a) + \frac{1}{2}(x-a)^T f^{''}(a)(x-a) = f^{'}(a) + (x-a)^T f^{''}(a) = 0 \tag{A-2}$$

$$x = a - [f^{'}(a)]^T [f^{''}(a)]^{-1} \tag{A-3}$$

The Newton Raphson process iterates this equation. More specifically, if x_0 is the starting point for the algorithm and x_1, x_2 are successive estimates defined recursively through the equation:

$$x_{i+1} = x_i - [f^{'}(x_i)]^T [f^{''}(x_i)]^{-1} \tag{A-4}$$

In case the function $f(x)$ is quadratic, the approximation is exact and the Newton Rapshon method converges to the maximum in one iteration. If the function is concave, then the method successfully converges to the right answer. In case the function is convex only for some values of x, then the algorithm may or may not converge. The method might converge to a local and not global maximum, a local minimum or it cycle between two points. The best method for driving convergence to the global maximum is to start the algorithm near the global maximum [45].

Bibliography

[1] R. E. P. N. for the 21st Century, "Renewables 2012 global status report," tech. rep., Renewable Energy Policy Network for the 21st Century, 2012.

[2] E. P. I. Association, "Global market outlook for photovoltaics 2013-2017," tech. rep., European Photovoltaic Industry Association, 2013.

[3] V. Quaschning, *Understanding Renewable Energy Systems [Multimedia Multisupport]*, vol. 1. Earthscan, 2005.

[4] A. D. Theocharis, V. P. Charalampakos, A. Drosopoulos, and J. Milias-Argitis, "Equivalent circuit of photovoltaic generator using newton-raphson algorithm," *COMPEL - The International Journal for Computation and Mathematics in Electrical and Electronic Engineering*, vol. 31, no. 4, pp. 1224–1245, 2012.

[5] M. Zeman, "Photovoltaic basics syllabus." University Lecture, 2011.

[6] H. J. Möller, *Semiconductors for solar cells.* Artech House Boston^ eMA MA, 1993.

[7] D. Rekioua and E. Matagne, *Optimization of Photovoltaic Power Systems: Modelization, Simulation and Control.* Springer, 2012.

[8] M. G. Villalva, J. R. Gazoli, *et al.*, "Comprehensive approach to modeling and simulation of photovoltaic arrays," *Power Electronics, IEEE Transactions on*, vol. 24, no. 5, pp. 1198–1208, 2009.

[9] S. Said, A. Massoud, M. Benammar, and S. Ahmed, "A matlab/simulink-based photovoltaic array model employing simpower systems toolbox," *Journal of Energy and Power Eng*, vol. 6, pp. 1965–1975, 2012.

[10] B. WILAMOWSKI and J. Irwin, *Power Electronics and Motor Drives (The Industrial Electronics Handbook).* CRC Press Taylor and Francis Group, 2011.

[11] A. Malla and A. Niraula, "Importance of balance of system in a solar pv application,"

[12] J. A. VENTRE *et al.*, *Photovoltaic systems engineering.* CRC press, 2004.

[13] P. B. Miro Zeman, "Photovoltaic systems reader." University Lecture, 2013.

[14] IEEE, "Recommended practice for utility interface of photovoltaic (pv) system, ieee std 929-2000," tech. rep., Institution of Electrical and Electronics Engineers, 2000.

[15] Wikipedia, "Islanding," 2013.

[16] U. Mohan, "Robins (2003) power electronics: Converters, applications, and design."

[17] S. V. Araújo, P. Zacharias, and R. Mallwitz, "Highly efficient single-phase transformerless inverters for grid-connected photovoltaic systems," *Industrial Electronics, IEEE Transactions on*, vol. 57, no. 9, pp. 3118–3128, 2010.

[18] A. Falk, M. Meinhardt, and V. Wachenfeld, "Efficiency and grid compatibility of photovoltaic inverters–state-of-the-art and future trends," in *Proceedings of the European Conference on Power Conversion and Intelligent Motion (PCIM), Nuremberg, Germany*, pp. 14–20, 2009.

[19] M. Calais, J. Myrzik, T. Spooner, and V. G. Agelidis, "Inverters for single-phase grid connected photovoltaic systems-an overview," in *Power Electronics Specialists Conference, 2002. pesc 02. 2002 IEEE 33rd Annual*, vol. 4, pp. 1995–2000, IEEE, 2002.

[20] C. Rodriguez and J. D. Bishop, "Organic architecture for small-to large-scale photovoltaic power stations," *Industrial Electronics, IEEE Transactions on*, vol. 56, no. 11, pp. 4332–4343, 2009.

[21] T. Esram and P. L. Chapman, "Comparison of photovoltaic array maximum power point tracking techniques," *Energy conversion, IEEE transactions on*, vol. 22, no. 2, pp. 439–449, 2007.

[22] S. Alghuwainem, "Matching of a dc motor to a photovoltaic generator using a step-up converter with a current-locked loop," *Energy Conversion, IEEE Transactions on*, vol. 9, no. 1, pp. 192–198, 1994.

[23] S. Lalouni, D. Rekioua, T. Rekioua, and E. Matagne, "Fuzzy logic control of stand-alone photovoltaic system with battery storage," *Journal of Power Sources*, vol. 193, no. 2, pp. 899–907, 2009.

[24] H. Cho, S. Yeo, C. Cim, V. Terzijia, and Z. Radojevic, "A steady-state model of the photovoltaic system in emtp," in *The International Conference on Power Systems Transients (IPST2009), Kyoto, Japan*, 2009.

[25] H. Hoidalen, "Atp draw version 5–users manual supplements," 2007.

[26] M. Popov, "Atpdraw-based models: non-linear elements, surge arresters and circuit breakers," in *European EMTP-ATP conference*, vol. 22, p. 23, 2008.

[27] T. Zacharias, J. Milias-Argitis, and V. Makios, "First-order circuits driven by a photovoltaic generator," *Solar cells*, vol. 31, no. 1, pp. 57–75, 1991.

[28] Siemens, "Solar module sm110/sm100," 2000.

[29] A. D. Theocharis and E. C. Pyrgioti, "Electromagnetic transient programs and the photovoltaic input," in *Environment and Electrical Engineering (EEEIC), 2013 12th International Conference on*, pp. 346–351, IEEE, 2013.

[30] W. F. Marion, B. Kroposki, K. Emery, J. Del Cueto, D. Myers, and C. Osterwald, *Validation of photovoltaic module energy ratings procedure at NREL*. National Renewable Energy Laboratory, 1999.

[31] A. Menti, T. Zacharias, and J. Milias-Argitis, "Harmonic distortion assessment for a single-phase grid-connected photovoltaic system," *Renewable Energy*, vol. 36, no. 1, pp. 360–368, 2011.

[32] B. McNeill and M. Mirza, "Estimated power quality for line commutated photovoltaic residential system," *Power Apparatus and Systems, IEEE Transactions on*, no. 10, pp. 3288–3295, 1983.

[33] A. Sarwar and M. J. Asghar, "Multilevel converter topology for solar pv based grid-tie inverters," in *Energy Conference and Exhibition (EnergyCon), 2010 IEEE International*, pp. 501–506, IEEE, 2010.

[34] S. Pyakuryal and M. Matin, "Implementation of ac to dc converter using thyristor in atp," *IOSR Journal of Engineering*, vol. 2, no. 11, pp. 6–11, 2012.

[35] S. Tunyasrirut, B. Wangsilabatra, and T. Suksri, "Phase control thyristor based soft-starter for a grid connected induction generator for wind turbine system," in *Control Automation and Systems (ICCAS), 2010 International Conference on*, pp. 529–534, IEEE, 2010.

[36] R. García-Valverde, C. Miguel, R. Martínez-Béjar, and A. Urbina, "Optimized photovoltaic generator–water electrolyser coupling through a controlled dc–dc converter," *International Journal of Hydrogen Energy*, vol. 33, no. 20, pp. 5352–5362, 2008.

[37] J. B. Zhang, P. Wang, Z. Zhou, and M. M. Cai, "An improved multistage variable-step mppt algorithm for photovoltaic system," *Applied Mechanics and Materials*, vol. 347, pp. 1833–1838, 2013.

[38] D. Sera, M. Valentini, and A. Raducu, "Real time photovoltaic array simulator for testing grid-connected pv inverters,"

[39] F. Ding, P. Li, B. Huang, F. Gao, C. Ding, and C. Wang, "Modeling and simulation of grid-connected hybrid photovoltaic/battery distributed generation system," in *Electricity Distribution (CICED), 2010 China International Conference on*, pp. 1–10, IEEE, 2010.

[40] J. M. M. A. V. Alberto, "Integration of solar and wind power with battery storage systems," Master's thesis, Faculdade de CiÃłncias e Tecnologia da Universidade de Coimbra, Departamento de Engenharia ElectrotÃľcnica e de Computadores.

[41] S.-K. Kim, J.-H. Jeon, C.-H. Cho, J.-B. Ahn, and S.-H. Kwon, "Dynamic modeling and control of a grid-connected hybrid generation system with versatile power transfer," *Industrial Electronics, IEEE Transactions on*, vol. 55, no. 4, pp. 1677–1688, 2008.

[42] Solarex, "Msx-60 and msx-64 photovoltaic modules," 1998.

[43] C. Keles, B. B. Alagoz, M. Akcin, A. Kaygusuz, and A. Karabiber, "A photovoltaic system model for matlab/simulink simulations,"

[44] S. A. Rahman and R. K. Varma, "Pscad/emtdc model of a 3-phase grid connected photovoltaic solar system," in *North American Power Symposium (NAPS), 2011*, pp. 1–7, IEEE, 2011.

[45] "Newton Raphson Algorithm." http://web.as.uky.edu/statistics/users/kviele/sta601s08/nummax.pdf, 2006. [Online; accessed 30-October-2013].

Glossary

List of Acronyms

PV	Photovoltaic
EPIA	European Photovoltaic Industry Association
EU	European Union
MPPT	Maximum Power Point Tracking
EMTP	Electromagnetic Transients Program
ATP	Alternative Transients Program
Si	Silicon
ASTM	American Society for Testing and Materials
AM	Air Mass
STC	Standard Test Conditions
BOS	Balance of System
IEEE	Institute of Electrical and Electronics Engineers
PWM	Pulse Width Modulation
ENRC	Equivalent Newton-Raphson Circuit
TACS	Transient Analysis of Control Systems
MER	Module Energy Ratings
SCR	Silicon-Controlled Rectifier
THD	Total Harmonic Distortion
IEEE	Institute of Electrical and Electronics Engineers

SVPWM Space Vector Pulse Width Modulation

SOC State of Charge